Study of Multi-Kilowatt Solar Arrays for Earth Orbit Applications

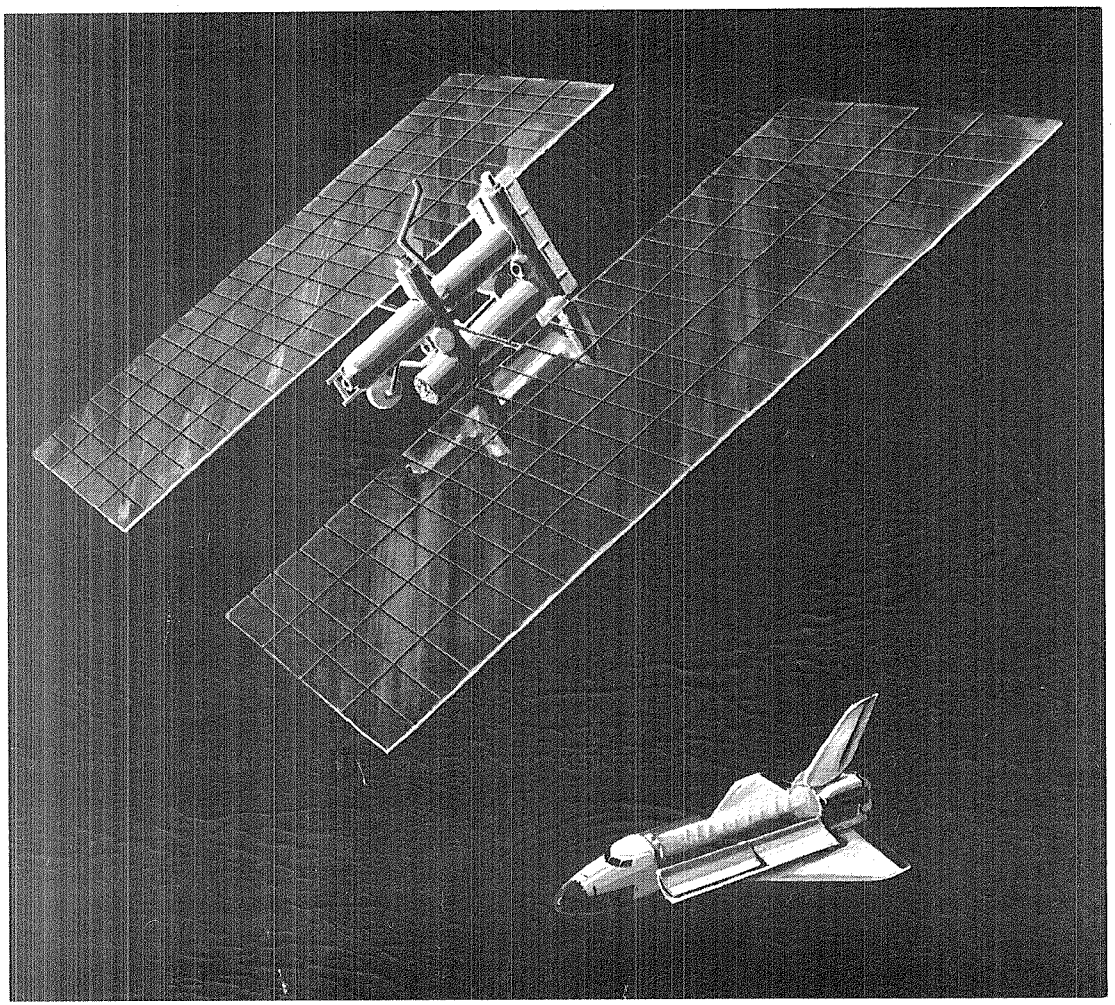

Spacecraft Engineering Division
TRW Space & Technology Group
One Space Park,
Redondo Beach, CA 90278

Final Technical Report
15 October 1983
Contract NAS 8-34131
Document Number 38172-6001-UE-00

Prepared by
Robert E. Patterson

Work Performed for:
Marshall Space Flight Center
National Aeronautics &
Space Administration
Huntsville, Alabama 35812

Study of Multi-Kilowatt Solar Arrays for Earth Orbit Applications

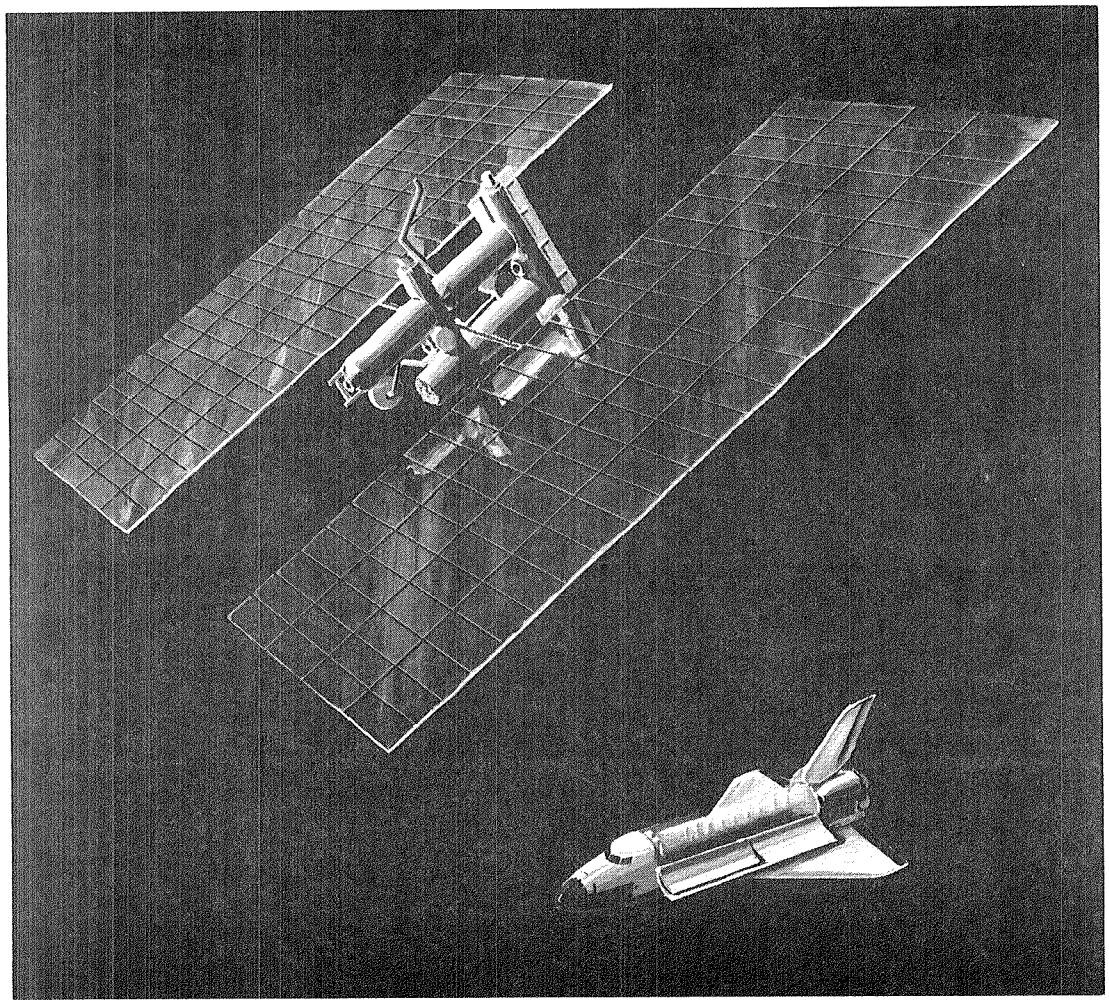

Spacecraft Engineering Division
TRW Space & Technology Group
One Space Park,
Redondo Beach, CA 90278

Final Technical Report
15 October 1983
Contract NAS 8-34131
Document Number 38172-6001-UE-00

Prepared by
Robert E. Patterson

Work Performed for:
Marshall Space Flight Center
National Aeronautics &
Space Administration
Huntsville, Alabama 35812

TABLE OF CONTENTS

FOREWORD

This report documents work performed by the TRW Space and Technology Group, Redondo Beach, California, for the NASA George C. Marshall Space Flight Center (NASA/MSFC), Huntsville, Alabama, under Contract NAS8-34131.

This final report is submitted in compliance with the contract statement of work and covers the entire contract period of performance from 19 November 1980 through 30 June 1983.

The study was managed for TRW by Robert E. Patterson of the Power Sources Engineering Department, Electrical Power Systems Laboratory, and for NASA/MSFC by William L. Crabtree and Ralph Carruth of the Power Branch.

The very helpful participation in this study by many personnel of TRW and NASA/MSFC is gratefully acknowledged.

CASSEGRAINIAN CONCENTRATOR SOLAR ARRAY PROJECT TEAM

IRA ALLARD	MANUFACTURING ENGINEERING
PETER BARRETT	DYNAMIC ANALYSIS
SAUL BASHIN	MECHANICAL DESIGN
ROD DOBSON	ELECTRICAL TESTING
HENRYK FLASHNER	CONTROLS
MARTIN GIEBLER	MECHANICAL DESIGN
JUDD HALL	MANUFACTURING ENGINEERING
DICK HARDGROVE	THERMAL ANALYSIS
JERRY JACOBY	OPTICAL DESIGN
GARY JOHNSON	CREW SYSTEMS/EVA ANALYSIS
LARRY KELLEY	THERMAL TESTING & ANALYSIS
ED LEE	MECHANICAL DESIGN MANAGER
WILLIAM PALMER	MECHANICAL DESIGN
ROBERT PATTERSON	ELECTRICAL DESIGN, PROJECT MANAGER
WILLIAM WINTERS	MATERIALS
CARL WOO	STRESS ANALYSIS

Introduction

INTRODUCTION

A miniaturized Cassegrainian concentrator (MCC) solar array concept is being developed with the objective of significantly reducing the recurring cost of multikilowatt solar arrays. The desired cost reduction is obtained as a result of using very small high efficiency solar cells in conjunction with low-cost optics.

The MCC single element concept is shown on the facing page. Incident solar radiation is reflected from a primary parabolic reflector to a secondary hyperbolic reflector and finally to a 4-millimeter diameter solar cell. A light catcher cone is used to improve off-axis performance. The solar cell is mounted to a heat fin. An element is approximately 13-millimeters thick which permits efficient launch stowage of the concentrator system panels without complex optical component deployments or retractions. The MCC elements are packed in bays within graphite epoxy frames and are electrically connected into appropriate series-parallel circuits.

A MCC single element with a 21-cm^2 entrance aperture and a 20 percent efficient, 0.25-cm^2 gallium arsenide solar cell has the same power output as 30 cm^2 of 11-percent efficiency (at 68°C) silicon solar cells. The MCC concept provides the potential for a significant reduction in array cost due to a 99 percent reduction in required cell area and a 30 percent reduction in array area relative to a planar array of equivalent power. The approach also offers early opportunities for the application of advanced high efficiency cell types that may be more readily available as small-area devices in large quantities from production facilities otherwise limited by market size and capital investment factors.

The analysis and rationale on precursor studies that led to the miniaturized Cassegrainian concentrator approach have been described elsewhere in detail (1, 2, 3, 4). This report covers all work accomplished under Contract NAS8-34131 and includes: (a) the design fabrication and testing of a miniaturized Cassegrainian concentrator (MCC) single element and a nine element MCC demonstration module, (b) MCC element and module design studies based on the performance of the demonstration hardware, and (c) a 100-kilowatt MCC solar array system concept study.

CASSEGRAINIAN CONCENTRATOR ARRAY REDUCES SOLAR CELL AREA AND ARRAY AREA

COMPARISON	PARAMETER	CONCENTRATOR	PLANAR
CONCENTRATOR ELEMENT VERSUS PLANAR CELLS OF EQUIVALENT POWER OUTPUT	CONFIGURATION	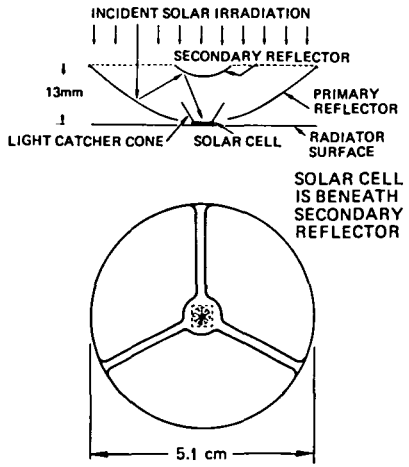	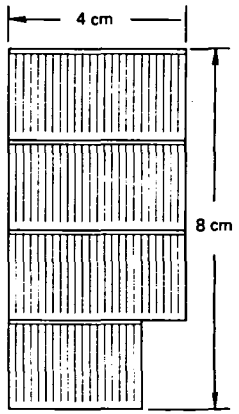
	CELL TYPE	GaAs, η = 20% AT 85°C	Si, η = 11% AT 68°C
	ELEMENT AREA	21 cm^2	30 cm^2
	CELL AREA	0.25 cm^2	30 cm^2
	OUTPUT	0.43 W	0.43 W
CONCENTRATOR ARRAY VERSUS PLANAR ARRAY OF EQUIVALENT POWER OUTPUT	RELATIVE SIZE	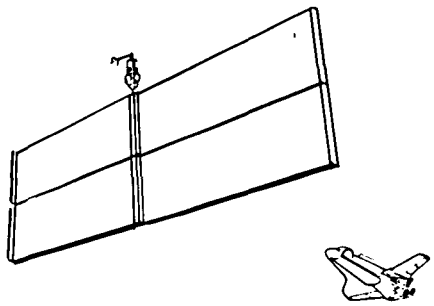 NET CONCENTRATION RATIO = 130	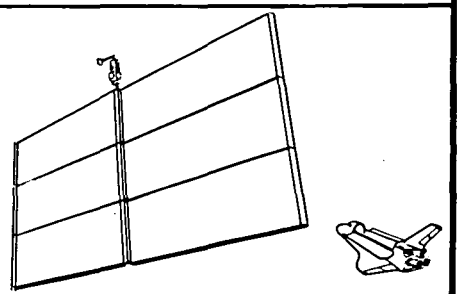 NET CONCENTRATION RATIO = 1
	AREAL DENSITY	160 W/m^2	110 W/m^2

Technical Summary

TECHNICAL SUMMARY

A miniaturized Cassegrainian concentrator (MCC) module has been designed, assembled, and tested. Results support technical feasibility. Thermal vacuum testing and analysis has confirmed earlier predictions that miniaturization results in acceptable solar cell temperatures with passive thermal control for a concentrator element with an effective concentration ratio of 130. Electrical performance of the demonstration hardware was as predicted at normal solar incidence. A light catcher cone improves off-pointing performance but its full predicted effectiveness has not been achieved.

A number of element and module design trade studies have been performed. A packing density study led to the selection of hexagonal close packing of untruncated elements as the baseline approach because it maximizes W/kg performance and minimizes element cost per unit power output. Electrical cell stack configuration, coverglass location, reflector material/configuration, and element radiator configuration studies have been performed. These studies identified multiple acceptable approaches.

A MCC solar array system study was performed to assess the practicality of assembling the basic MCC element into a total array system capable of producing multihundred kilowatts of power for Space Platform/Space Station or other low earth orbit long lifetime missions. Preliminary mechanical and electrical subsystems were developed in order to determine first order performance characteristics. Results of the study support the feasibility of a 100-kilowatt MCC array system with beginning-of-life performance of 160 W/m^2 and 28 W/kg. It would occupy approximately 8 linear feet of Shuttle Cargo Bay in the fully stowed configuration.

The performance numbers are based on 20 percent efficient (at operating temperature) solar cells and 0.25-millimeter thick electroformed nickel optics. These performance numbers can be improved upon significantly with the development of higher efficient solar cells and/or lighter weight optics.

TECHNICAL SUMMARY

NINE-ELEMENT CASSEGRAINIAN CONCENTRATOR DEMONSTRATION MODULE	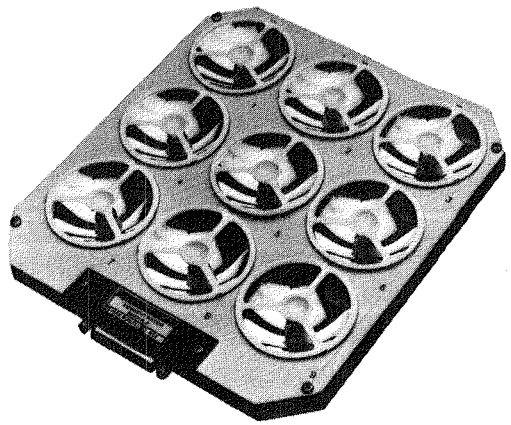	• TEST RESULTS SUPPORT TECHNICAL FEASIBILITY • 85°C CELL TEMPERATURE IN LOW EARTH ORBIT CONFIRMED BY THERMAL VACUUM TEST • CELL STACK ASSEMBLED USING CONVENTIONAL JOINING PROCESSES • OPTICAL ELEMENTS ALIGNED USING MECHANICAL INTERFERENCE FIT
100 KW BOL CASSEGRAINIAN CONCENTRATOR SOLAR ARRAY SYSTEM STUDY	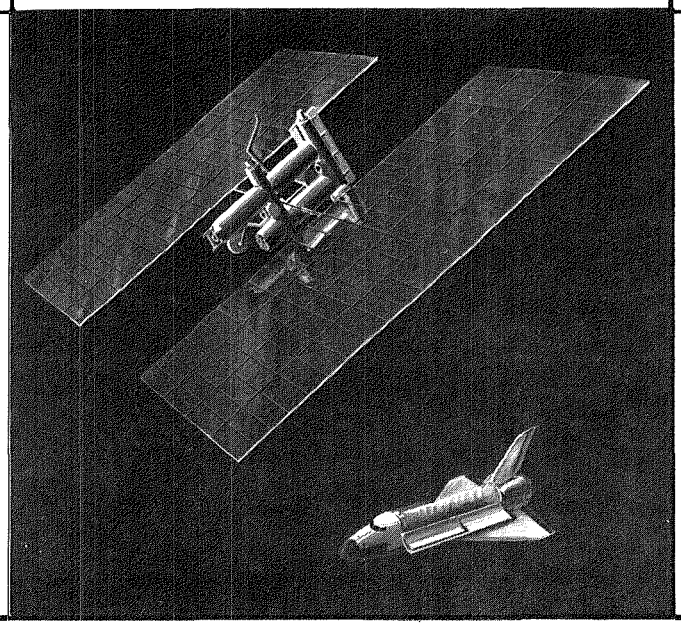	• TWO WING DESIGN BASELINED BUT CONFIGURATIONS ARE NOT CONSTRAINED • FOLD-OUT RIGID PANELS WITH FOLDING BEAM SUPPORT (USED ON SKYLAB) • MODULAR CONCEPT (12.5 KW PER SUBWING MODULE) • ACCURATE ELEMENT POINTING (MAXIMUM RSS OF 1.1°) • 160 W/m^2 (CURRENT TECHNOLOGY) • 28 W/kg (CURRENT TECHNOLOGY) • POTENTIAL OF 60 W/kg WITH TECHNOLOGY DEVELOPMENT • ERECTABLE (EVA) ARRAY OPTIONAL

Demonstration Hardware Design and Assembly

- Element Design
- Cell Stack Assembly Parts Diagram
- Alignment Fixture for Element Assembly
- Cell Stack Detail
- Element Optical Component Assembly
- Nine-Element Demonstration Module

BASELINE CONCENTRATOR ELEMENT DESIGN

This section describes the design of the miniaturized Cassegrainian concentrator demonstration hardware. Incident solar radiation is reflected from a primary parabolic reflector to a secondary hyperbolic reflector and finally to a solar cell. The solar cell is mounted to a molybdenum heat spreader which is mounted to a 0.25-millimeter thick aluminum heat fin. The primary and secondary reflectors are designed such that they have a common focal point in the plane of the entrance aperture, an f-number of 0.25, and rim angle of 90 degrees. This design yields a height of 12.7 millimeters which corresponds to a concentrator panel thickness similar to that of conventional rigid planar solar panels.

The optical reflectors are made of electroformed nickel with a 2000-angstrom rhodium primer coating, a 1200-angstrom aluminum reflective coating, and a 2500-angstrom silicon monoxide protective coating. The solar cells are 0.25 millimeter thick and are made of silicon with 0.5 ohm-cm base resistivity. Their junction depth is 4000 to 5000 angstroms. The cells have back surface reflectors and silicon monoxide antireflective coatings.

This design is for feasibility demonstration hardware. It is anticipated that actual flight hardware will have a number of design changes to enhance performance such as reduced secondary support blockage, silver reflective coatings to increase reflectance, high efficiency gallium arsenide solar cells, and lighter weight optics. Design improvements to the baseline demonstration hardware are discussed throughout this report.

BASELINE CONCENTRATOR ELEMENT DESIGN (ELECTROFORMED NICKEL)

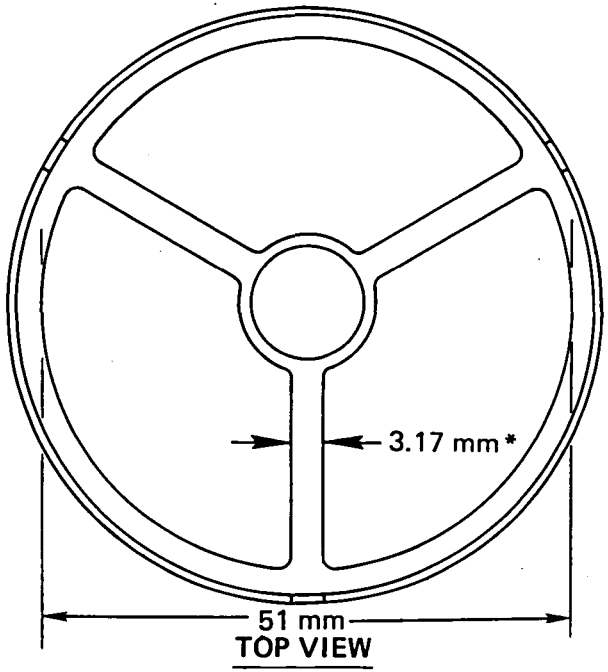

TOP VIEW

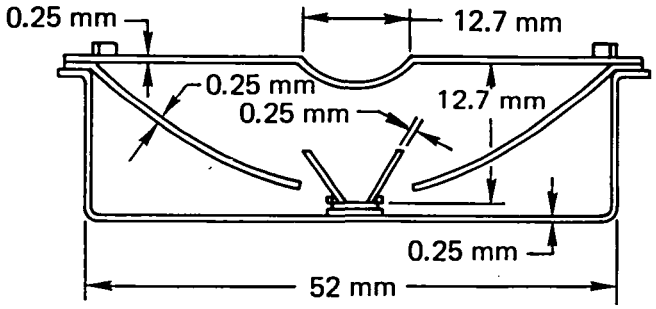

CROSS SECTION

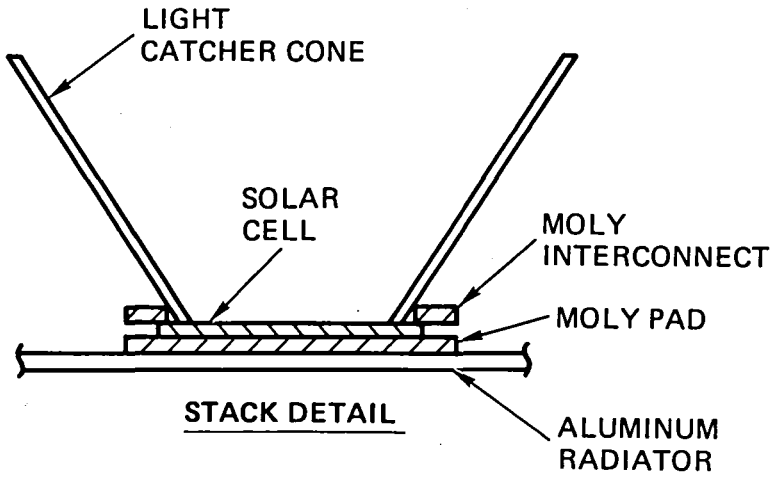

STACK DETAIL

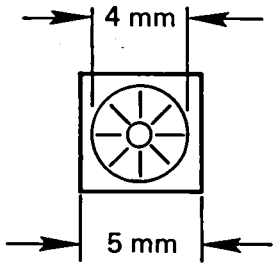

SOLAR CELL DETAIL

*SUPPORT WIDTH TO BE REDUCED ON FUTURE DEVELOPMENT HARDWARE

CELL STACK ASSEMBLY PARTS DIAGRAM

The parts required for cell stack assembly are shown. The aluminum cup acts as both a radiator and a convenient support structure for the optical elements. The cup is 0.25 millimeter thick and is nickel plated to permit soldering. The molybdenum pad between the cell and the cup is used to reduce the shear stress on the cell back contact during thermal cycling since the thermal expansion coefficient of molybdenum is much closer to that of silicon than it is to the coefficient of aluminum. The molybdenum interconnect on the top side of the cell similarly reduces shear stresses on the front cell contact and provides a surface for cone attachment.

CELL STACK ASSEMBLY PARTS DIAGRAM

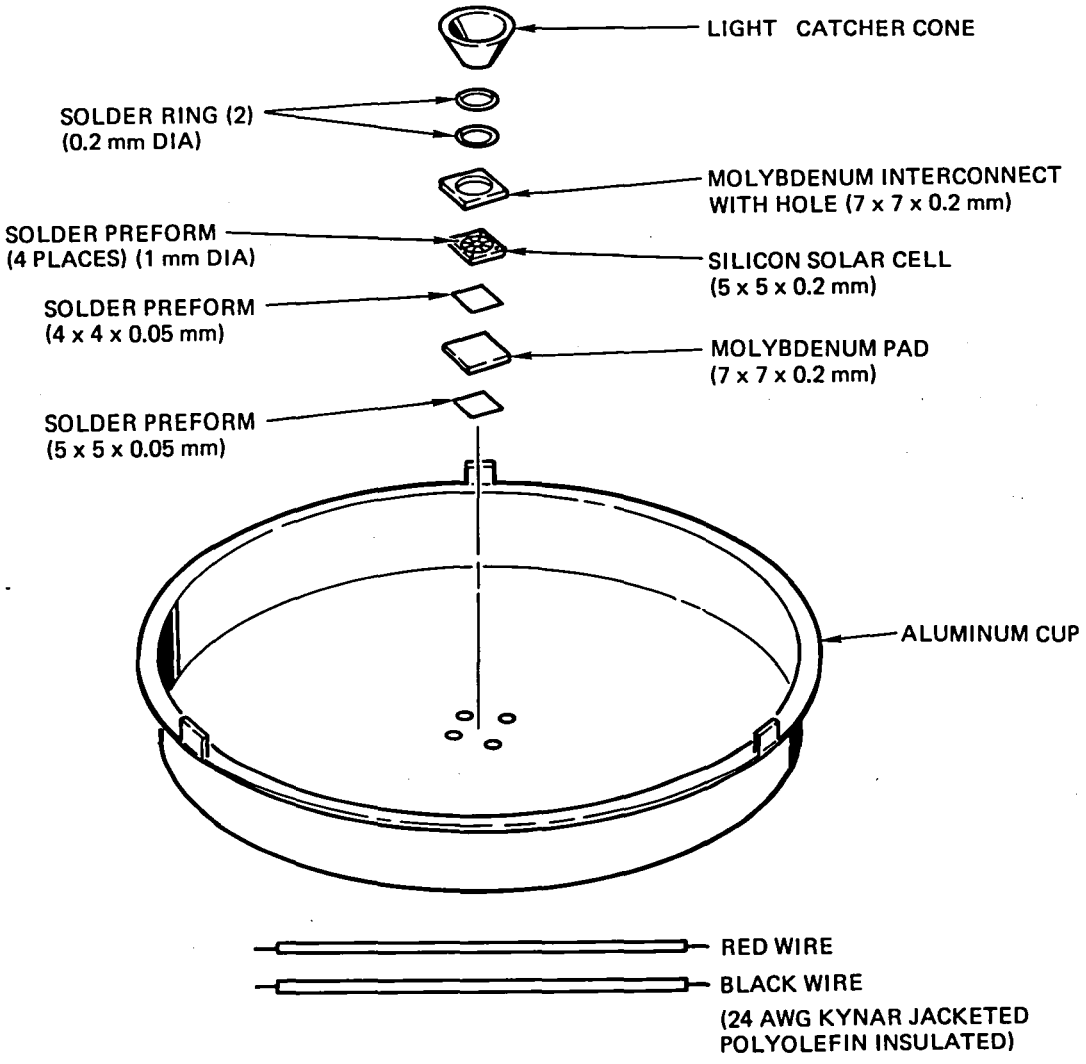

ALIGNMENT FIXTURE FOR CELL STACK CENTERING

The cell stack is centered inside the cup using an alignment fixture that provides four pins for centering the cell stack elements inside the cup. The stack assembly is held in place with springs while it is heated in a vapor phase condensation reflow soldering unit. This process enables all cell stack joining to be accomplished in one operation and, consequently, is well suited for low cost assembly.

ALIGNMENT FIXTURE FOR CENTERING CELL STACK

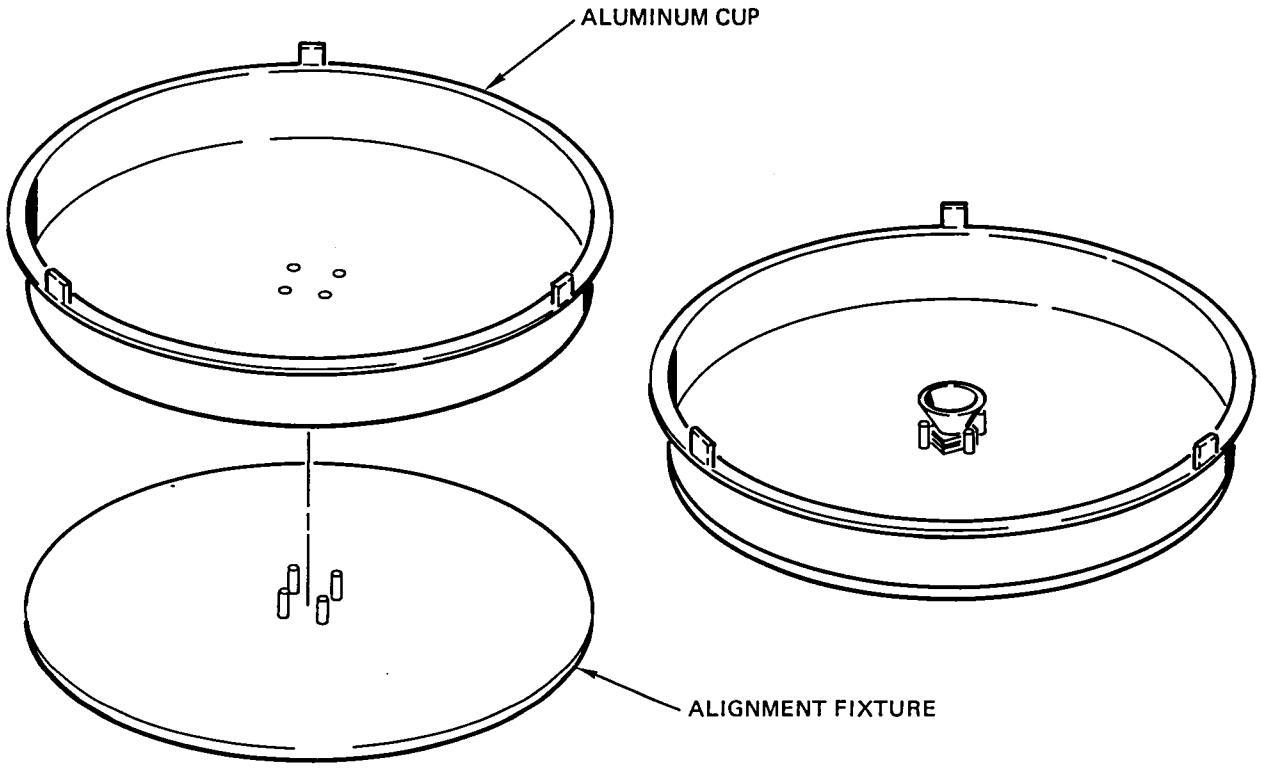

CELL STACK ASSEMBLY DETAIL

Negative and positive wire leads are attached to the top side of the molybdenum interconnect and to the aluminum cup, respectively, as shown. SN-62 solder is used for all electrical attachments and for the cone attachment.

CELL STACK DETAIL

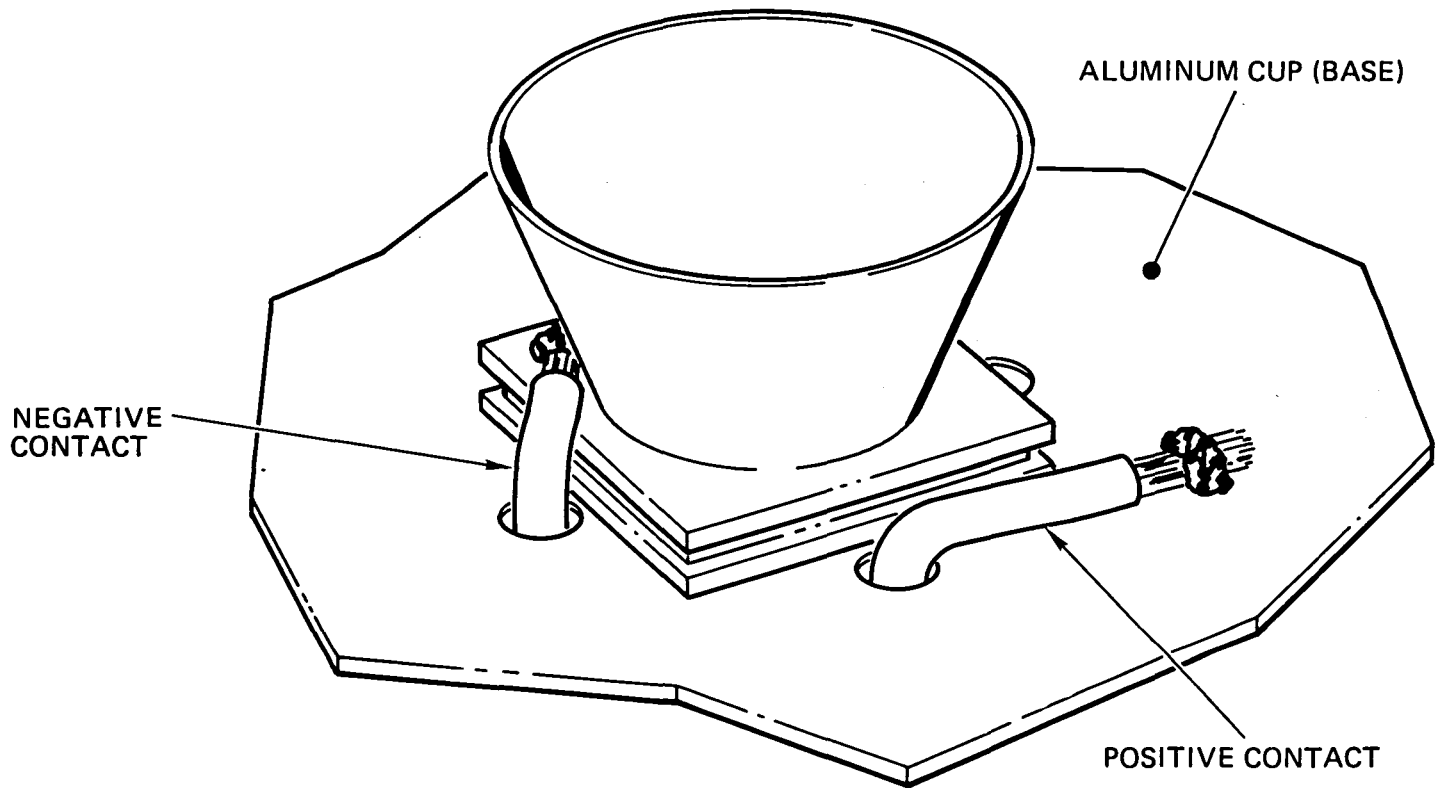

SINGLE ELEMENT ASSEMBLY

The approach used for the single element assembly is shown. The primary and secondary reflectors are supported on the lip of the aluminum cup and are aligned and secured by bending each of the three cup tabs over the flanges of the reflectors.

CUP PROVIDES SELF ALIGNMENT FOR SINGLE ELEMENT ASSEMBLY

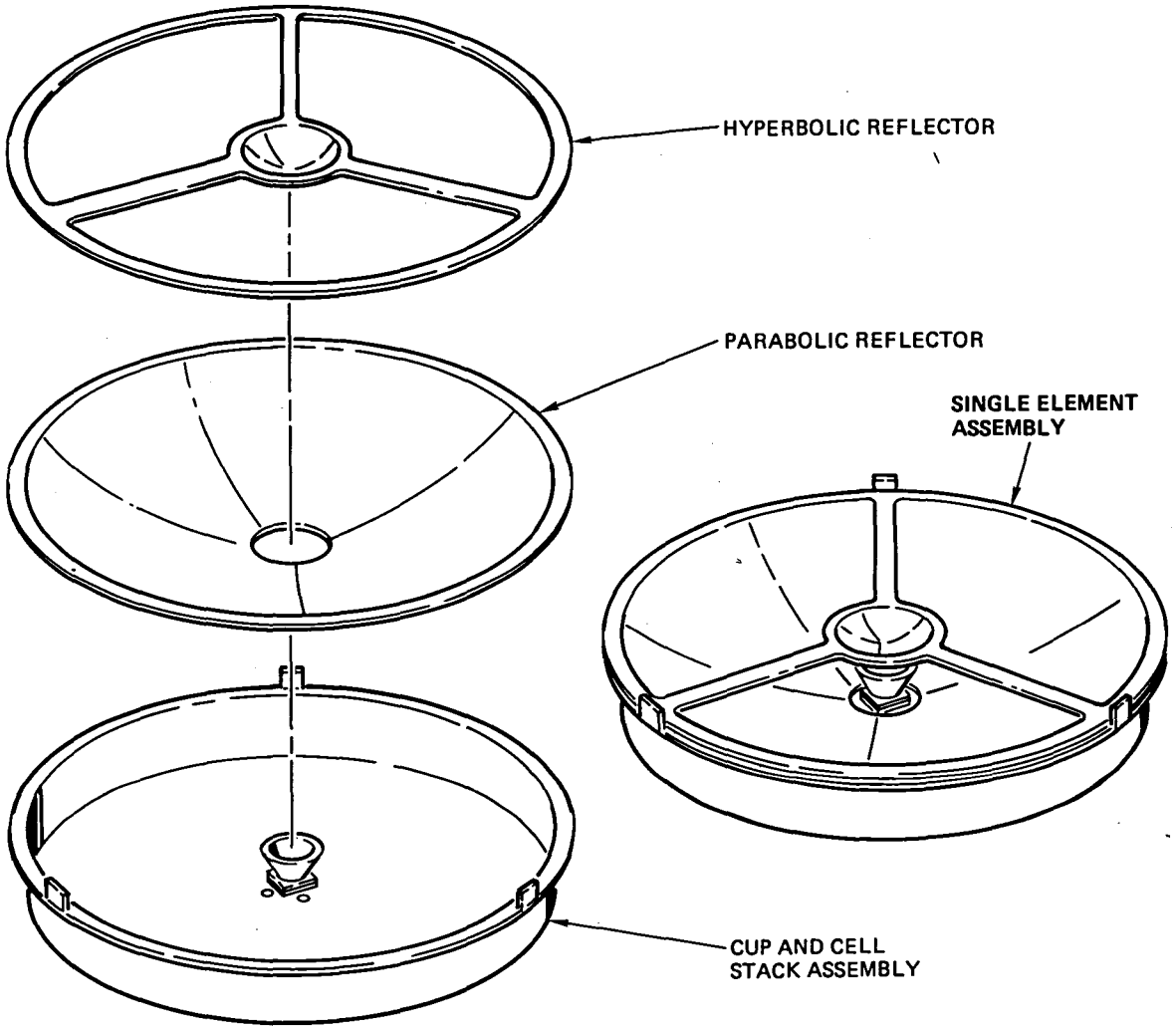

NINE ELEMENT CASSEGRAINIAN CONCENTRATOR DEMONSTRATION MODULE

Nine additional elements were assembled for the demonstration module. The assembled elements were bonded to a honeycomb panel and interconnected such that each element could be tested individually and all could be tested in either series or parallel circuits.

The elements of the demonstration module are arranged orthogonally for assembly and test convenience only, rather than in a closely packed hexagonal pattern. A simple "spider" arrangement supports the secondary hyperbolic reflector. The wide spider legs produce a large blockage loss contribution. No attempt was made to reduce this loss by substituting a more complex support structure since it was desired for the purpose of initial demonstration to use off-the-shelf commercial electroforming techniques without requiring complex mandrel tooling.

NINE-ELEMENT CASSEGRAINIAN CONCENTRATOR DEMONSTRATION MODULE

NINE ELEMENT CASSEGRAINIAN CONCENTRATOR DEMONSTRATION MODULE (BACK VIEW)

The back view of the demonstration module is shown. The white disks are the bottoms of the aluminum cups which support the reflectors. They are painted white to minimize earth shine and albedo effects in low earth orbit. Negative and positive leads are brought out individually from each element and attached to a connector. The four holes in the center of each element are the cell stack centering holes.

NINE-ELEMENT CASSEGRAINIAN CONCENTRATOR DEMONSTRATION MODULE (BACK VIEW)

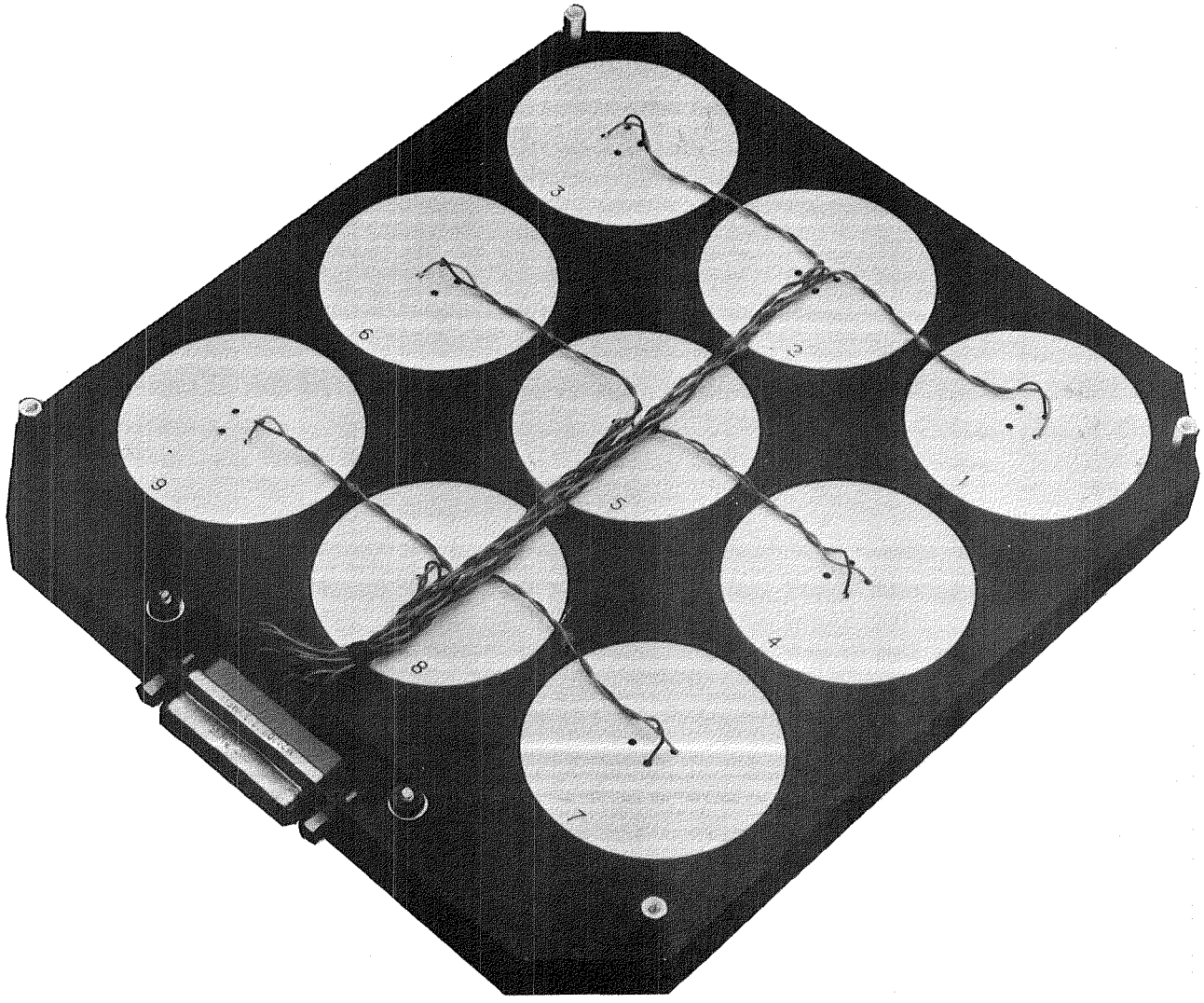

TRW

Test Description and Results

- Reflectance
- Reflector/Cell Misalignment
- Electrical Performance at Normal Incidence
- Electrical Performance Off-Axis
- Thermal Vacuum

TEST SETUP FOR REFLECTANCE MEASUREMENTS

The test setup for reflectance measurements is shown. The beam splitter, variable neutral density filter, and second silicon photo diode enable real time data correction for beam intensity variation. Vendor-supplied spectral reflectance data for aluminum reflectors supports the use of a He-Ne laser light source. The reflectance for aluminum at the He-Ne wavelength is reasonably representative of the average broadband reflectance for aluminum between 0.4 and 1 micron.

TEST SETUP FOR REFLECTANCE MEASUREMENTS

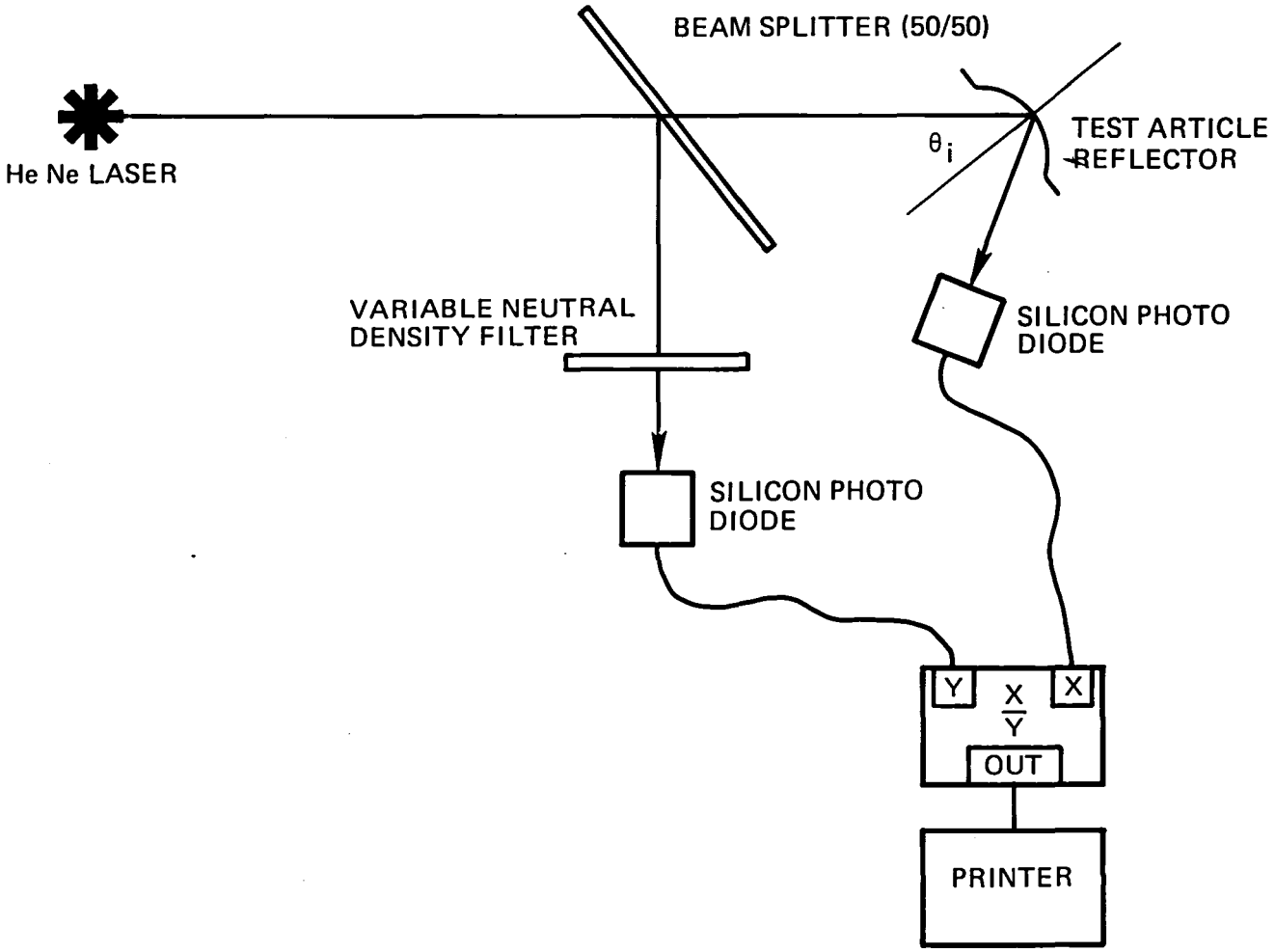

REFLECTANCE DATA

The test setup for the reflectance data is shown on Page 4-3. Reflectance data as a function of angle of incidence was obtained over the appropriate range of angles for each reflector and is presented. A solar simulator was used as the light source for one set of measurements on the parabolas. This data point is identified. Measured reflectance was in good agreement with vendor supplied data.

REFLECTANCE DATA SHOWS GOOD COATING REPRODUCIBILITY

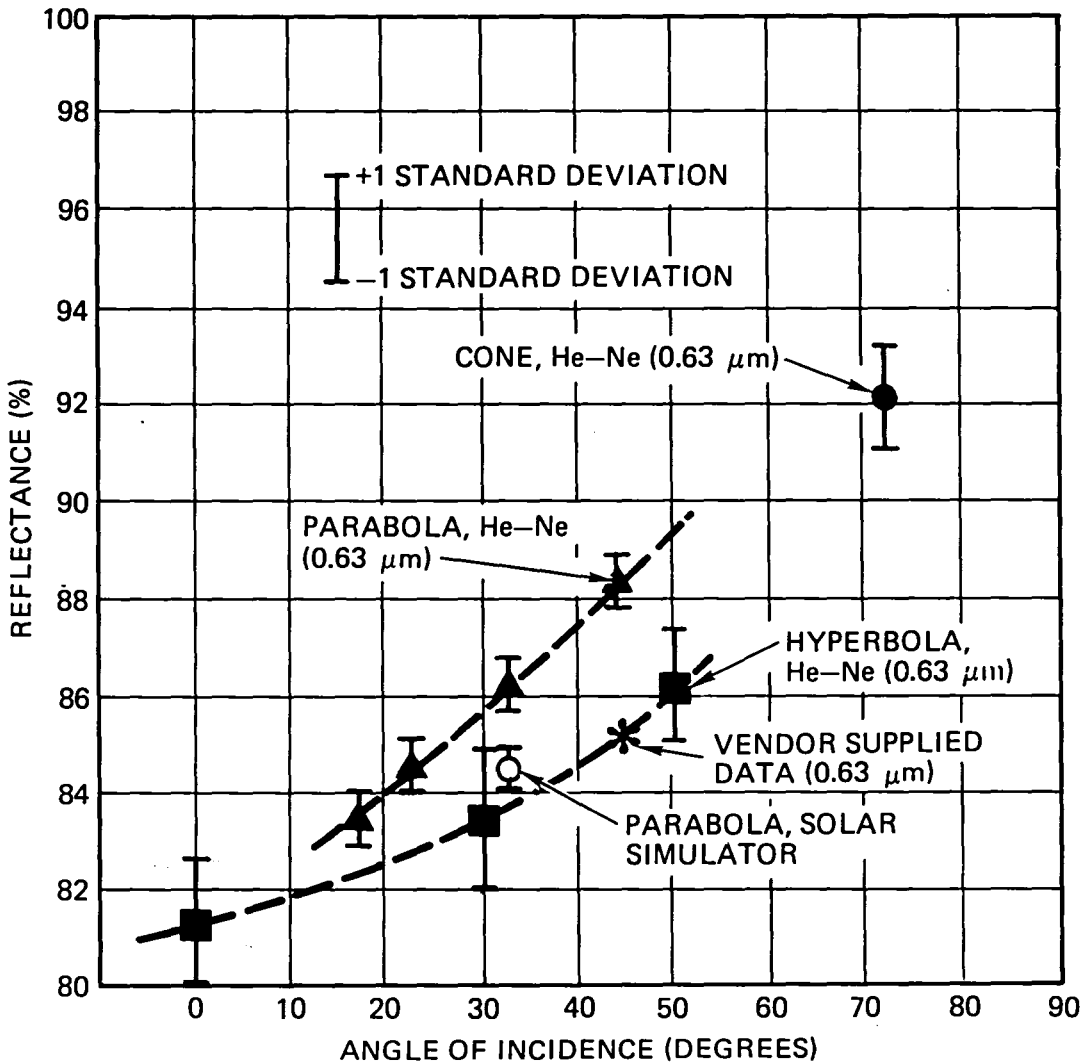

ALTERNATE REFLECTOR COATINGS

Reflectance can be improved by using an enhanced aluminum coating or a silver coating as shown (vendor-supplied data). Space experiments are planned for the high performance coatings to determine environmental stability.

ALTERNATE REFLECTOR COATINGS OFFER IMPROVED REFLECTANCE

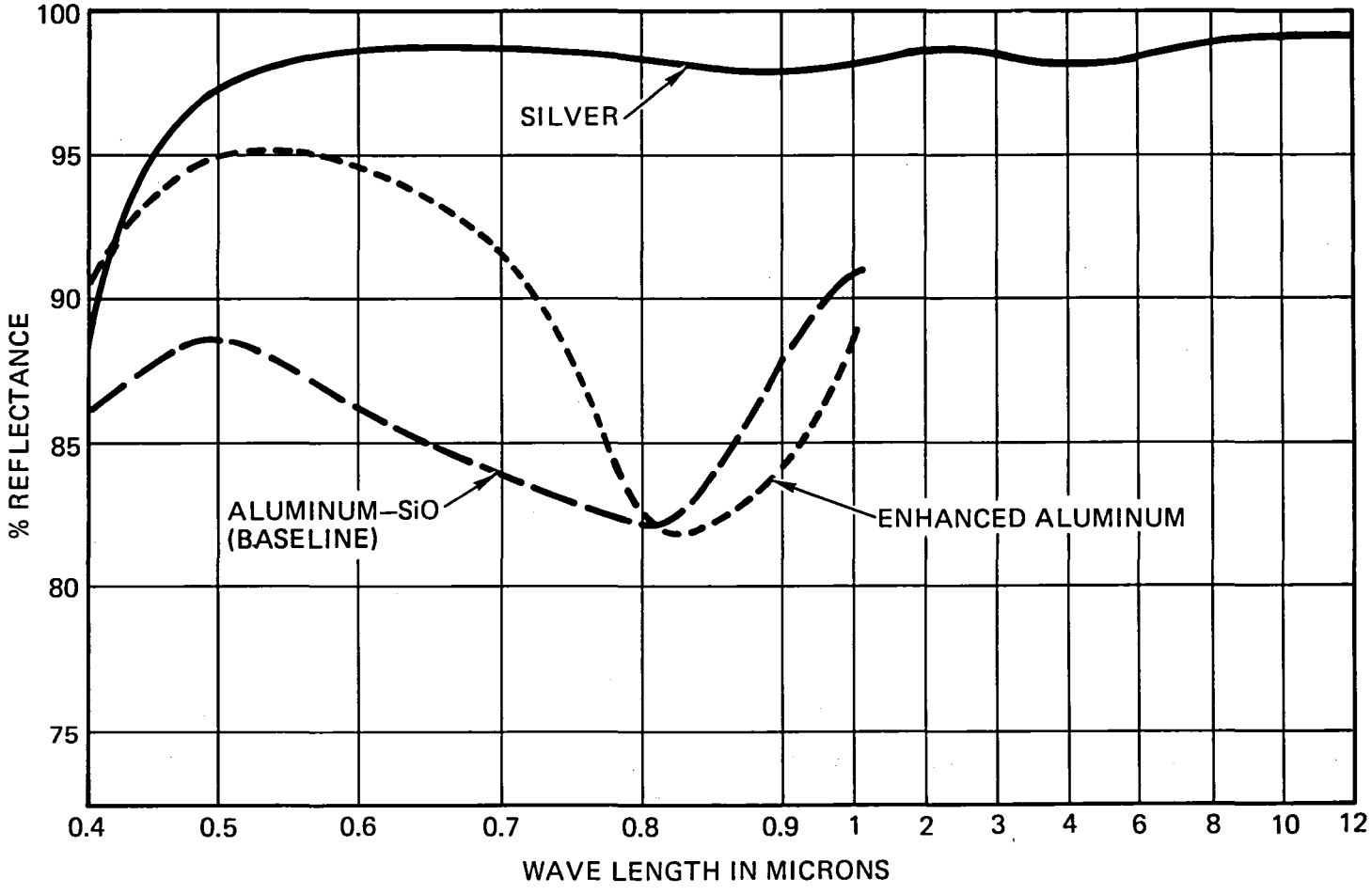

TEST SETUP FOR CELL MISALIGNMENT MEASUREMENTS

The test setup for cell misalignment measurements along the optical axis is shown. The angular sensitivity of the concentrator to incident radiation imposes stringent requirements on the degree of collimation of the light source. Conventional solar simulators are not sufficiently collimated for accurate characterization of the optical components. For this reason a He-Ne laser was used for the illumination source. A spatial filter was used to expand the laser beam and a collimating lens was used to redirect the divergent beam from the spatial filter as a collimated beam incident on the concentrator element. Maximum illumination intensity on the silicon photodiode was approximately 20 W/m^2.

The silicon photodiode was coupled to a LVDT (linear variable differential transformer). Using a micrometer adjustment, the photodiode could be translated along the axis of the optical system. The LVDT transformed Y translation of the photodiode into a proportional electrical signal which in turn was input to an X-Y recorder. A 4-millimeter diameter aperture was used to restrict measured illumination to that which would be incident on a 4-millimeter diameter active area solar cell. The output of the photodiode was input to the X-Y recorder. Results of the Y-axis translational measurements are presented on Page 4-11.

TEST SET-UP FOR CELL MISALIGNMENT MEASUREMENTS

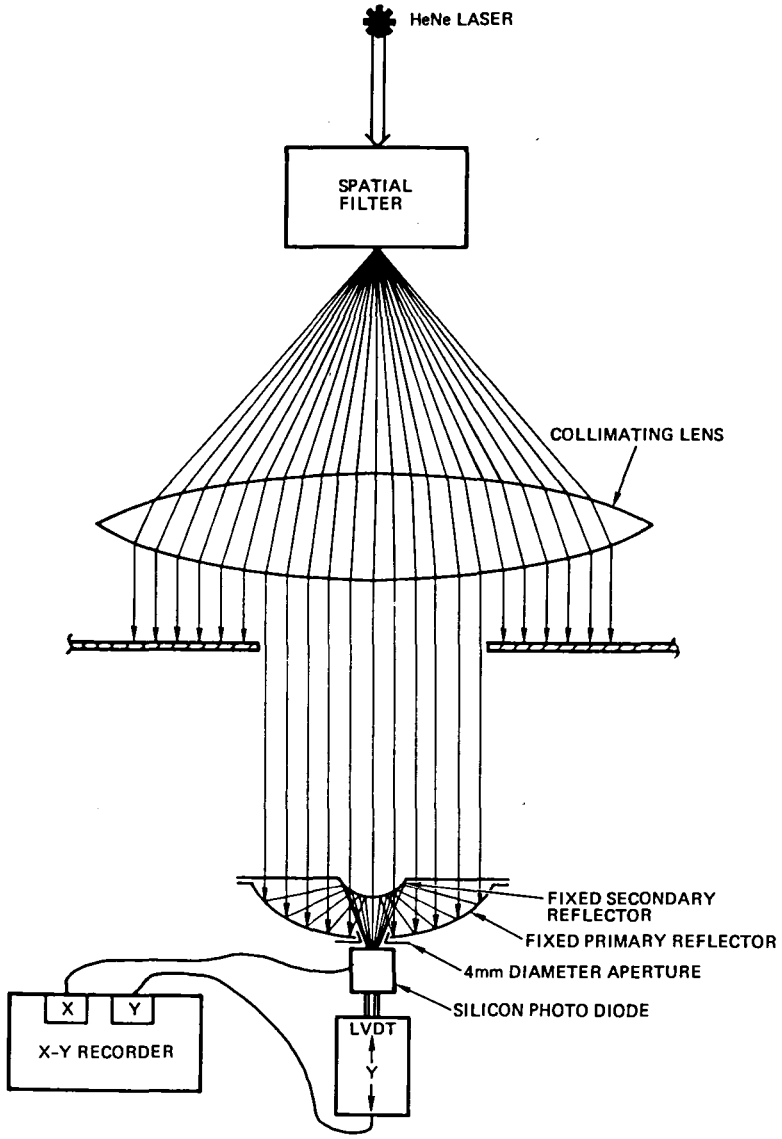

CELL MISALIGNMENT ALONG OPTICAL AXIS

The test setup for this data is shown on Page 4-9. The results indicate that the concentrator performance is relatively insensitive to cell location along the optical axis from the plane of the clearance hole in the center of the parabola to a position 0.025 in behind this plane. This result is as expected since the system is designed to have the cell operate between the hyperbola and the system focal point in the unfocused portion of the conical illumination beam. This result suggests that a cell stack tolerance of $\pm$0.1 millimeter can be permitted without having a significant effect on optical performance. Such a tolerance on cell stack assembly is readily achievable.

The misalignment testing has been performed with normal incident illumination and with one component misalignment at a time. The compound effects of multiple component misalignment and nonnormal incident illumination need to be investigated in order to more accurately define alignment tolerances for future hardware design.

OPTICAL SYSTEM PERFORMANCE RELATIVELY INSENSITIVE TO CELL MISALIGNMENT ALONG OPTICAL AXIS

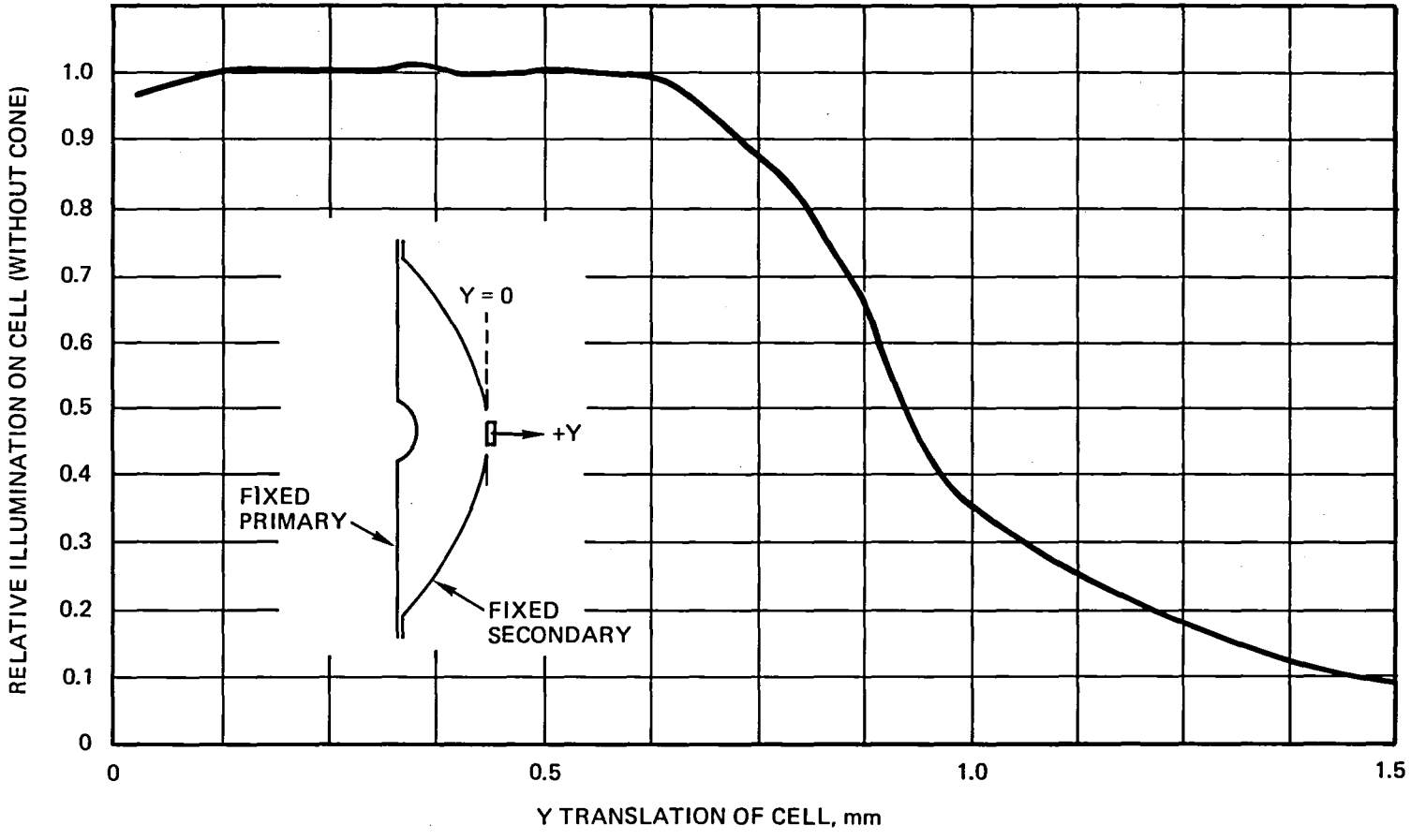

SECONDARY REFLECTOR TRANSLATIONAL MISALIGNMENT TEST SETUP

The test setup for determining the effect of secondary mirror misalignment on optical system performance is shown. A wire was bonded to the secondary mirror which coupled it to a LVDT (linear variable differential transformer). Using a micrometer adjustment, the secondary reflector could be translated in the entrance aperture plane of the optical system. The LVDT transformed X translation of the secondary reflector into a proportional electrical signal which in turn was input to an X-Y recorder. Illumination at the cell position was measured with a silicon photodiode. A 4-millimeter diameter aperture was used to restrict measured illumination to that which would be incident on a 4-millimeter diameter active area solar cell. The output of the photodiode was input to the X-Y recorder. Results of the secondary reflector X-axis translational measurements with and without the light catcher cone are presented on Pages 4-15 and 4-17, respectively.

SECONDARY REFLECTOR TRANSLATIONAL MISALIGNMENT MEASUREMENTS TEST SET-UP

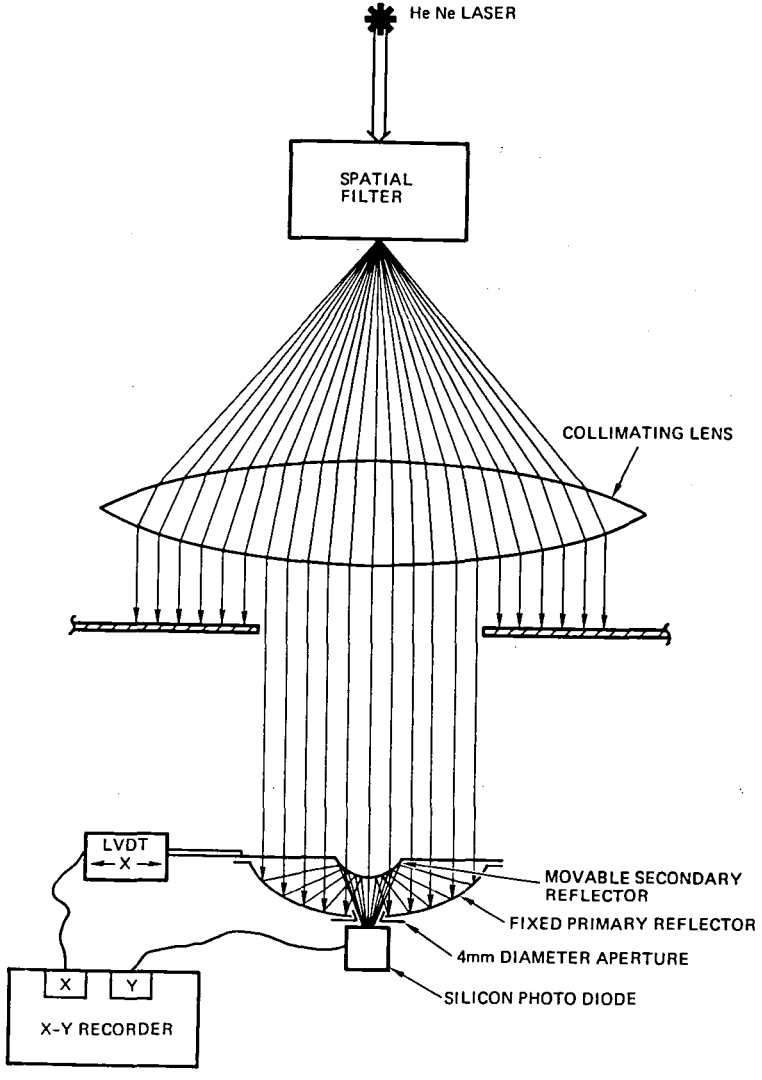

TRANSLATIONAL MISALIGNMENT OF SECONDARY REFLECTOR (WITH CONE)

The test setup for this data is shown on Page 4-13. The results indicate that with a light catcher cone the secondary reflector can be misaligned (in the plane of the entrance aperture) with respect to the primary reflector by as much as $\pm$0.020 inch without significant degradation of optical performance (approximately 3 percent). This data led to the present interference fit design of the single element assembly. An X-translation tolerance of $\pm$0.005 inch can be achieved using the interference fit design. Consequently, it is anticipated that optical alignment can be achieved by hardware design.

The misalignment testing has been performed with normal incident illumination and with one component misalignment at a time. The compound effects of multiple component misalignment and nonnormal incident illumination need to be investigated in order to more accurately define alignment tolerances for future hardwre design.

REFLECTIVE PERFORMANCE AS A FUNCTION OF SECONDARY REFLECTOR TRANSLATIONAL MISALIGNMENT (WITH CONE)

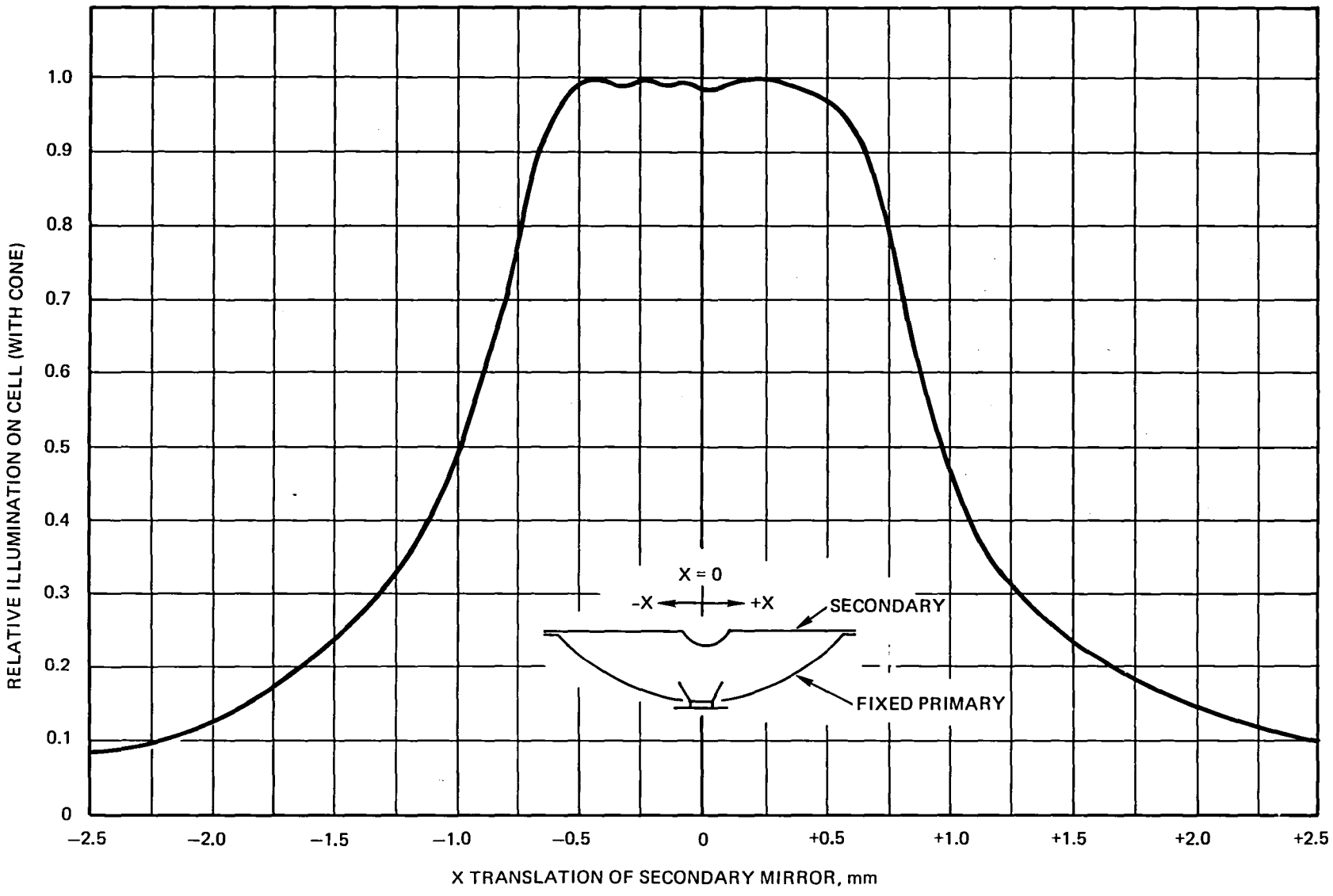

TRANSLATIONAL MISALIGNMENT OF SECONDARY REFLECTOR (WITHOUT CONE)

The test setup for this data is shown on Page 4-13. The results indicate that removing the light catcher cone reduces the allowable translational misalignment of the secondary reflector.

The misalignment testing has been performed with normal incident illumination and with one component misalignment at a time. The compound effects of multiple component misalignment and nonnormal incident illumnation need to be investigated in order to more accurately define alignment tolerances for future hardware design.

REFLECTIVE PERFORMANCE AS A FUNCTION OF SECONDARY REFLECTOR TRANSLATIONAL MISALIGNMENT (WITHOUT CONE)

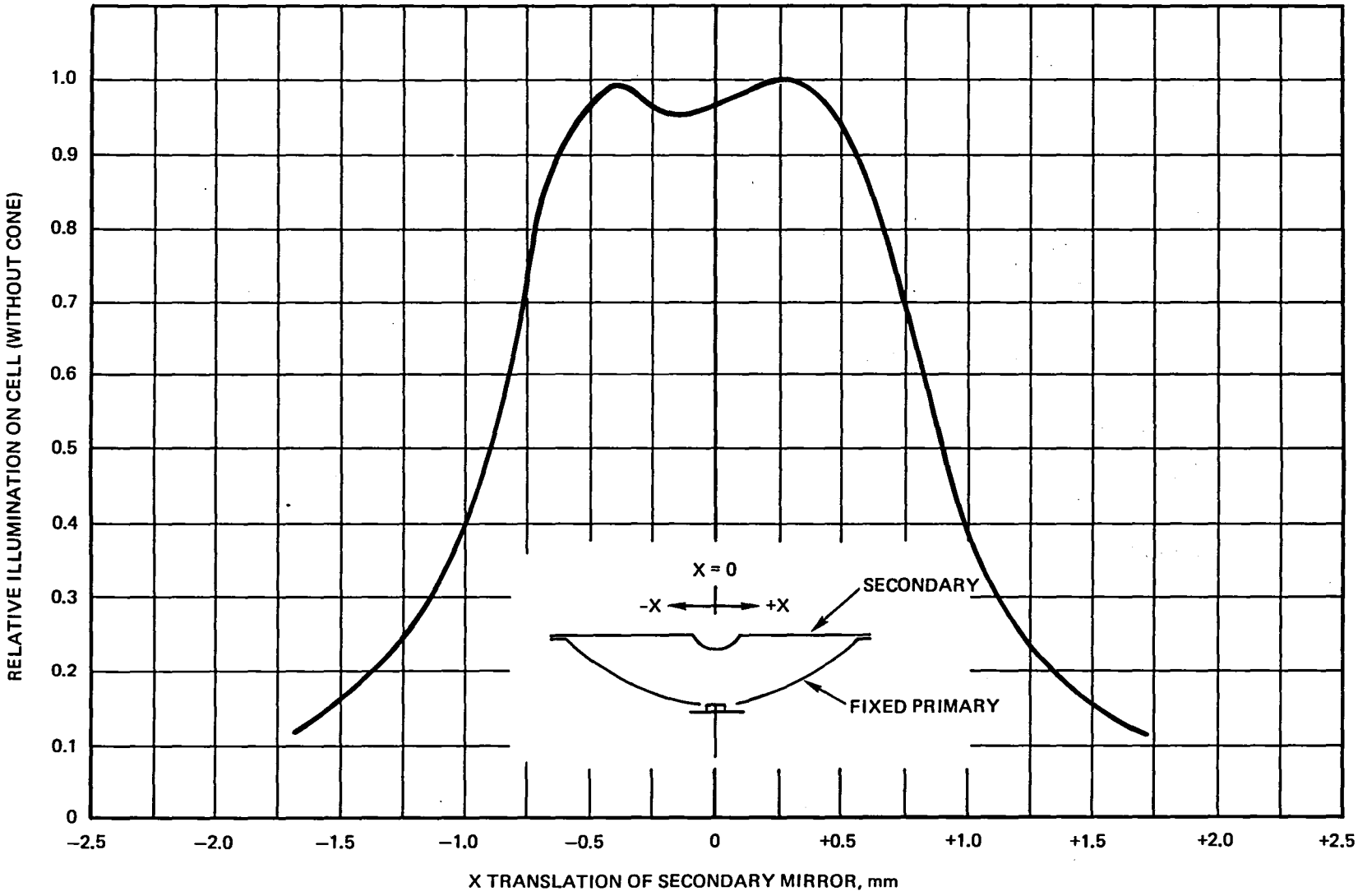

TEST SETUP FOR SECONDARY REFLECTOR MISALIGNMENT ALONG THE OPTICAL AXIS

The test setup for determining the effect of secondary reflector misalignment along the optical axis is shown. The light source is identical to that described on Page 4-8. A target was attached to the secondary reflector. A microscope was coupled to a LVDT (linear variable differential transformer). Using a micrometer adjustment, the secondary reflector was moved along the optical axis. The microscope was used to sight the target on the secondary reflector. The LVDT transformed Y translation of the secondary reflector into a proportional electrical signal which was in turn input to an X-Y recorder. Results of the secondary reflector Y-axis translational measurements are presented on Page 4-21.

TEST SET-UP FOR SECONDARY REFLECTOR MISALIGNMENT ALONG OPTICAL AXIS

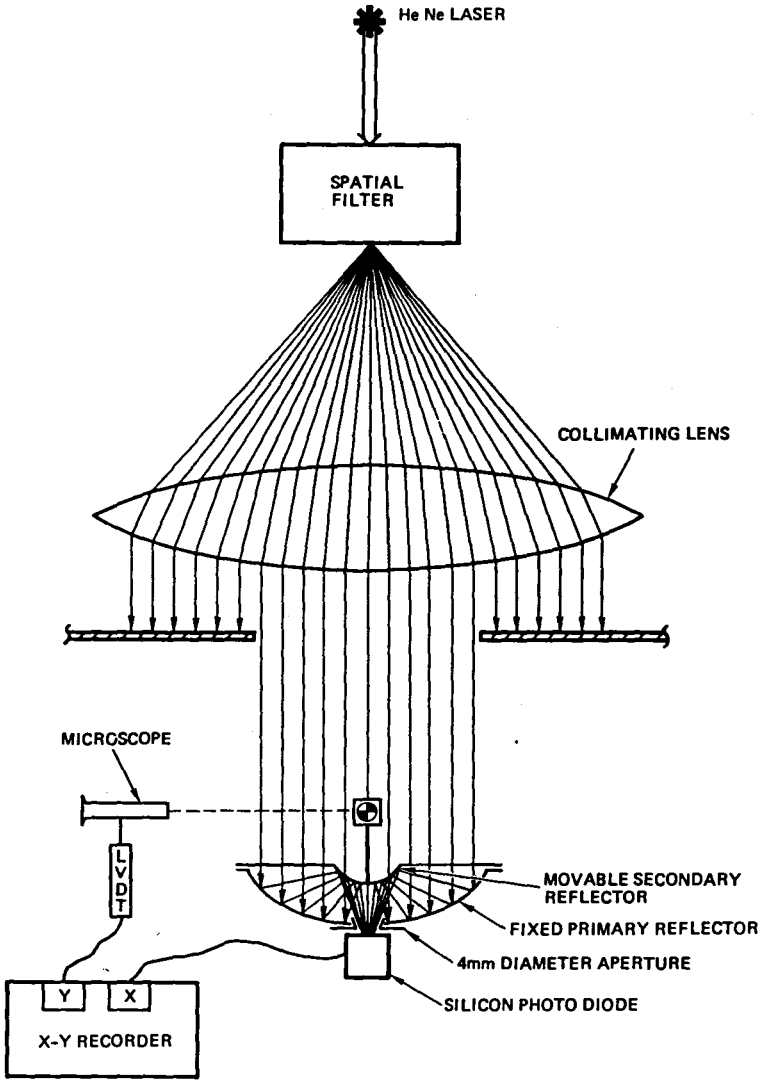

SECONDARY REFLECTOR MISALIGNMENT ALONG THE OPTICAL AXIS

The test setup for this data is shown on Page 3-2. The results show that performance falls off as the secondary reflector is moved toward the primary reflector and is relatively constant as the secondary reflector is moved away from the primary reflector. The reason for this is that light rays converge from the primary reflctor to the secondary reflector. As the secondary reflector moves closer to the primary reflector the light beam cross section increases and the outer rays in the beam miss the secondary reflector. As the secondary reflector moves away from the primary reflector the light beam cross section decreases and all rays in the beam continue to hit the secondary reflector.

The misalignment testing has been performed with normal incident illumination and with one component misalignment at a time. The compound effects of multiple component misalignment and nonnormal incident illumination need to be investigated in order to more accurately define alignment tolerances for future hardware design.

SECONDARY REFLECTOR MISALIGNMENT ALONG OPTICAL AXIS

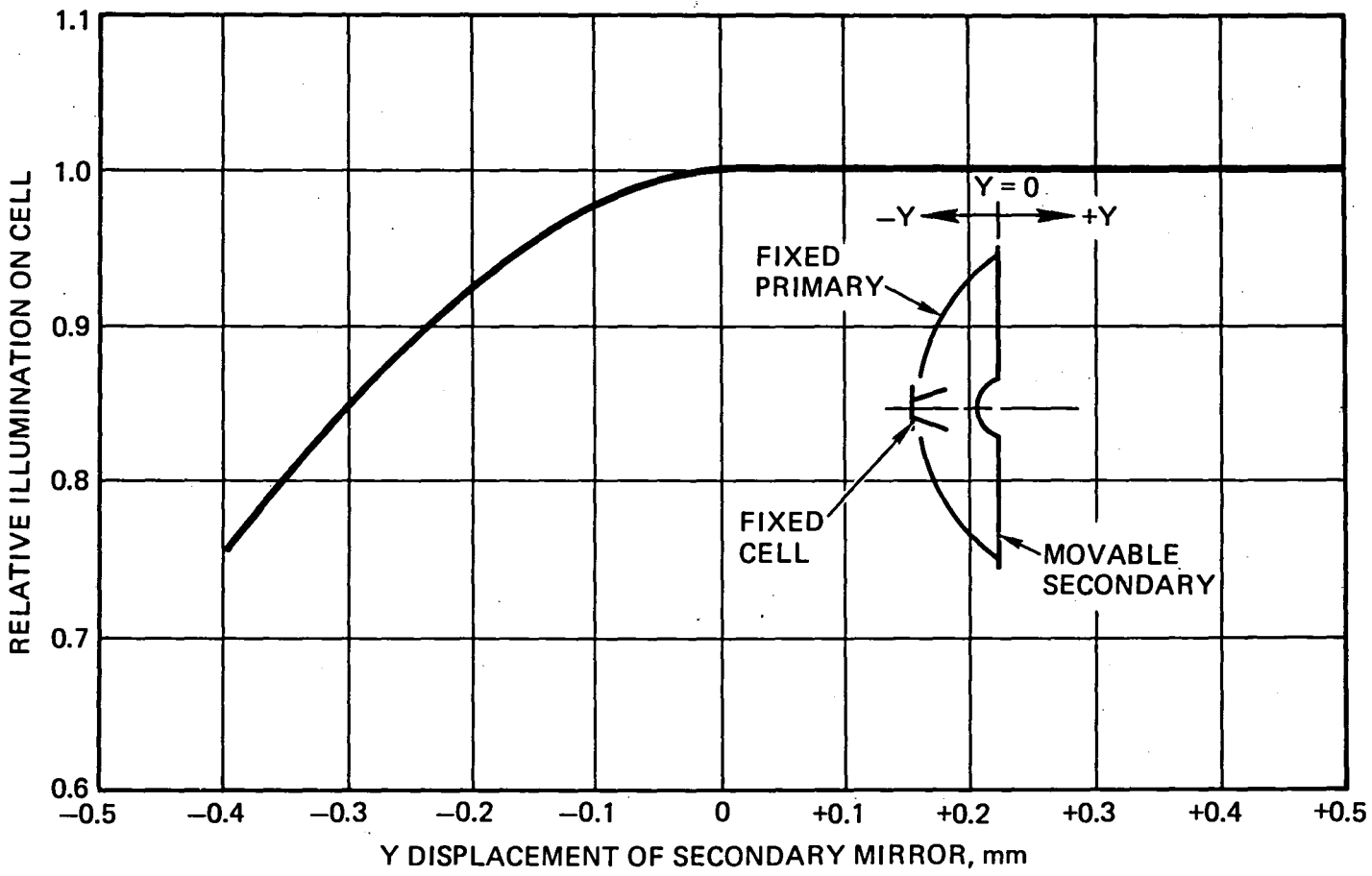

ELECTRICAL PERFORMANCE DATA FOR EACH ELEMENT AT NORMAL INCIDENCE

Element performance without concentration (mirrors removed and light catcher cone baffled) was determined for each of the nine elements in the demonstration module using a solar simulator. This data is presented in Column 2. The nine element demonstration module was tested at the Table Mountain Observatory (JPL/NASA facility) in Wrightwood, California, using a motorized solar tracker to determine element performance with concentration. Natural sunlight provides an excellent light source consistent with the concentrator imposed requirement of high collimated illumination. A standard cell was placed at the bottom of a tube so that its view factor was similar to that of a concentrator cell in an element. This was done to neutralize the effect of diffuse illumination on the standard cell since the concentrator element "sees" very little diffuse illumination (light entering concentrator at off-axis angles greater than 4 degrees does not reach the concentrator cell). Column 3 presents element performance (with reflectors) corrected to 135 mW/cm^2 illumination intensity. The effective concentrator ratio for each element is presented in Column 4. Optical efficiency for each element which is the ratio of effective concentration ratio to geometric concentration ratio (times 100 percent) is presented in Column 5. Optical efficiency is the ratio of illumination reaching the concentrator solar cell to that which enters the entrance aperture of the concentrator element. Factors which influence optical efficiency are presented on Page 4-25.

ELECTRICAL PERFORMANCE DATA FOR EACH ELEMENT AT NORMAL INCIDENCE

①	②	③	④	⑤
ELEMENT NUMBER	CELL I_{SC} AT 135 mW/cm^2 WITHOUT CONCENTRATION (mA)	ELEMENT I_{SC} CORRECTED FOR INTENSITY (135 mW/cm^2) WITH CONCENTRATION (mA)	EFFECTIVE CONCENTRATION RATIO ③ ÷ ②	OPTICAL EFFICIENCY ④ ÷ 163* x 100%
1	3.4	305	90	55
2	3.4	309	91	56
3	3.5	311	89	55
4	3.6	335	93	57
5	3.2	289	90	55
6	3.6	314	87	53
7	3.6	317	88	54
8	3.5	308	88	54
9	3.6	313	87	53
$\bar{X}$	3.5	311	89 (132)	55 (.81)
S	0.14	12	1.98	1.2
$S/\bar{X} \cdot 100\%$	3.9%	3.8%	2.2%	2.2%

*163 = GEOMETRIC CONCENTRATION RATIO

DEMONSTRATION MODULE OPTICAL EFFICIENCY BREAKDOWN

Factors which influence optical system efficiency are presented. The computed optical efficiency of 0.56 (product of individual measured factors) is in good agreement with the system measurement of 0.55 presented on Page 4-23. Future development hardware will improve on optical system efficiency. Changing to silver reflectors will increase primary and secondary reflectance to 0.95. Secondary support blockage can be reduced to 4 percent. With these changes, it is projected that optical system efficiency can be increased up to 0.81.

DEMONSTRATION MODULE OPTICAL EFFICIENCY BREAKDOWN

ELEMENT/PARAMETER	MEASURED VALUE	OPTICAL TRANSMISSION FACTOR
PRIMARY REFLECTOR REFLECTANCE	0.84	$F_1 = 0.84$
SECONDARY REFLECTOR REFLECTANCE	0.84	$F_2 = 0.84$
SECONDARY REFLECTOR BLOCKAGE	6%	$F_3 = 0.80$
SECONDARY REFLECTOR SUPPORT BLOCKAGE	14%	

COMPUTED OPTICAL EFFICIENCY = $F_1 \times F_2 \times F_3 = 0.56$

PRELIMINARY OFF-POINTING TEST RESULTS

A single element and the nine element demonstration module were tested at the Table Mountain Observatory (JPL/NASA facility) in Wrightwood, California, using a motorized solar tracker to determine off-axis performance. Results of this test are presented and show that although the cone improves off-axis performance over that predicted without a cone, the total predicted effectiveness of the cone has not been achieved. Improved methods for measuring off-axis performance are being developed at TRW. Additional testing and analysis are required to reconcile differences between predicted and measured off-axis performance.

PRELIMINARY OFF-POINTING TEST RESULTS FOR SINGLE ELEMENT AND NINE-ELEMENT MODULE

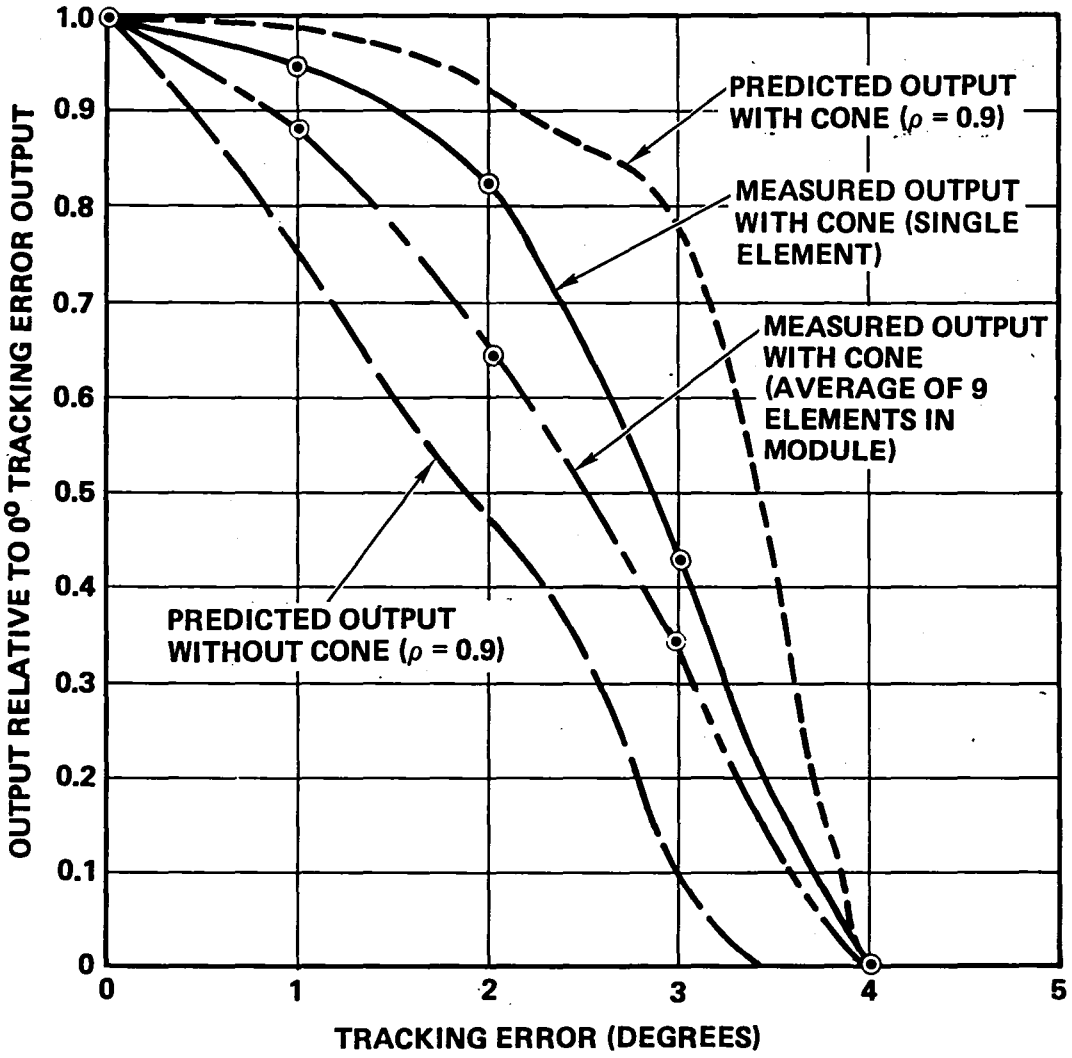

- ADDITIONAL TESTING IS REQUIRED TO RECONCILE DIFFERENCES BETWEEN PREDICTED AND MEASURED PERFORMANCE

THERMAL VACUUM TEST AND ANALYSIS

A thermal vacuum test was performed on a single concentrator element to verify experimentally the thermal performance of the miniaturized Cassegrainian concentrator concept. The element design corresponds to that shown on Page 3-3. The thermal vacuum test provided temperature distribution data corresponding to selected values of absorbed heat flux on the cell. The resulting temperature distributions, computed areas, and estimated emittances and view factors were then used to calculate net radiant heat flow rates from various locations on the element to the surrounding heat sink shroud. Reasonable adjustments were made to the estimated emittances and view factors until a single set of parameters was found that provided an overall best heat balance for all five runs that were performed. Each run had a different input heating rate, and one run had a widely different shroud temperature. With the itemized heat balance of the tested configuration "calibrated," other configurations that could not be readily examined experimentally were considered analytically by two separate representations, a three-node model and a multinode model (up to 18 nodes).

THERMAL TEST AND ANALYSIS VERIFY INITIAL THERMAL PREDICTIONS

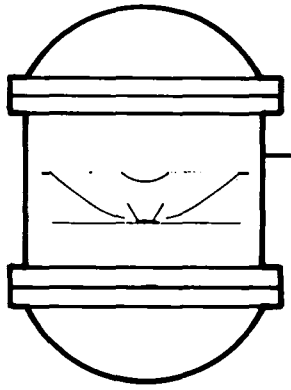

THERMAL VACUUM TEST

RUN NO.	Q_{in}	NODE 1	NODE 16
1	Q_1	T_{11}	T_{116}
2	Q_2	T_{21}	T_{216}
3	Q_3	T_{31}	T_{316}
4	Q_4	T_{41}	T_{416}
5	Q_5	T_{51}	T_{516}

NODAL TEMPERATURE DISTRIBUTIONS FOR DIFFERENT HEAT INPUTS

$Q_{in} = Q_{out}$ TO "CALIBRATE" THERMAL RESISTANCES

THREE NODE MODEL

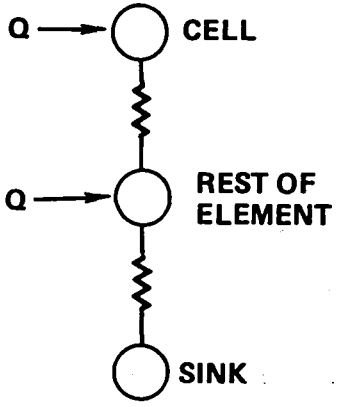

THREE-NODE MODEL DEVELOPED BASED ON ANALYSIS OF TEMPERATURE DISTRIBUTION DATA

SPACE PREDICTIONS

SPECIFY ELEMENT DESIGN PARAMETERS

THREE NODE MODEL

The closed-form three node representation is considered to be a useful tool for preliminary parametric trade-off studies. A diagram of the three node analytical representation of the tested solar concentrator configuration is shown. The thermal resistance (R = 9.6°C/W) was selected to produce a minimum root-mean-squared difference between the measured cell temperatures and those computed by the indicated equation for cell temperature.

The following computation illustrates how the above equation can be used to compute cell temperature for a specific design. Design assumptions for an improved element design (higher optical efficiency than for demonstration hardware) are presented on Page 4-33. The sum of the radiative factors ($\Sigma\mathcal{F}A$) is calculated to be 28.8 cm^2 as shown on Page 4-35. The heat input calculations are shown on Page 4-37 with Q_{in} equal to 1.784 watts and Q_{cell} equal to 1.380 watts. The cell temperature is computed to be 63°C using calculated values for $\Sigma\mathcal{F}A$ from Page 4-35 and for Q_{in} and Q_{cell} from Page 4-37. This temperature corresponds to a geosynchronous orbit as it does not include the effects of earth emission or albedo. The corresponding average temperature for a 235 nautical mile orbit would be approximately 87°C using the three node representation. For comparison, a cell temperature of 85°C was calculated using the 18 node model.

THREE NODE MODEL DEVELOPED FOR PERFORMING PRELIMINARY DESIGN TRADE STUDIES

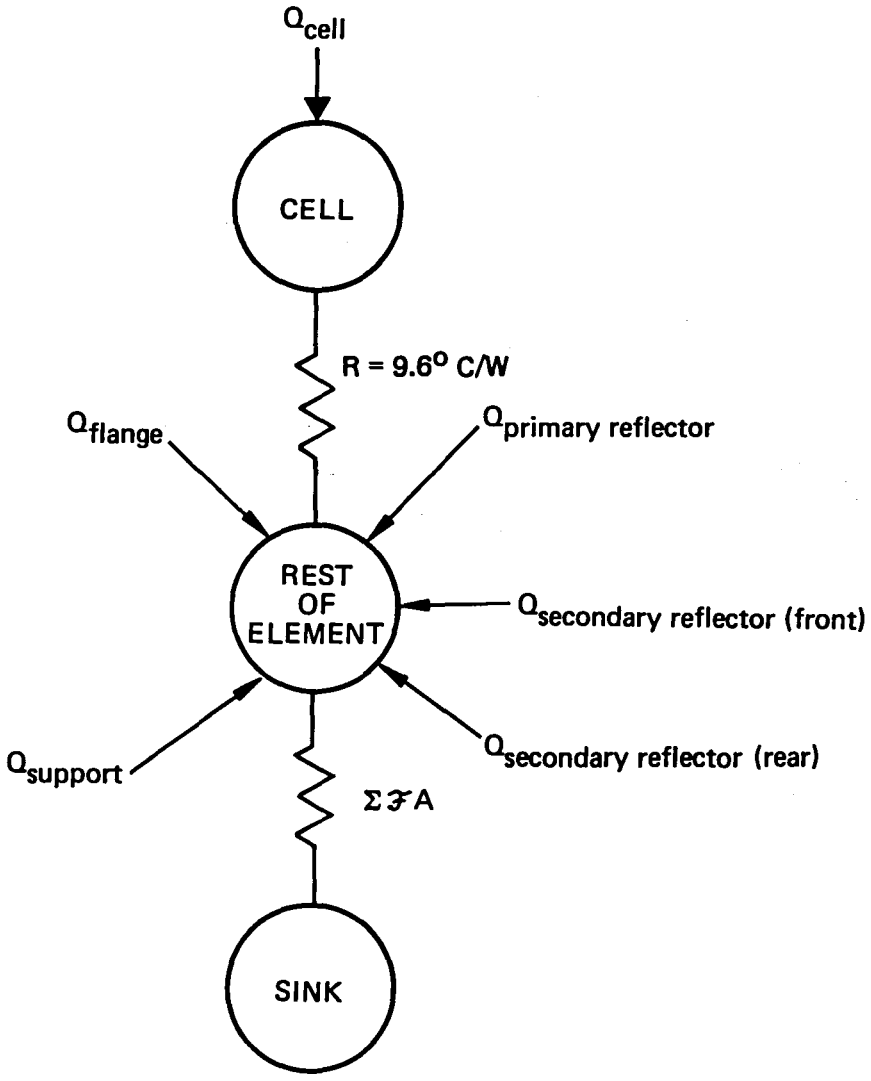

$$T_{cell} \approx \left[\frac{Q_{in}}{\sigma \Sigma \mathcal{F} A} + T^4_{sink}\right]^{1/4} + R\, Q_{Cell}$$

T_{cell} AND T_{sink} ARE ABSOLUTE TEMPERATURES

σ = STEFAN – BOLTZMAN CONSTANT

Q_{in} = SUM OF ALL HEAT INPUTS

Q_{cell} = HEAT INPUT TO THE CELL

$\Sigma \mathcal{F} A$ = SUM OF ALL RADIATION FACTORS

ASSUMPTIONS FOR THERMAL CALCULATIONS

These are the assumptions which were the basis for the three node calculations on Page 4-30 and for the multinode calculation which was made to support the 100-kilowatt array performance prediction summarized on Page 6-103. The assumptions are based on using GaAs solar cells (20 percent efficient at operating temperature) and silver coatings (95 percent reflectance).

ASSUMPTIONS FOR THERMAL CALCULATIONS FOR IMPROVED DESIGN

PARAMETER	SYMBOL	VALUE
INCIDENT SOLAR FLUX	S	0.135 W/cm^2
REFLECTOR ABSORPTANCE	α_r	0.05
CELL EFFICIENCY (AT OPERATING TEMPERATURE)	η	20%
CELL ABSORPTANCE	α_c	0.80
SECONDARY REFLECTOR BLOCKAGE	B_p	0.06
SECONDARY SUPPORT BLOCKAGE	B_s	0.05
FLANGE ABSORPTANCE	α_f	0.20
REFLECTOR BACKSIDE ABSORPTANCE	α_b	0.20
SECONDARY SUPPORT ABSORPTANCE	α_s	0.20
APERTURE AREA	A_a	21.23 cm^2

THERMAL RADIATION FACTOR CALCULATION

This shows some intermediate results using the three node model calculation described on Pages 4-30 and 4-31. The table also defines the areas and assumed radiometric properties of the components that make up a single concentrator element.

THERMAL RADIATION FACTOR CALCULATION FOR IMPROVED DESIGN

EMITTANCE SURFACE	AREA A		HEMISPHERICAL EMITTANCE ϵ_H	VIEW FACTOR F	$A\epsilon_H F = A\mathcal{F}$
	cm^2	SYMBOL			(cm^2)
CONE, OUTSIDE	1.143	A_{ci}	0.88	0.9	0.90
CONE, INSIDE	1.168	A_{co}	0.02	0.9	0.02
CELL/PAD	0.659	A_c	0.70	0.7	0.32
RADIATOR	21.23	A_r	0.88	1.0	18.68
HEXAGONAL FLANGE (REAR)	3.40	A_f	0.88	1.0	2.99
PRIMARY REFLECTOR	19.99	A_p	0.02	0.9	0.36
HEXAGONAL FLANGE (FRONT)	3.40	A_f	0.85	1.0	2.89
SECONDARY SUPPORT (FRONT)	1.06	A_s	0.85	1.0	0.90
SECONDARY SUPPORT (REAR)	1.06	A_s	0.20	0.9	0.19
SEC. REFLECTOR (FRONT)	1.27	A_{sm}	0.85	1.0	1.08
SEC. REFLECTOR (REAR)	1.27	A_{sm}	0.02	0.9	0.02
MISC EDGES	1.00	A_m	0.5	0.9	0.45
					$\Sigma = 28.8$

HEAT INPUT CALCULATION

This shows some intermediate results using the three node model described on Pages 4-30 and 4-31.

HEAT INPUT CALCULATION FOR IMPROVED DESIGN

HEAT INPUT	SYMBOL	RELATIONSHIP	VALUE (W)
HEXAGONAL FLANGE	Q_f	$S A_f \alpha_f$	0.091
SECONDARY SUPPORT	Q_s	$S A_s \alpha_s$	0.028
SECONDARY REFLECTOR (REAR)	Q_{srr}	$S A_{sm} \alpha_b$	0.034
PRIMARY REFLECTOR	Q_{pr}	$S A_a (1-B_p-B_s) \alpha_r$	0.128
SECONDARY REFLECTOR (FRONT)	Q_{srf}	$S A_a (1-B_p-B_s)(1-\alpha_r) \alpha_r$	0.122
CELL	Q_{cell}	$S A_a (1-B_p-B_s)(1-\alpha_r)(1-\alpha_r)(\alpha_c-\eta)$	1.380
TOTAL INPUT	Q_{in}	$Q_f + Q_s + Q_{srr} + Q_p + Q_{srf} + Q_{cell}$	1.784

CELL TEMPERATURE OF IMPROVED DESIGN USING THREE NODE MODEL

The three node model described on Page 4-30 was used to generate the parametric data presented on the facing page. Assumptions, radiation factors, and heat input calculations are the same as those presented on Pages 4-33, 4-35, and 4-37, respectively, with the exception that variable heat absorptance and cell efficiency were to generate the parametric data. For comparison, a data cell temperature of 85°C was calculated using the 18 node model for a cell net heat absorptance of 0.6 which is in good agreement with the 87°C cell temperature calculated with the three node model.

MAXIMUM OPERATING CELL TEMPERATURE OF IMPROVED DESIGN USING THREE-NODE MODEL

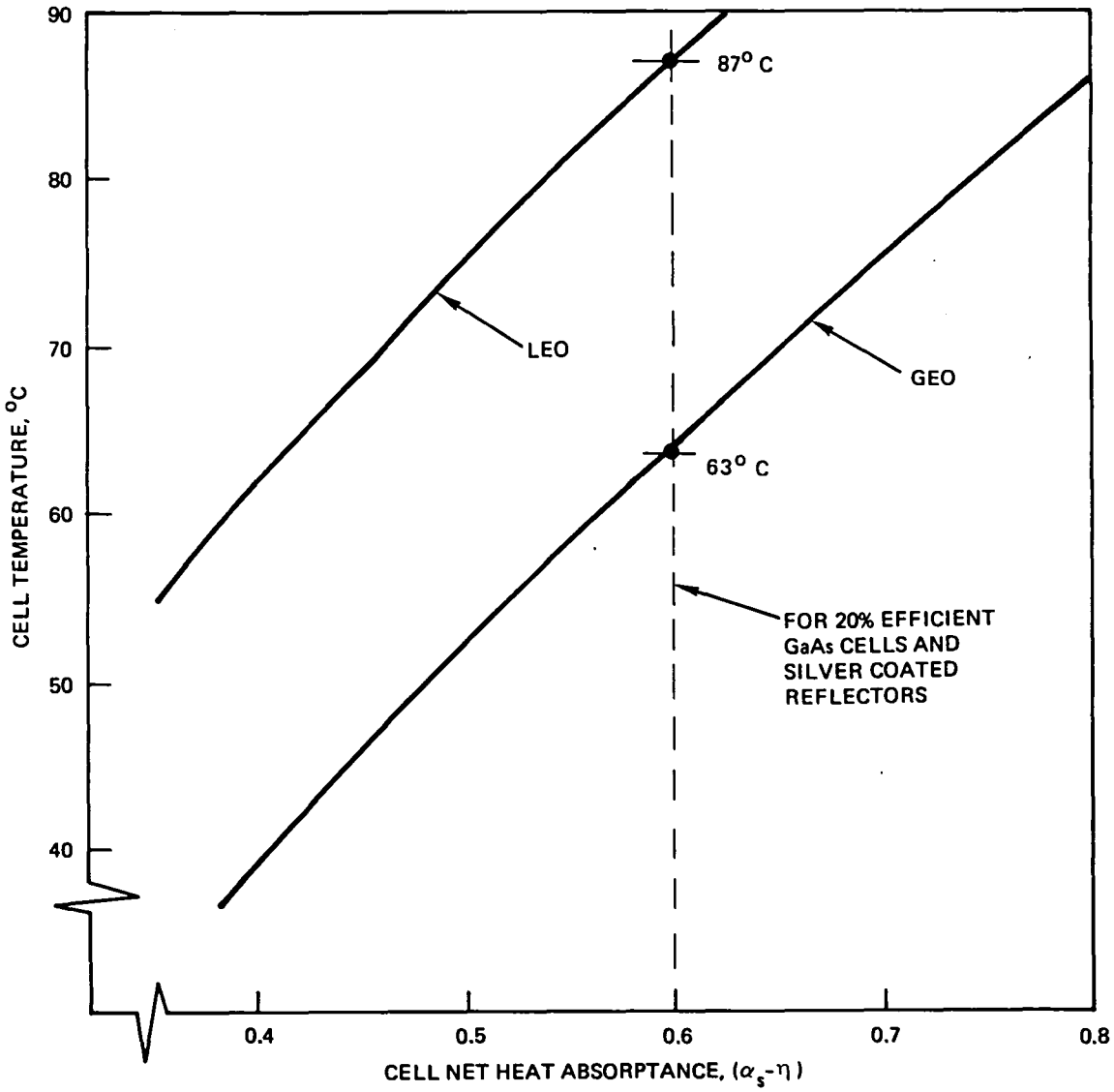

TRW

Element and Module Design Studies

- Packing Density
- Cell Stack Electrical Configuration
- Coverglass Location
- Reflector Material/Configuration

PACKING DENSITY STUDY SUMMARY

The performance of the concentrator solar array concept is a function of the packing efficiency obtained when individual elements are arranged into panels. A trade study was performed to determine the interaction of area, power output, and weight for two geometrical arrangements of elements: square and hexagonal. Details of the packing density study are presented on Pages 5-4 through 5-11.

Results of the packing density study indicate that untruncated hexagonal close packing maximizes W/kg performance and minimizes element cost per unit power output. For this reason it was selected as the baseline packing approach for the array system design study presented in Section 6. The performance prediction presented on Page 6-103 is based on untruncated hexagonal close packing.

PACKING DENSITY STUDY SUMMARY

OBJECTIVE: SELECT A BASELINE PACKING GEOMETRY WHICH MINIMIZES $/W AND MAXIMIZES PERFORMANCE (W/kg AND W/m^2)

APPROACH: DETERMINE THE INTERACTION OF AREA, POWER OUTPUT, WEIGHT, AND COST FOR HEXAGONAL AND SQUARE PACKING OF CONCENTRATOR ELEMENTS AS A FUNCTION OF ELEMENT TRUNCATION

RESULTS: UNTRUNCATED HEXAGONAL CLOSE PACKING SELECTED AS BASELINE APPROACH BECAUSE IT MAXIMIZES W/kg PERFORMANCE AND MINIMIZES ELEMENT COST PER UNIT POWER OUTPUT. W/kg AND W/m^2 CANNOT BE MAXIMIZED SIMULTANEOUSLY SINCE TRUNCATION BOTH DEGRADES W/kg PERFORMANCE AND IMPROVES W/m^2 PERFORMANCE

PACKING APPROACHES

The configuration of the individual optical elements was varied from untruncated to fully truncated for each geometry in which the primary mirror aperture is either hexagonal or square as shown. In this figure the element width is a measure of truncation. A 52.5-millimeter wide element corresponds to an untruncated element whereas a 37.5-millimeter wide element corresponds to a fully truncated square and a 45.5-millimeter wide element corresponds to a fully truncated hexagonal element.

PACKING APPROACHES

HEXAGONAL PACKING OF CONCENTRATOR ELEMENTS WITH ELEMENT WIDTH INDICATED

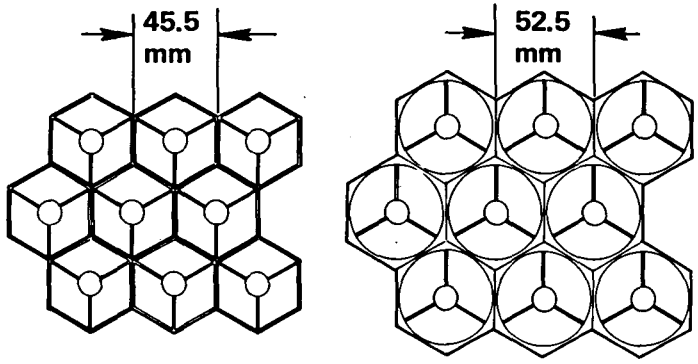

FULLY TRUNCATED NO TRUNCATION

SQUARE PACKING OF CONCENTRATOR ELEMENTS WITH ELEMENT WIDTH INDICATED

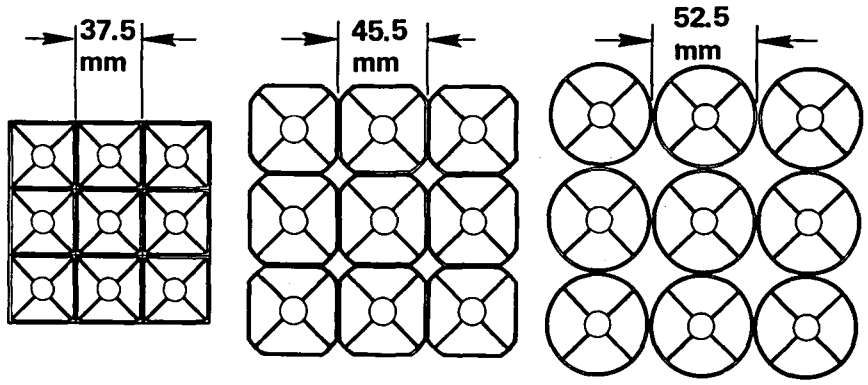

FULLY TRUNCATED PARTIALLY TRUNCATED NO TRUNCATION

PACKING FACTOR AS A FUNCTION OF ELEMENT WIDTH

For planar arrays, the packing factor is defined as the ratio of the sum of all solar cell areas to the corresponding gross substrate area. For concentrator arrays, the packing factor is defined as the ratio of the sum of all primary mirror aperture areas to the corresponding gross panel/frame area. Packing factor is seen to increase for both geometries as element truncation is increased (element width reduced).

PACKING FACTOR AS A FUNCTION OF ELEMENT WIDTH

TRUNCATION IMPROVES ELEMENT PACKING FACTOR

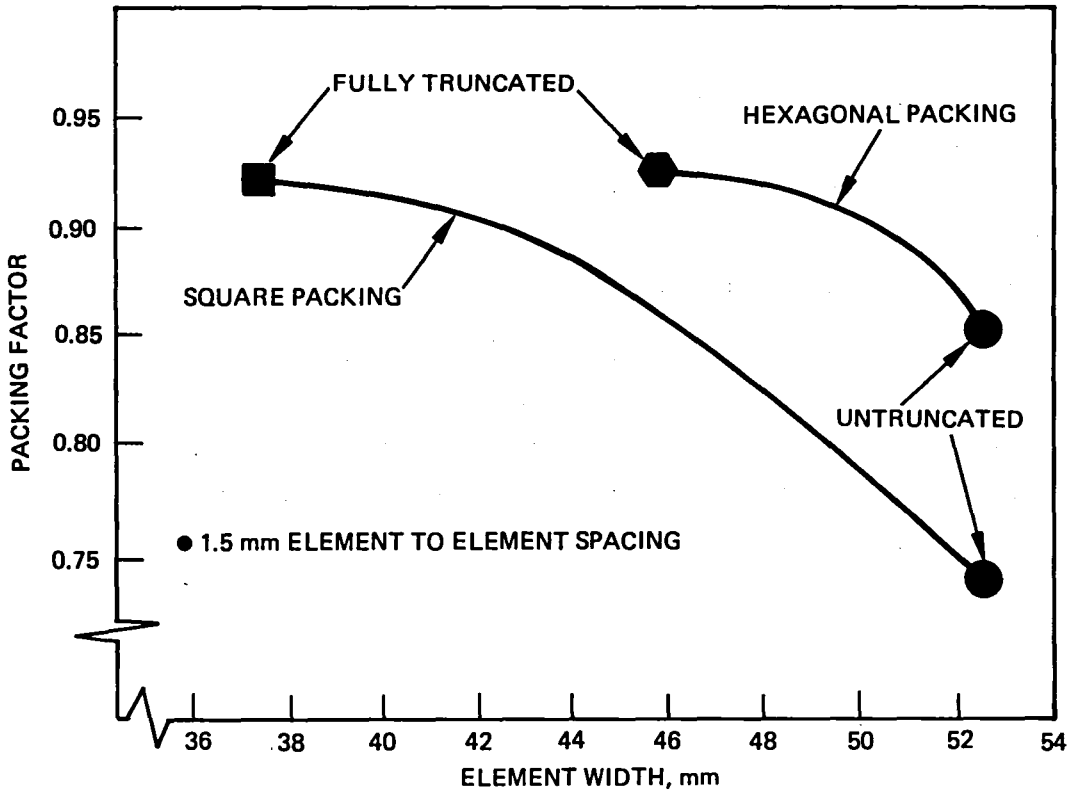

SPECIFIC PERFORMANCE AS A FUNCTION OF ELEMENT WIDTH

The mass of the concentrator element is distributed with a large fraction located centrally about each element's optical axis. Therefore, truncation does not reduce the element's weight as rapidly as element area and mirror aperture area decrease, and the maximum W/kg and minimum kg/m^2 performance is achieved with elements at or near untruncated dimensions.

Packing factor does not optimize at the same element width as the specific performance factor. This allows the concentrator array designer to determine which requirement (weight or area) drives his design, and trade weight for area, or vice versa, to optimize his design (e.g., 10 percent reduction in array weight by increasing array area by 7 percent or vice versa.

SPECIFIC PERFORMANCE AS A FUNCTION OF ELEMENT WIDTH

TRUNCATION DEGRADES SPECIFIC PERFORMANCE

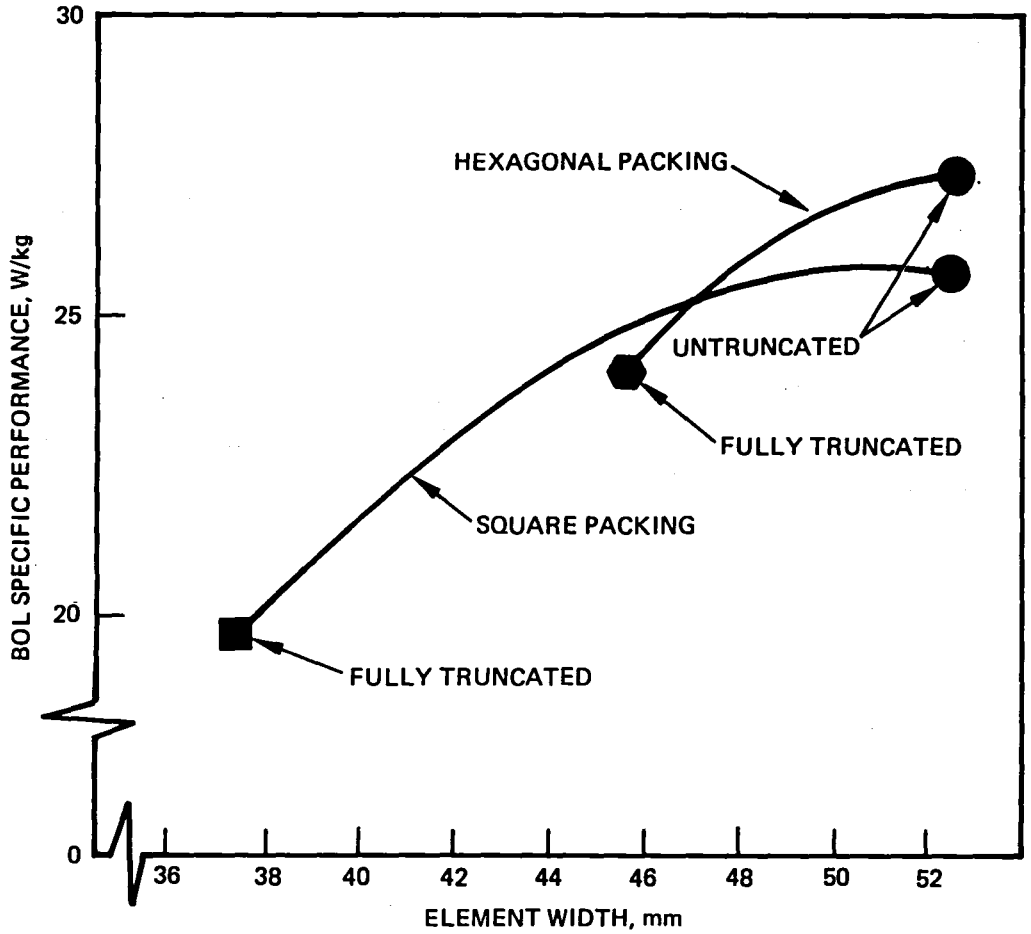

RELATIVE ELEMENT COST/UNIT POWER AS A FUNCTION OF ELEMENT WIDTH

Element truncation reduces primary reflector area and thereby reduces element output. Therefore, truncation increases the number of elements required relative to untruncated elements for the same power requirement. Assuming comparable truncated and untruncated element unit cost, relative element cost per unit power output increases with truncation.

RELATIVE ELEMENT COST/UNIT POWER AS A FUNCTION OF ELEMENT WIDTH

TRW

TRUNCATION INCREASES ELEMENT COST PER UNIT POWER OUTPUT

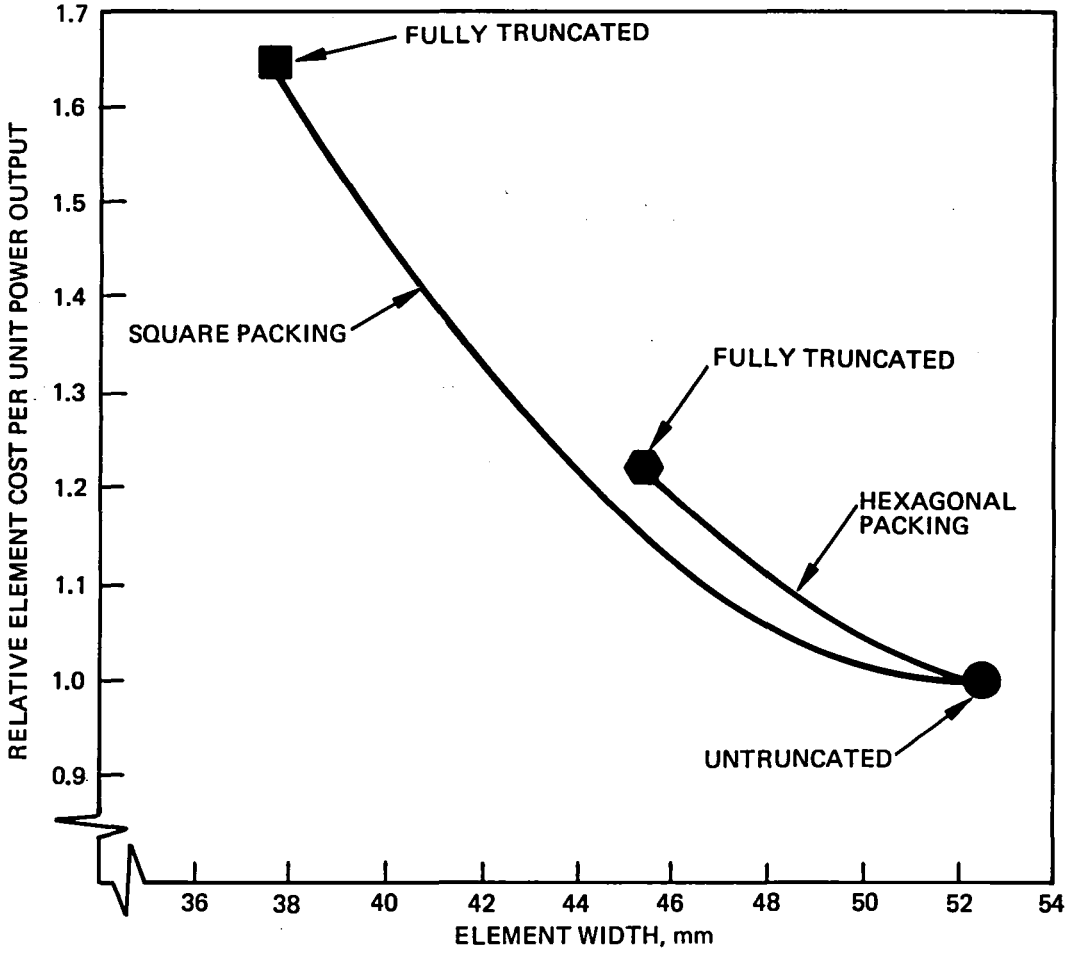

ELEMENT ELECTRICAL DESIGN

The solar cells in the miniconcentrator array are electrically connected in parallel and series in the same fashion as on a planar array. Three different approaches for making series connections are shown. These approaches are discussed on Pages 5-14 and 5-15.

ELECTRICAL DESIGN

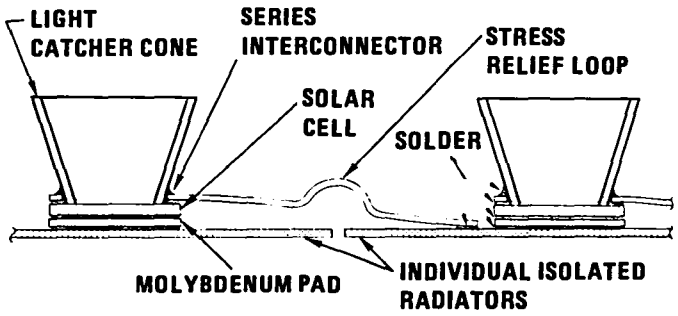

BASELINE DESIGN REQUIRES ELECTRICAL ISOLATION OF EACH ELEMENT RADIATOR

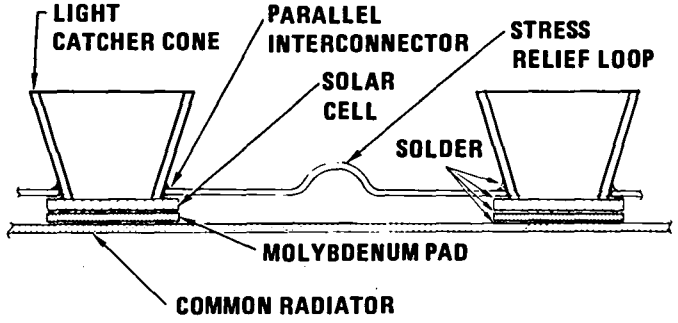

OPTION A DESIGN REQUIRES ELECTRICAL ISOLATION OF EACH MODULE

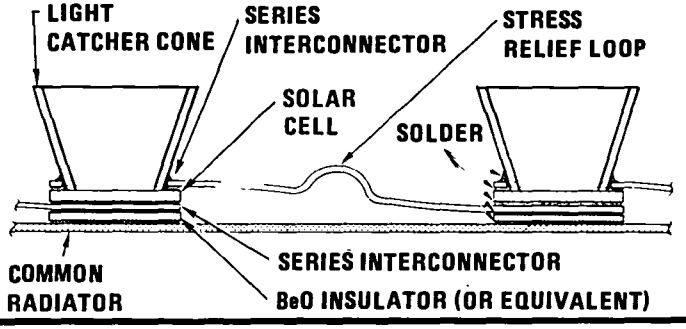

OPTION B DESIGN INCREASES CELL STACK COST BUT REDUCES ARRAY ASSEMBLY COST

ELECTRICAL CONFIGURATION TRADE

The baseline approach was selected for the demonstration hardware only because it avoided the high cost of producing only a few of the special size beryllium oxide (BeO) insulators. The cell-to-heat sink temperature gradient is about 1°C for direct cell-to-fin bond with either molybdenum or BeO. The cost impact of insulating the fins from a grounded frame and from each other may well be comparable to the cost of the BeO insulators. Future studies need to investigate these issues more fully, because the advantages of BeO insulators (Option B) appear most attractive for flight hardware use.

ELECTRICAL CONFIGURATION TRADE

OPTION	CELL/FIN INTERFACE	FIN/MODULE INTERFACE	MODULE/ PANEL INTERFACE	ADVANTAGES	DISADVANTAGES
BASELINE	CONDUCTIVE	DIELECTRIC	CONDUCTIVE	• LOWEST COST • SIMPLE CELL BONDING	• FIN/MODULE INSULATION MORE DIFFICULT
A	CONDUCTIVE	CONDUCTIVE	DIELECTRIC	• LOW COST • MODULES OF CELLS IN PARALLEL ARE SERIES-CONNECTED • GOOD FOR LARGER ARRAYS • GOOD HOT SPOT PROTECTION	• MODULE/PANEL INSULATION MORE DIFFICULT
B (MOST LIKELY CANDIDATE FOR FLIGHT HARDWARE)	DIELECTRIC	CONDUCTIVE	CONDUCTIVE	• ALL FINS GROUNDED • GREATEST FLEXIBILITY IN CELL SERIES AND PARALLEL CONFIGURATION FOR SMALLER ARRAYS • NO EXPOSED POTENTIALS • EASIEST ARRAY ASSEMBLY	• HIGH COST FOR BeO INSULATOR (∼$1.25 PER WATT)

COVERGLASS LOCATION

Three options for installing a coverglass in front of the concentrator solar cells are illustrated. Each configuration has technical and economic considerations that need be examined.

COVERGLASS LOCATION TRADE STUDY SUMMARY

DESIGNATION	SCHEMATIC	MASS/ELEMENT* (MG)	INTENSITY THROUGH COVER
BASELINE: COVER ATTACHED TO TOP OF CONE	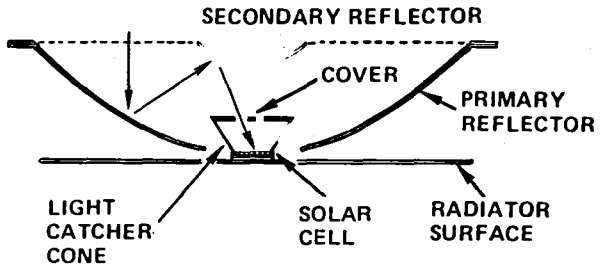	37	23 SUNS
OPTION A: COVER ATTACHED TO BASE OF CONE	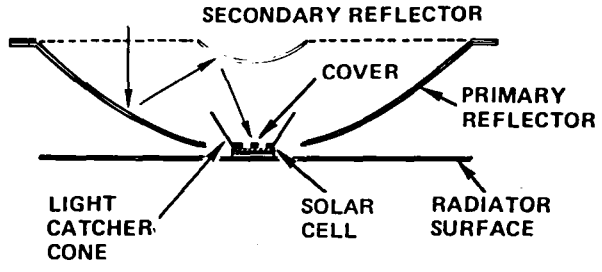	7	129 SUNS
OPTION B: COVER ATTACHED TO ENTRANCE APERATURE RIM	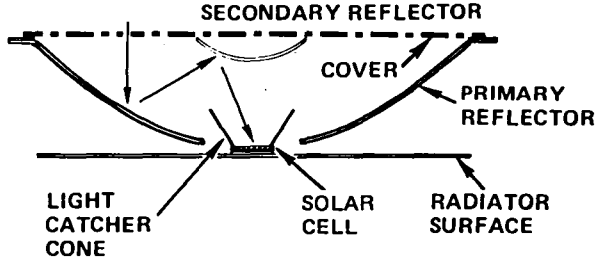	1168	1 SUN

*FOR 0.25mm THICK COVER.

OPTICAL ELEMENT MATERIAL PROCESS SUMMARY

Key to reducing the recurring cost of concentrator arrays are low-cost optical elements. Requirements for the reflectors include: conformance to theoretical surface shape, high degree of specular reflectance (0.85 with aluminum coating and 0.95 with silver coatings), physical stability in the temperature range between -100° and +100°C for 60,000 cycles in LEO or more, ability to withstand natural space radiation environment for 5 to 10 years without significant degradation, and low-cost producibility.

The four basic material and fabrication methods shown in the table were examined. Electroformed nickel (0.010 inch thick) was selected as the baseline design based on availability only. This material and fabrication method was used on the nine element demonstration module hardware and is currently being used to produce low-cost reflectors for high performance flashlights (approximately $2 per element). Future development will be directed toward the other approaches as funding for such development becomes available.

OPTICAL ELEMENT BASE MATERIAL/PROCESS SUMMARY

BASE MATERIAL*	THICKNESS	MANUFACTURING PROCESS	ADVANTAGES	DISADVANTAGES
NICKEL	0.010"	ELECTROFORMED	• OPTICAL PERFORMANCE HAS BEEN DEMONSTRATED	• WEIGHT • REQUIRES SEPARATE RADIATOR
COPPER	0.010"	ELECTROFORMED	• SURFACE ACCURACY HAS BEEN DEMONSTRATED • SEPARATE RADIATOR NOT REQUIRED	• WEIGHT
ALUMINUM	0.010"-0.030"	STAMPED	• LIGHTER WEIGHT • SEPARATE RADIATOR NOT REQUIRED	• OPTICAL PERFORMANCE HAS NOT BEEN DEMONSTRATED
PLASTIC	0.020"-0.040"	INJECTION MOLDED	• LIGHTER WEIGHT	• OPTICAL PERFORMANCE HAS NOT BEEN DEMONSTRATED • REQUIRES SEPARATE RADIATOR

* SILVER COATING AND PROTECTIVE OVERCOATING APPLIED TO BASE MATERIAL.

Spacecraft Engineering Division
TRW Space &
Technology Group

TRW

100 kW Array System Design Study

- Design Requirements
- Study Summary
- Mechanical Design
- Dynamic Analysis
- Electrical Design
- Array Performance Prediction

KEY FIRST-ORDER ARRAY SYSTEM DESIGN REQUIREMENTS

Key first-order array system design requirements were defined to provide a focus for the development of a representative array system concept for a "Space Station Type" application. Array area and W/kg performance requirements are consistent with previous concentrator array performance predictions (Reference 5). Element alignment requirements are based on the predicted element off-pointing performance shown on Page 4-27 of this report. The key design driver for this study is minimum cost per kilowatt at the array system level.

KEY FIRST-ORDER ARRAY SYSTEM DESIGN REQUIREMENTS FOR CONCENTRATOR SOLAR ARRAY

PARAMETER	REQUIREMENT/DESIGN GOAL
ORBIT	235 NMI, 57° INC
BOL POWER	100 KW
ARRAY AREA	650 m^2 MAXIMUM
BOL SPECIFIC POWER	27 W/KG MINIMUM
ELEMENT ALIGNMENT*	(A) ±3 DEGREE MAXIMUM (FROM NORMAL INCIDENCE) (B) 1.5 DEGREE MAXIMUM RMS (ALL ELEMENTS)
ARRAY ASSEMBLY	(A) SELF-DEPLOYABLE (B) ERECTABLE (EVA)
DEPLOYED DYNAMIC CHARACTERISTICS	COMPATIBILITY WITH SPACE PLATFORM DYNAMIC MODEL
STOWED DYNAMIC CHARACTERISTICS	COMPATIBILITY WITH SHUTTLE LAUNCH ENVIRONMENTS
BOL COST	100 TO 150 $/W

* INCLUDES THERMAL DISTORTION, MANUFACTURING TOLERANCES, DYNAMIC DISTORTION, AND CONTROL SENSING ERROR.

100-KILOWATT BOL CASSEGRAINIAN CONCENTRATOR SOLAR ARRAY SYSTEM STUDY SUMMARY

Summary results of the 100-kilowatt system study are presented to provide a general view of the overall concept that was developed on this program. Details of the 100-kilowatt array system which support the summary results are presented in this section.

100KW BOL CASSEGRAINIAN CONCENTRATOR SOLAR ARRAY SYSTEM STUDY SUMMARY

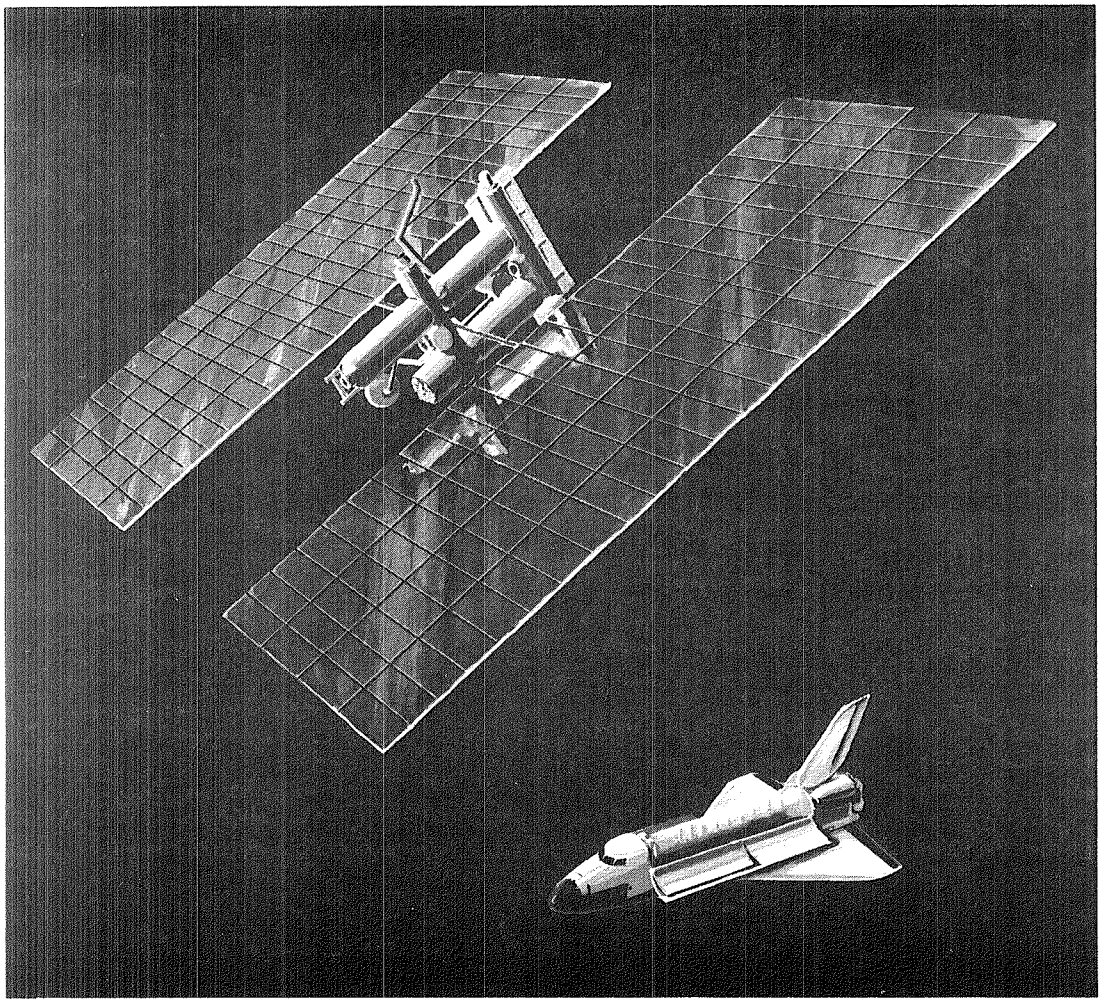

- TWO-WING DESIGN BASELINED BUT CONFIGURATIONS ARE NOT CONSTRAINED
- FOLD-OUT RIGID PANELS WITH FOLDING BEAM SUPPORT (USED ON SKYLAB)
- MODULAR CONCEPT (12.5 KW PER SUBWING MODULE)
- ACCURATE ELEMENT POINTING (MAXIMUM RSS OF 1.1^{o})
- 160 W/m^2 (CURRENT TECHNOLOGY)
- 28 W/kg (CURRENT TECHNOLOGY)
- POTENTIAL OF 60 W/kg WITH TECHNOLOGY DEVELOPMENT
- ERECTABLE (EVA) ARRAY OPTIONAL

MECHANICAL DESIGN AND PERFORMANCE OUTLINE

The mechanical design and performance section starts at the concentrator element level and builds up to the concentrator array configuration. Most of the mechanical design effort was on deployable concepts. Array analysis was performed only on the deployable concepts. The major thrust of the array analysis effort was to determine the dynamic characteristics of a large (100kW) concentrator solar array system.

MECHANICAL DESIGN AND PERFORMANCE OUTLINE

- CONCENTRATOR ELEMENT DESIGN CONFIGURATIONS
- ELEMENT SUPPORT PANEL DESIGN CONFIGURATIONS
- DEPLOYABLE ARRAY CONFIGURATION
  - DESIGN DETAILS
  - STOWAGE IN ORBITER CARGO BAY
  - ASSEMBLY TO SPACE STATION
- ERECTABLE ARRAY CONFIGURATIONS
  - CONCEPT A
  - CONCEPT B
- DEPLOYABLE ARRAY ANALYSIS
  - THERMAL DISTORTION
  - MANUFACTURING TOLERANCES
  - WEIGHT SUMMARY
  - DYNAMIC RESPONSE

CONCENTRATOR ELEMENT DESIGN

Two basic types of element configurations have been considered:

1) The integral radiator design utilizes the primary reflector as the radiator.

2) The separate radiator design uses a thin metal disk (or sheet) for the radiator.

Either type can be used for any of the panel concepts which are presented and discussed in this section. However, the separate radiator design is shown in most of the figures and it was selected as the baseline design for performance predictions. Additional trade studies are required to determine which approach is the most cost effective at the array system level.

CONCENTRATOR ELEMENT DESIGN

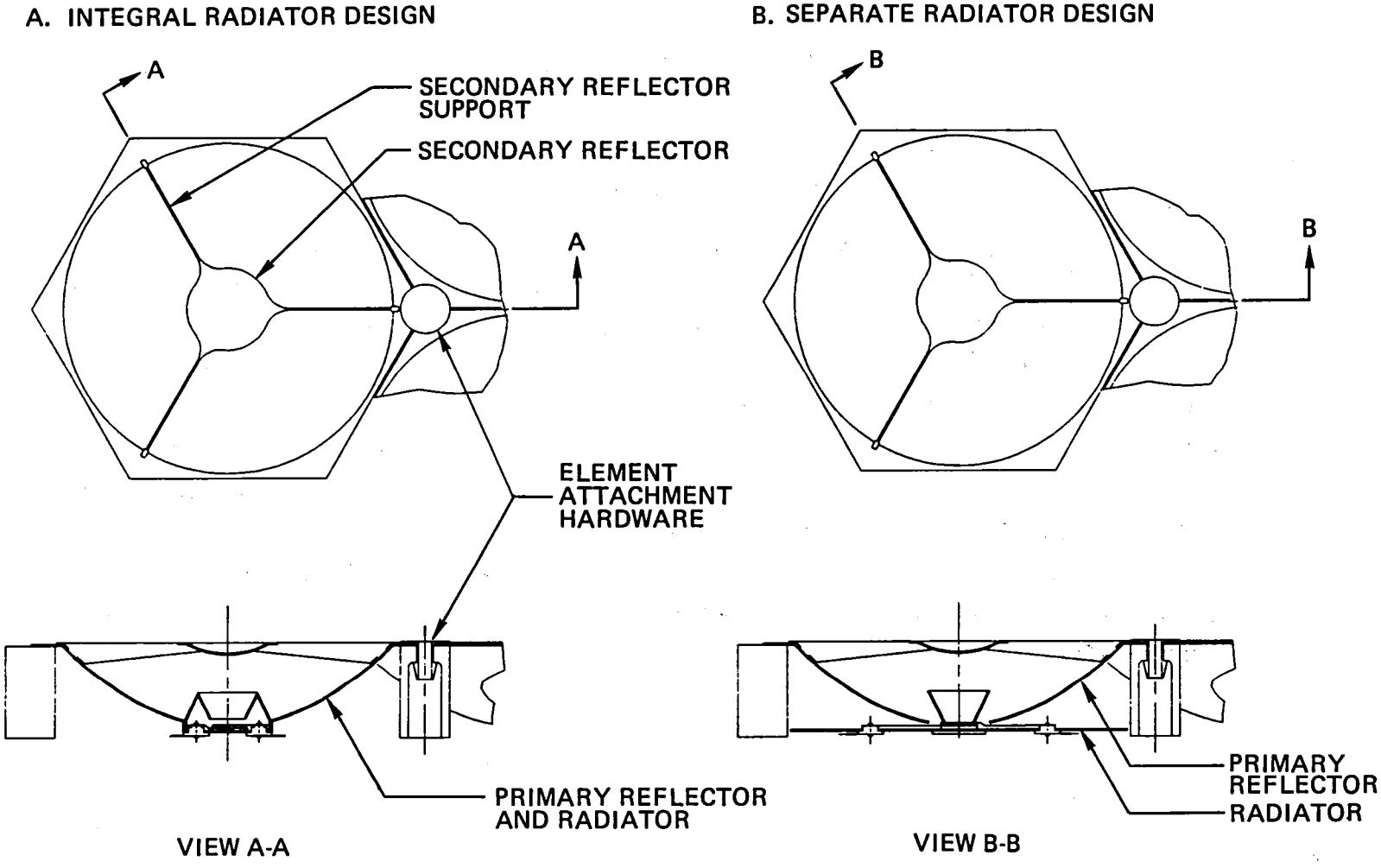

MULTIPLE ELEMENT MODULE ASSEMBLY CONCEPT

This is an assembly concept with a sandwich construction of multiple primary reflectors serving as the front face sheet and a multiple radiator back face sheet.

The multiple element concept offers the potential advantage of reduced panel assembly cost with respect to the single element concept. However, using electroformed nickel reflectors and an aluminum radiator results in a thermal expansion mismatch and the multiple element sandwich structure bows as a function of panel temperature. Preliminary analysis indicates that a 2- by 2-foot multiple element subpanel bows such that elements at the edges are misaligned $\pm$0.25 degree relative to an element in the center of the module during normal operation in a low earth orbit (235 nautical miles). Thus, performance predictions for the multiple element sandwich concept include a misalignment component at the panel level due to thermal distortion of 0.28 degrees (0.25 degrees for the subpanel and 0.03 degrees for a graphite frame).

MULTIPLE ELEMENT MODULE ASSEMBLY CONCEPT

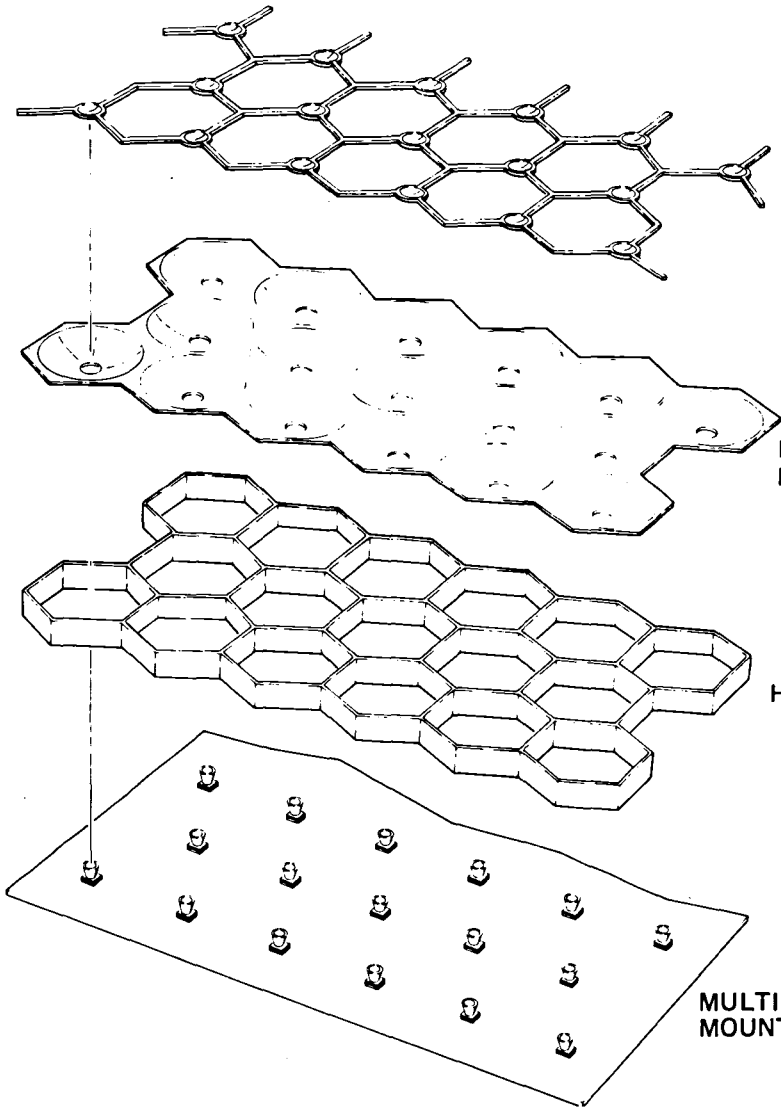

PANEL CONCEPT WITH MULTIPLE ELEMENT, HEX ALUMINUM CORE AND SEPARATE RADIATOR

This illustrates a multiple element sandwich module (24 by 27 inches) mounted in a 48- by 110-inch panel with four support points for each module. The support points are slotted to thermally isolate the modules from the panel frame. The gap between adjacent panels is also shown.

PANEL CONCEPT WITH MULTIPLE ELEMENTS, HEX ALUMINUM CORE AND SEPARATE RADIATOR

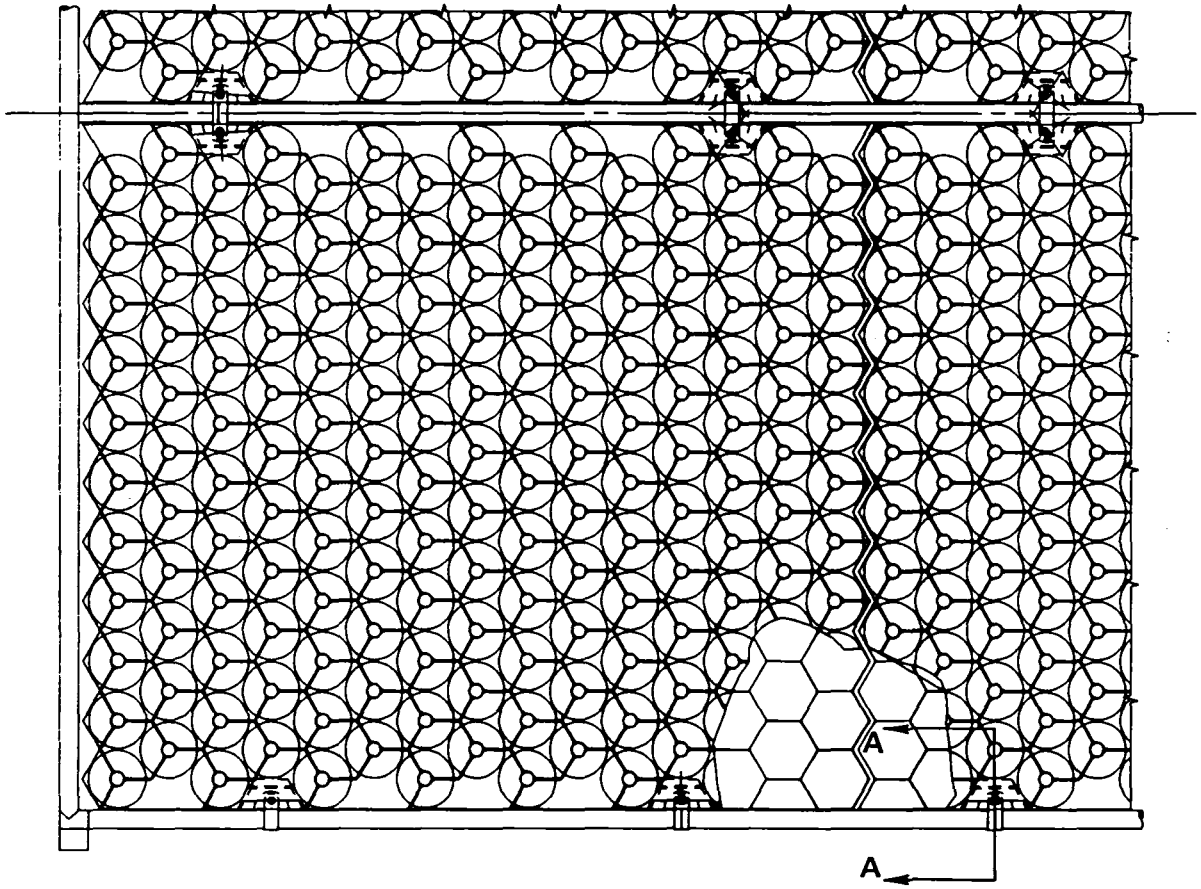

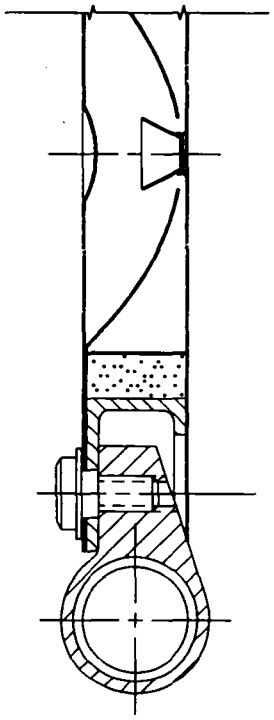

SECTION A–A

INDIVIDUAL ELEMENT MODULE ASSEMBLY CONCEPT

The single element assembly concept is shown in this figure. The single elements are assembled in a grid structure. Tooling for the assembly process is designed to achieve accurate element alignment and accurate element-to-element alignment. This approach is compatible with any of the element material and fabrication processes listed on Page 5-19 and any of the grid concepts listed on Page 6-23.

INDIVIDUAL ELEMENT MODULE ASSEMBLY CONCEPT

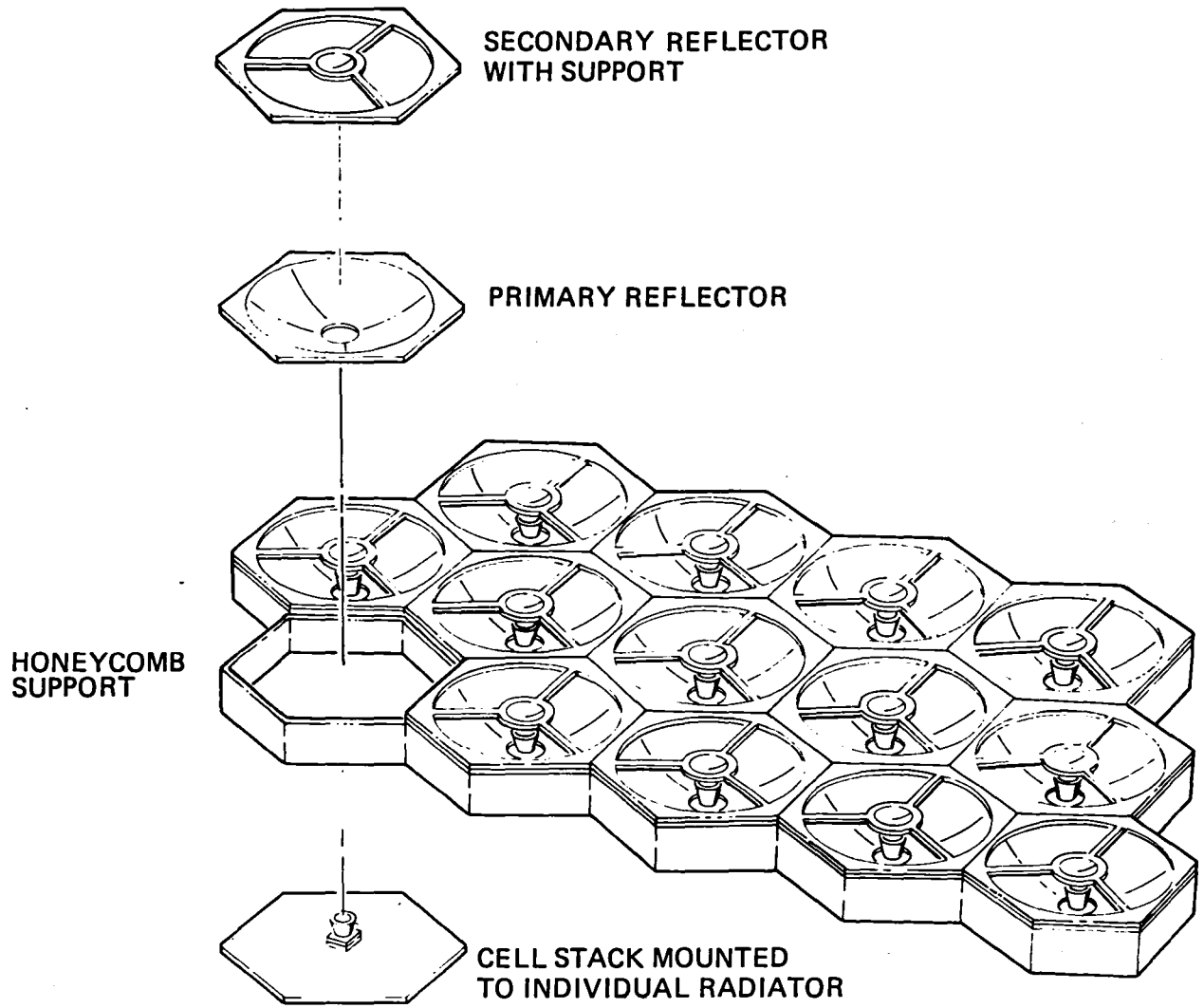

COVERGLASS LOCATION

Three options for installing a coverglass in front of the concentrator solar cells are illustrated. Each configuration has technical and economic considerations that require future examination.

PANEL CONCEPT WITH HEXAGONAL GRID ELEMENT SUPPORT STRUCTURE AND TUBULAR FRAME

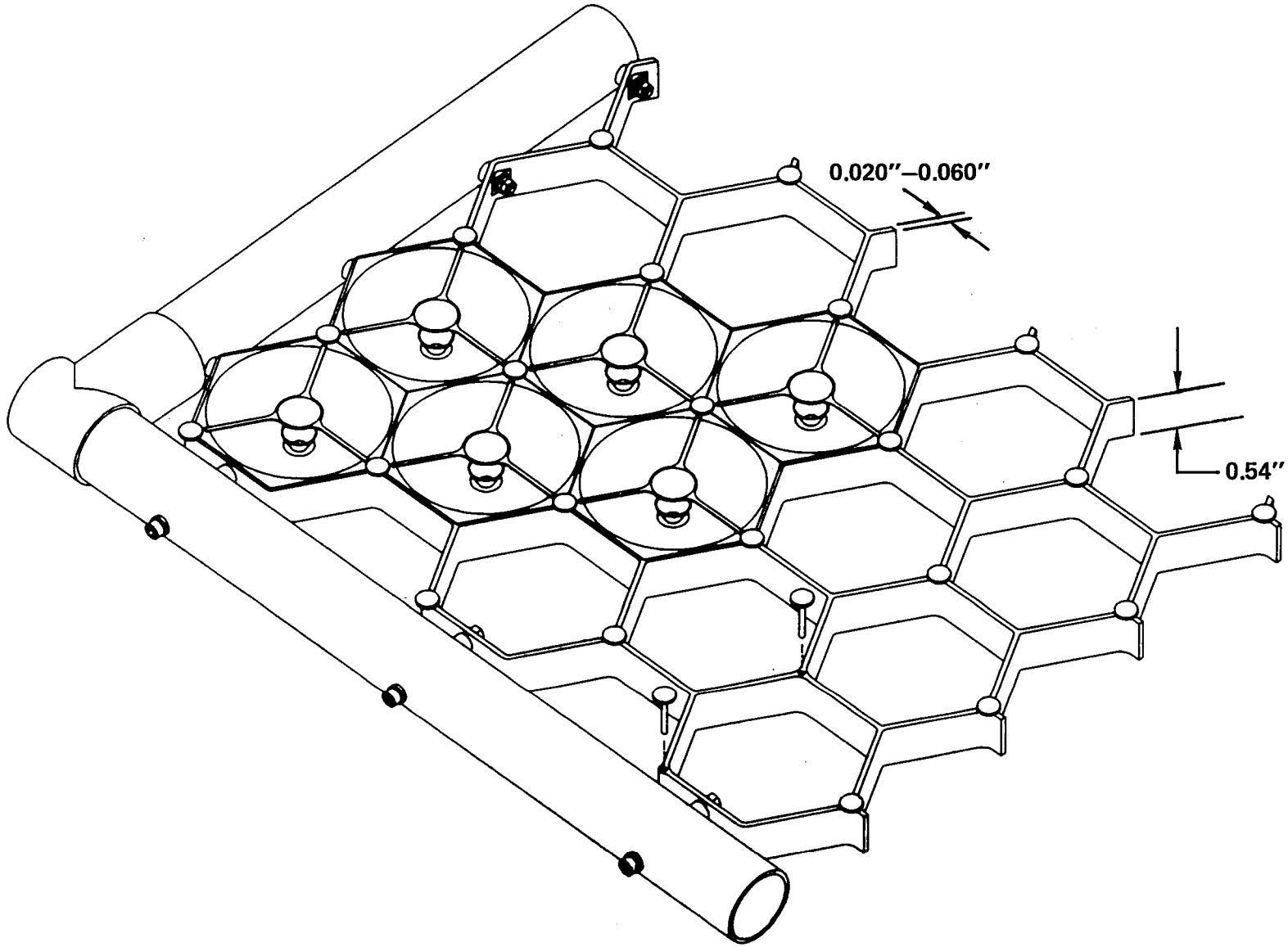

PANEL CONCEPT WITH TRI-HEX GRID ELEMENT SUPPORT STRUCTURE AND TUBULAR FRAME

The individual elements are supported by a number of Tri-Hex grid substrate modules with a graphite tubular frame to minimize thermal distortion for this configuration. The grid material could be Kevlar epoxy or graphite epoxy or plastic.

PANEL CONCEPT WITH TRI-HEX GRID ELEMENT SUPPORT STRUCTURE AND TUBULAR FRAME

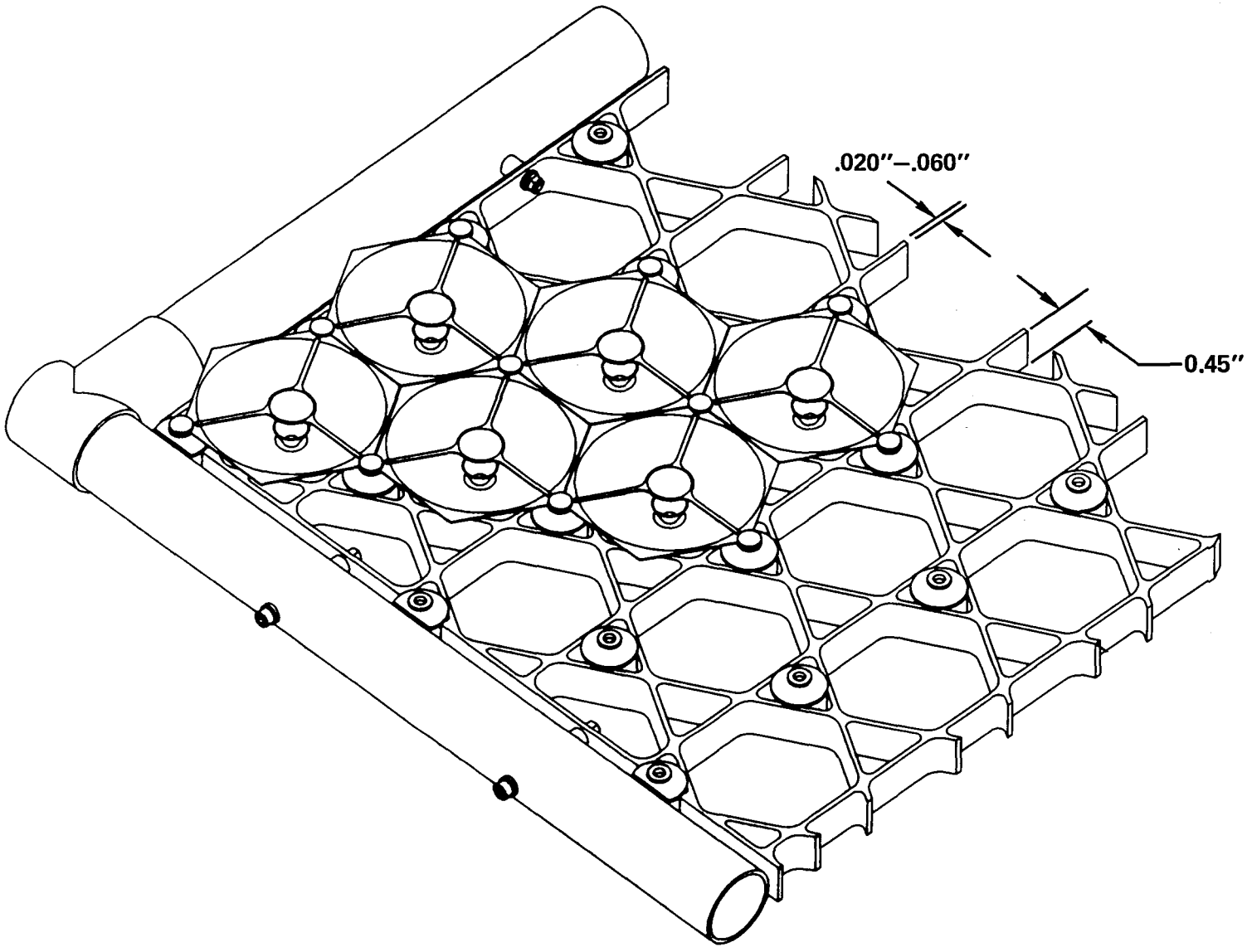

ONE-PIECE TRI-HEX GRID WITH INTEGRAL FRAME

The substrate for this configuration is made of Kevlar epoxy or graphite epoxy to minimize thermal distortion. The entire panel is a one piece construction with an integral frame. This configuration made of graphite epoxy was selected as the base-line for performance predictions.

PANEL CONCEPT WITH TRI-HEX GRID ELEMENT SUPPORT STRUCTURE AND INTEGRAL FRAME

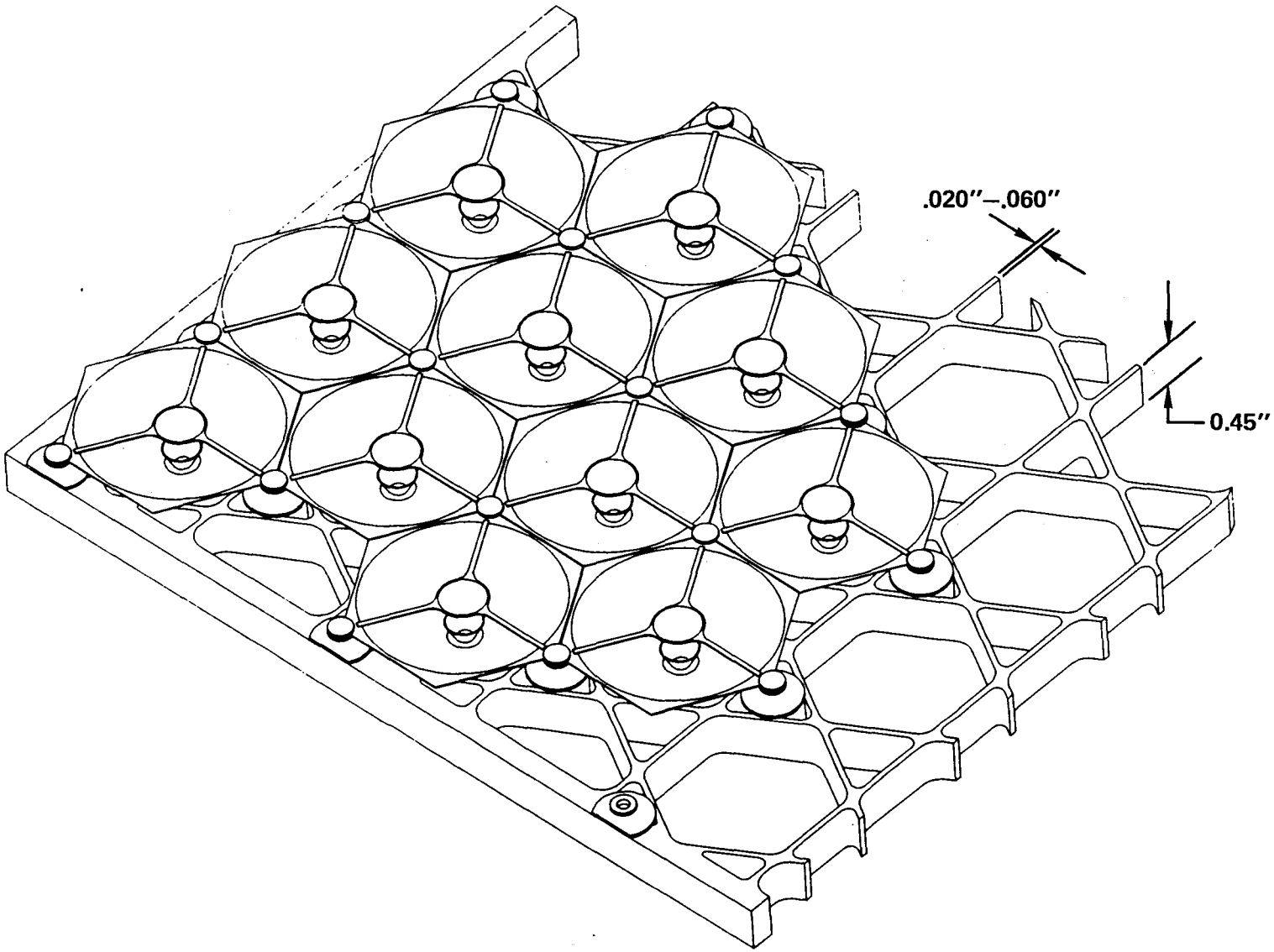

PANEL STRUCTURAL CONFIGURATION SUMMARY

Several single element support structure concepts were identified on this program and are compared to the mulitple element concept. The integral frame Tri-Hex graphite grid (shown on Page 6-21) was selected as the baseline for the purpose of performance predictions. Further design and analysis are required to perform a meaningful trade study with respect to the different panel concepts. The key design driver is cost per kilowatt at the array system level. Parameters which influence cost per kilowatt at the array system level include materials, process, configurations, mass properties, packing densities, operating temperatures, thermal distortions, manufacturing tolerances, dynamic distortions, and assembly costs.

PANEL STRUCTURAL CONFIGURATION SUMMARY

CONSTRUCTION	GRID/MATERIAL	GRID MFG. PROCESS	PANEL OFF-POINTING ERROR*	GRID MATERIAL COST	GRID FAB COST
FRAME/OPEN GRID	HEX/GRAPHITE	FORMED STRIPS/BONDED	0.13°	MODERATE	MODERATE
FRAME/OPEN GRID	HEX/KELVAR	FORMED STRIPS/BONDED	0.23°	LOW	MODERATE
FRAME/OPEN GRID	TRI HEX/PLASTIC	INJECTION MOLDED	NOT ANALYZED	LOWEST	LOWEST
INTEGRAL FRAME/ OPEN GRID	TRI-HEX GRAPHITE	FILAMENT WINDING	0.03°	MODERATE	LOW
INTEGRAL FRAME/ OPEN GRID	TRI-HEX/KELVAR	FILAMENT WINDING	0.23°	LOW	LOW
FRAME/SANDWICH**	HEX/ALUMINUM	FORMED STRIPS/BONDED	0.28°	LOW	MODERATE

* DUE TO THERMAL DISTORTION

** MULTIPLE ELEMENT DESIGN

FOLDED BOX BEAM DEPLOYMENT

The deployment concept illustrated in this figure is the same approach used on Skylab and now being employed on the Gamma Ray Observatory spacecraft.

FOLDED BOX BEAM DEPLOYMENT OF CONCENTRATOR SOLAR ARRAY SUB-WING

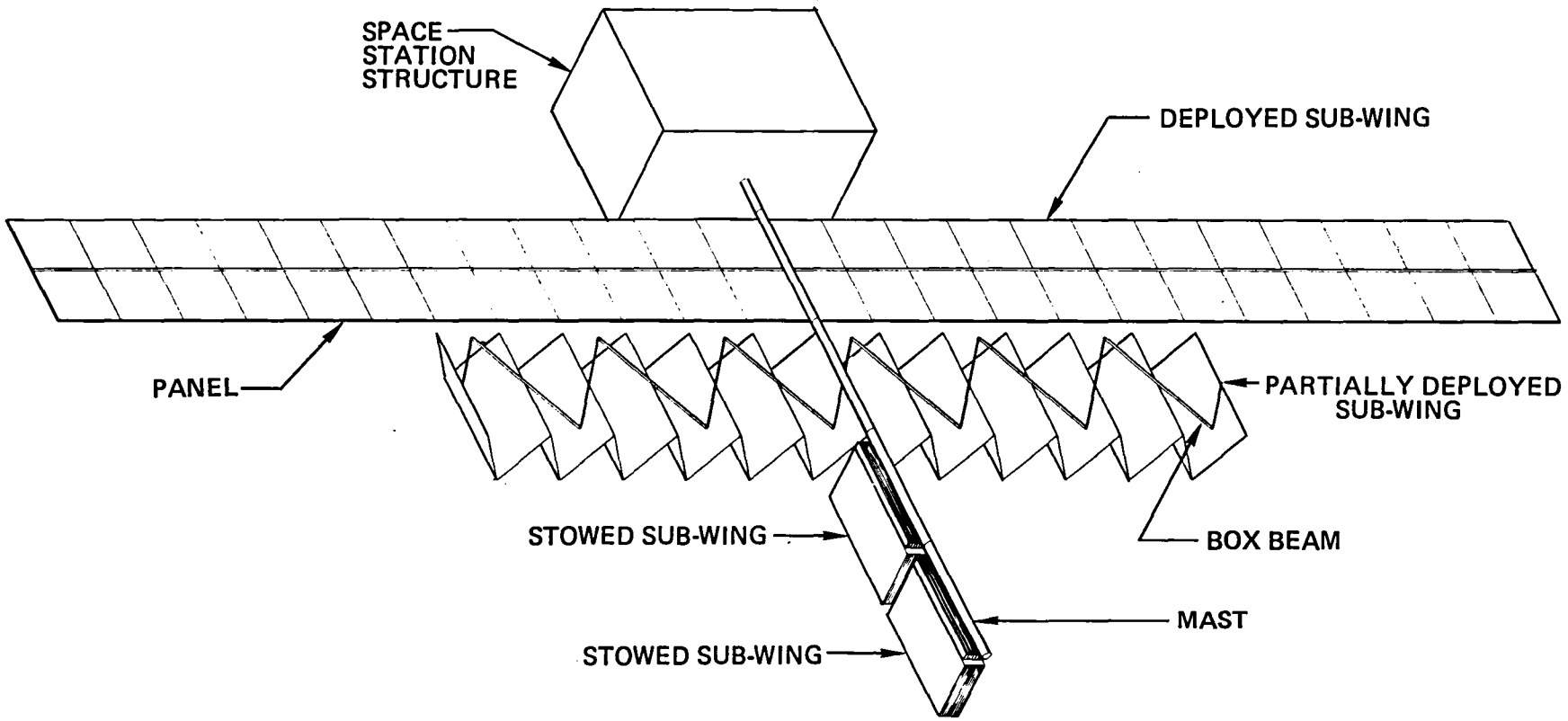

MAJOR COMPONENTS OF A 100-KILOWATT (BOL) CONCENTRATOR SOLAR ARRAY

This figure shows the size of the deployed 100-kilowatt array and identifies the location and name for each of the major components.

MAJOR COMPONENTS OF A 100-KW (BOL) CONCENTRATOR SOLAR ARRAY FOR LEO APPLICATIONS

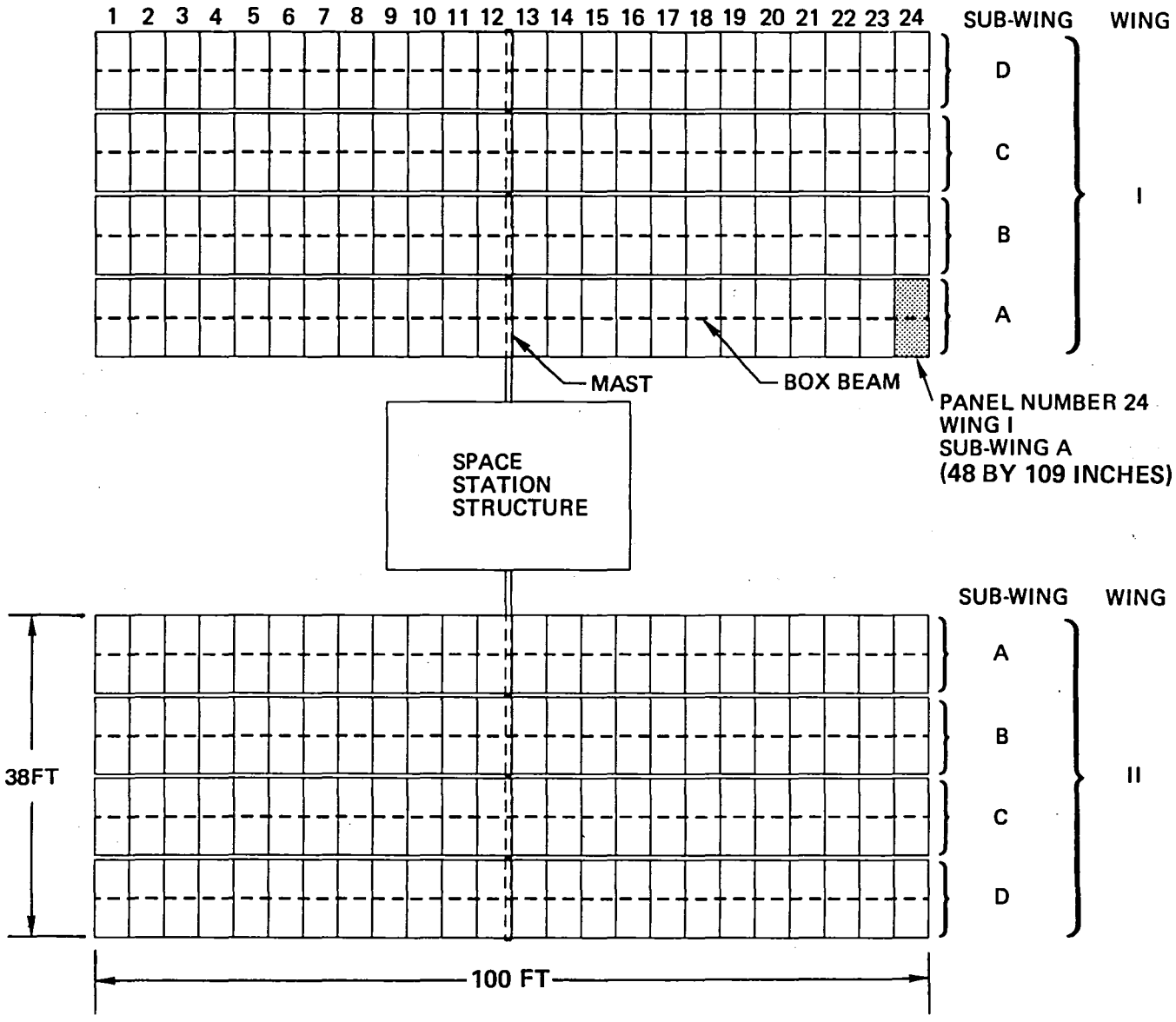

DEPLOYMENT MECHANISM CONCEPT

This figure shows a stowed subwing and enlarged views of the pivot joint between the mast and the folding beam, the deployment motor and linkage, and the mast/panel bracket. The pivot joint has two, tapered, mating surfaces which are preloaded with a flexure to eliminate free play. During deployment the beam is rotated 90 degrees relative to the mast with a motor and toggle linkage. The motor is a stepper motor with harmonic gearing. The electrical connectors are mated at the same time as the subwing mating mechanism.

DEPLOYMENT MECHANISM CONCEPT IDENTICAL TO GAMMA RAY OBSERVATORY (GRO) BASELINE DESIGN

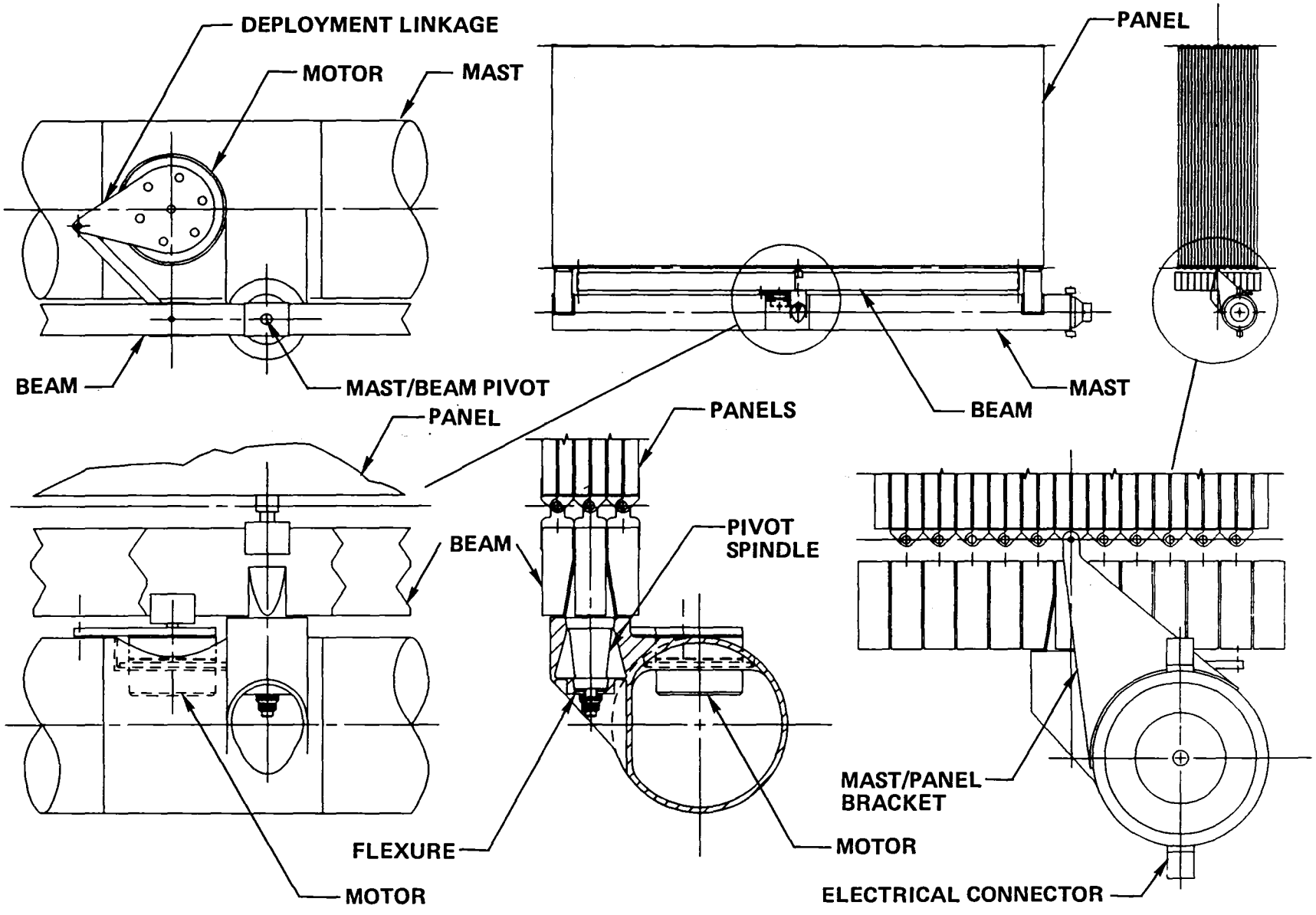

ONE SUBWING DEPLOYED

A deployed subwing with components and dimensions is shown with a view of the mast/beam pivot and deployment mechanism.

ONE SUB-WING DEPLOYED-FOR 100KW DEPLOYABLE CONCENTRATOR ARRAY

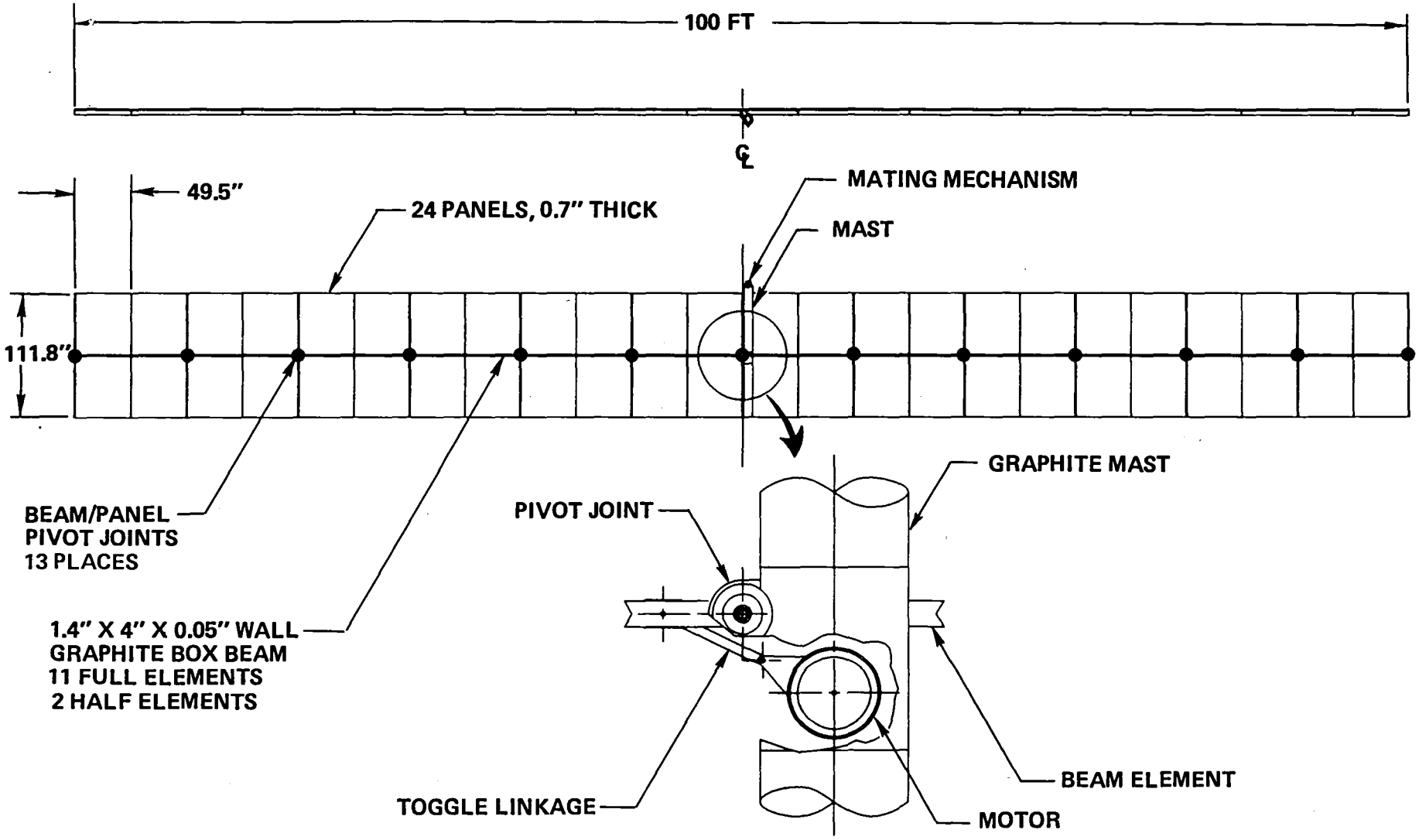

TYPICAL PANEL LAYOUT

A typical panel configuration is shown with details of the panel/beam pivot joint, hinges, and electrical harness routing.

TYPICAL PANEL LAYOUT FOR DEPLOYABLE 100-KW CONCENTRATOR SOLAR ARRAY

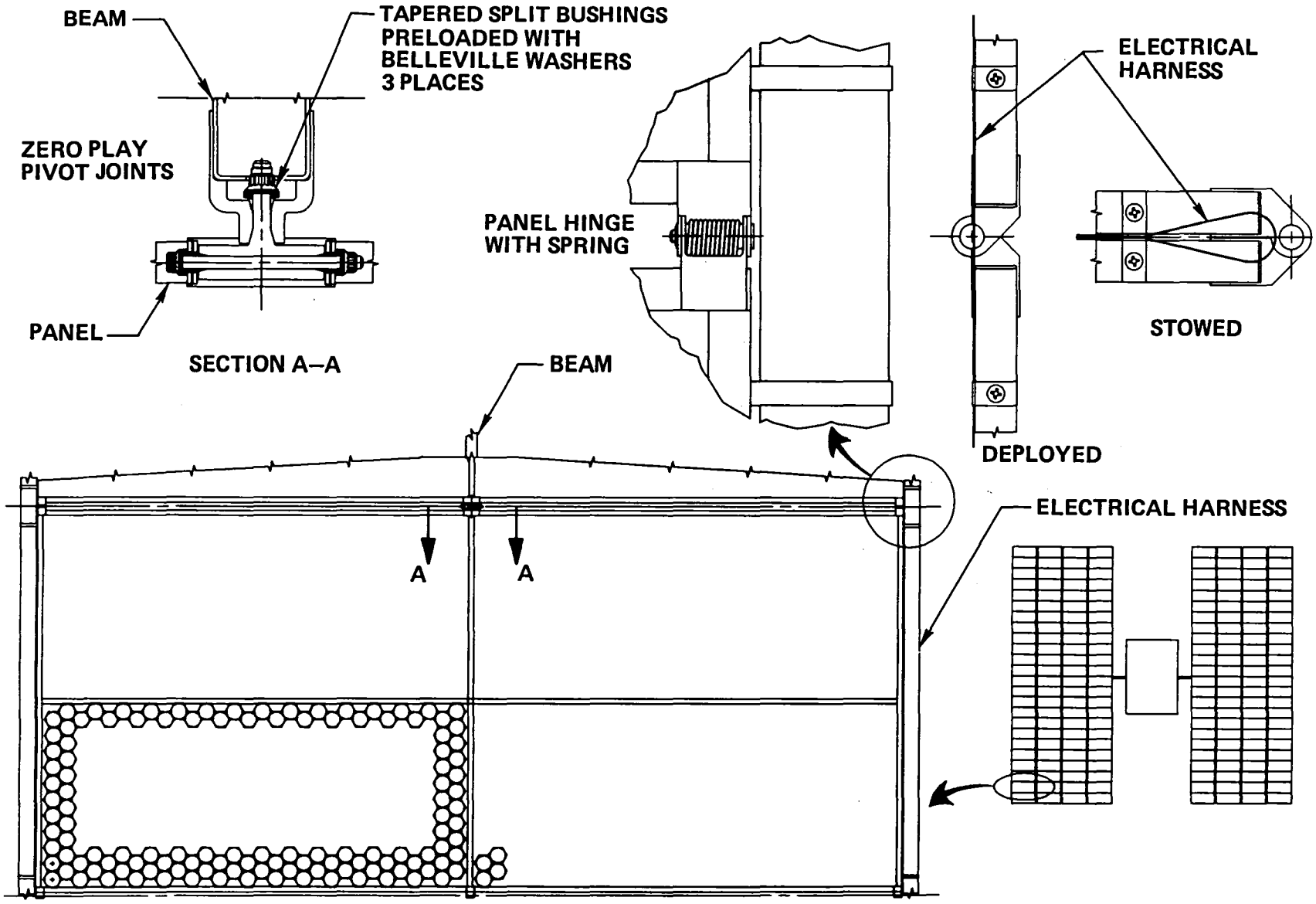

FOLDING BEAM HINGE DETAILS

The folding beam hinge details and the stops for positioning the panels when deployed are illustrated. The stops are adjustable so that the panels can be precisely aligned during ground testing prior to flight use.

FOLDING BEAM HINGE DETAILS WITH STOP TO POSITION PANELS ACCURATELY WHEN DEPLOYED

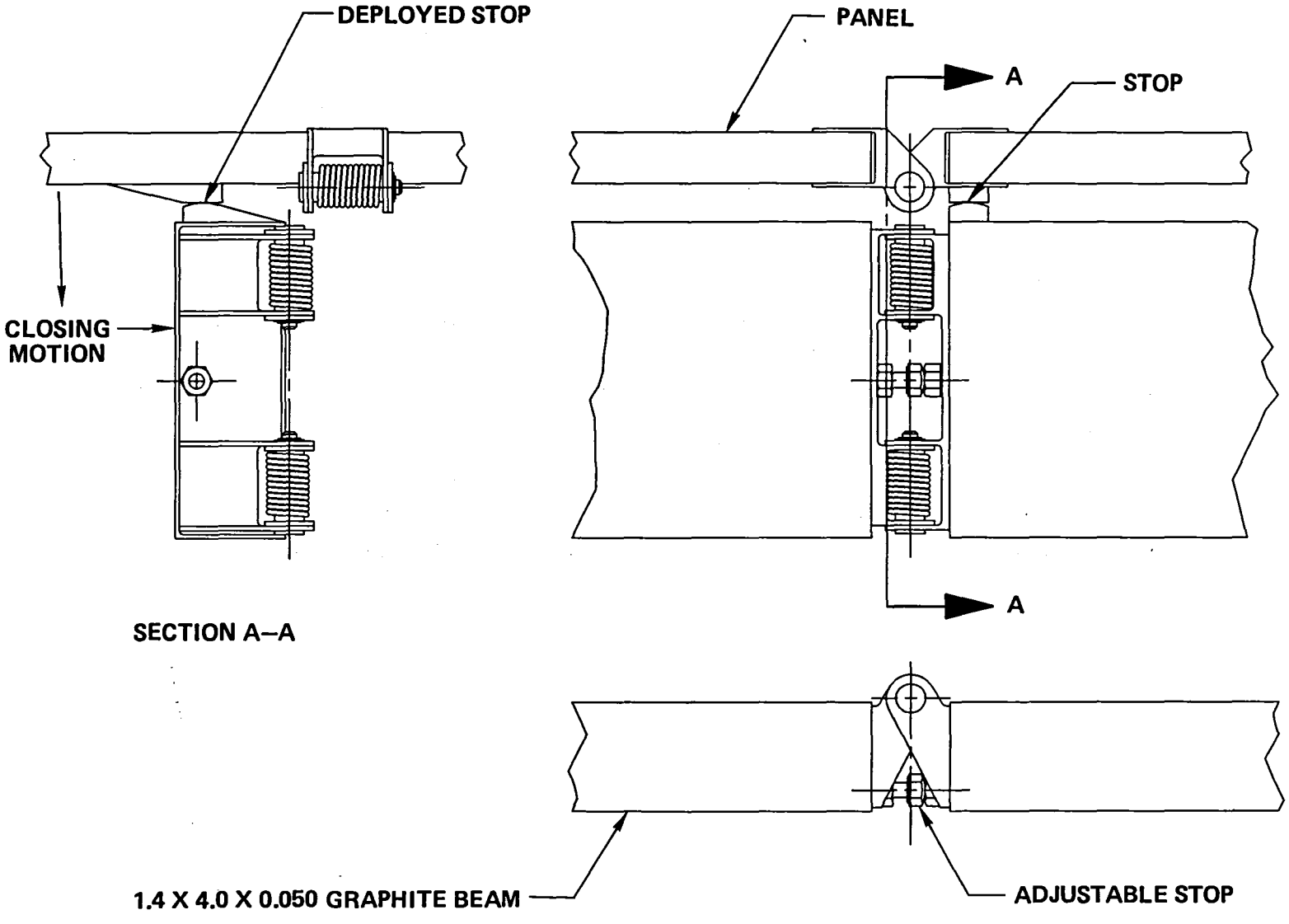

SUBWING MATING MECHANISM

This figure shows the two halves of the subwing mating mechanism one at each end of a subwing mast. This system was tested on the Space Platform program. It was used for attaching the spacecraft to shuttle and payloads to the spacecraft. The Remote Manipulator System (RMS) will place the male end into the receptacle of the female end so that the roller will be within the capture range of the latch as indicated by a switch closure. The motor will then be turned on and will drive the latch closed pulling the two halves together and mating the electrical connectors. Mating can be accomplished with up to an initial ± 4 degree misalignment about any axis.

SUB-WING MATING MECHANISM SCALED FROM SPACE PLATFORM BERTHING MECHANISM HARDWARE

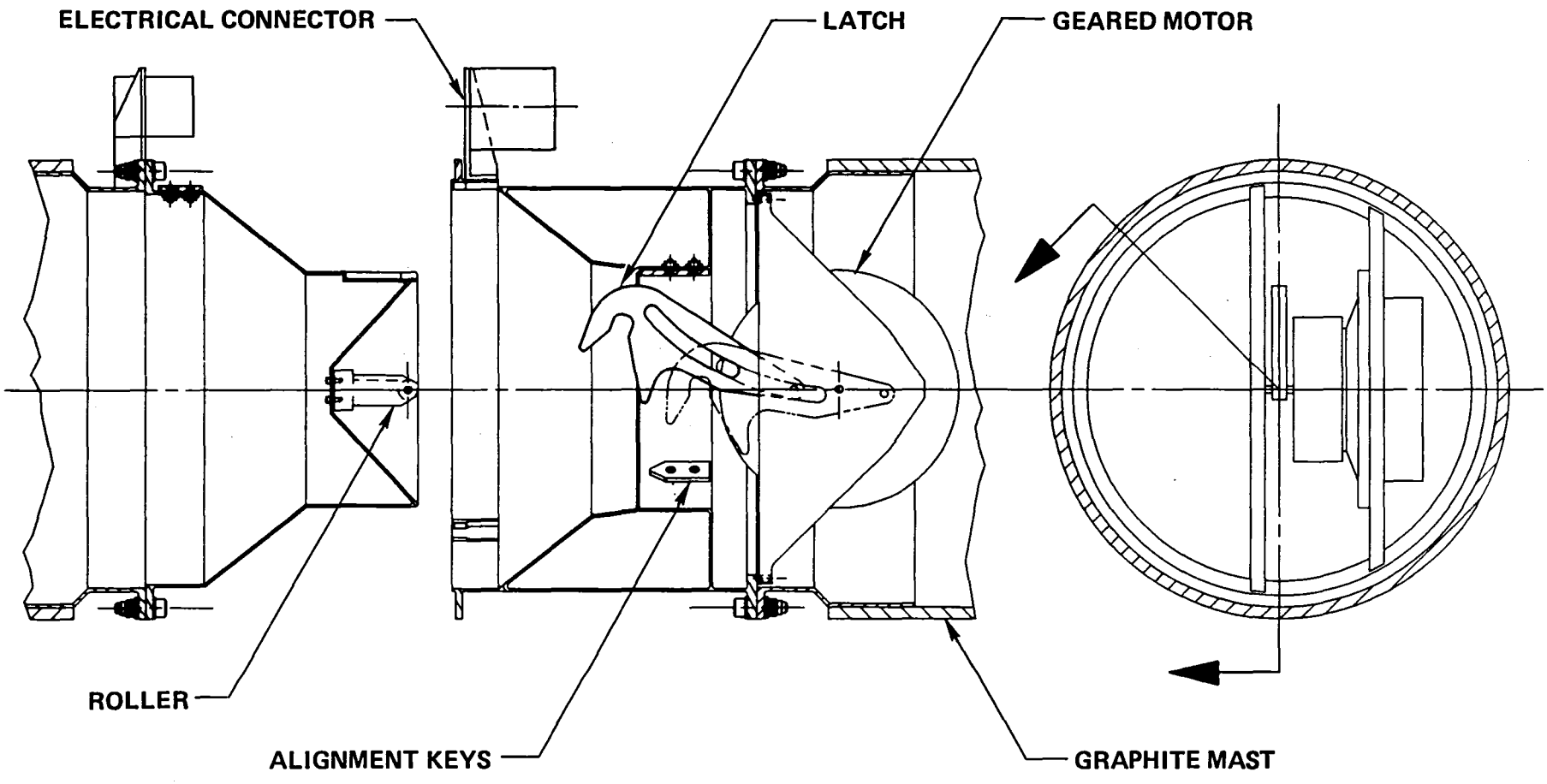

STOWED DEPLOYABLE 100-KILOWATT CONCENTRATOR SOLAR ARRAY

This figure shows that a stowed 100-kilowatt concentractor array requires less than 8 linear feet along the main axis of the shuttle cargo bay. This includes the array panels and panel support structure (masts and folding box beams). This efficient storage is achieved by miniaturization of the Cassegranian concentrator element which results in a 0.5-inch panel thickness. A detail cut-away view of stowed concentrator panels is shown on Page 6-41.

STOWED DEPLOYABLE 100-KW CONCENTRATOR SOLAR ARRAY

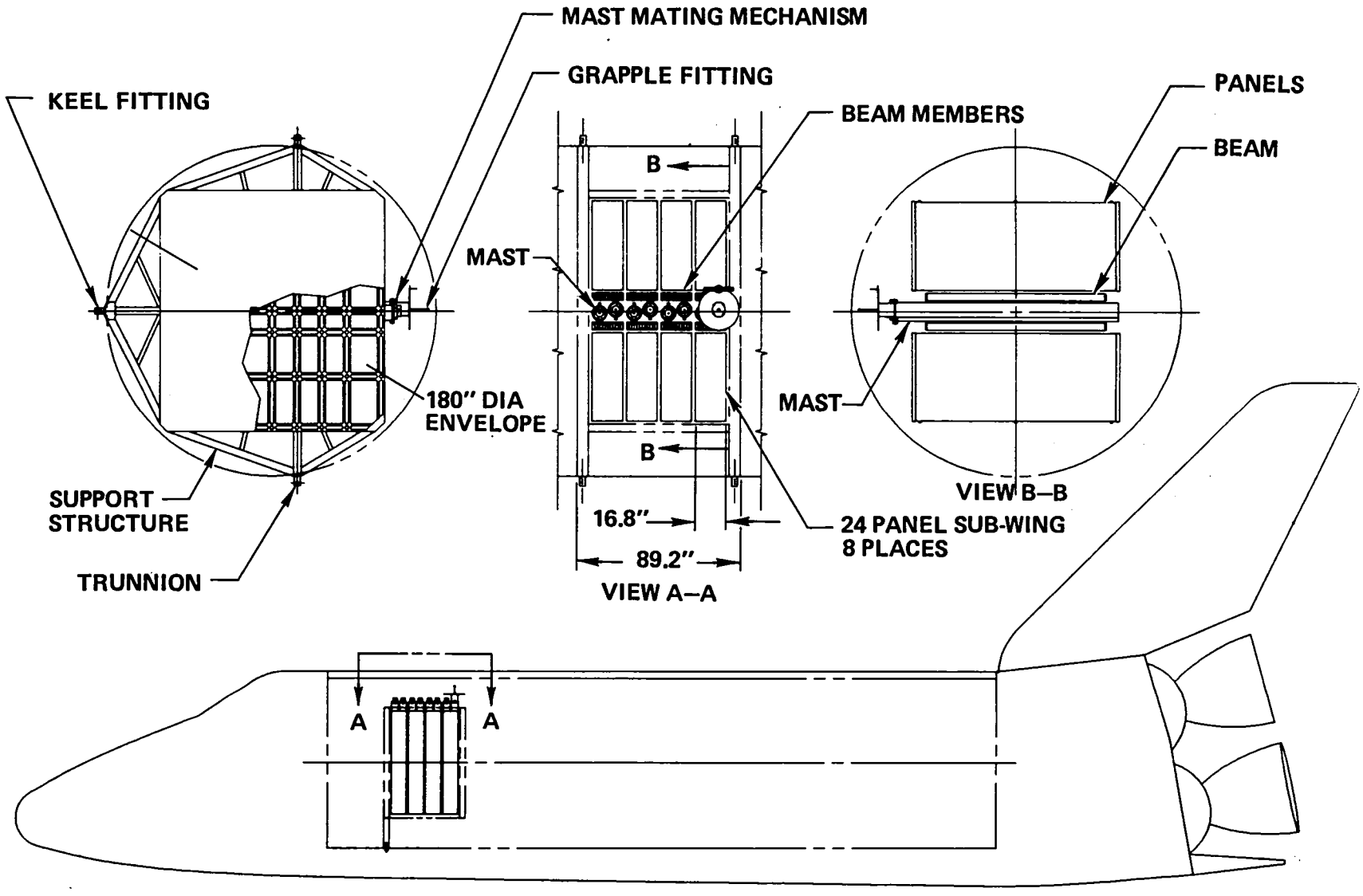

CUT-AWAY OF STOWED CONCENTRATOR PANELS

This figure shows a detailed cut-away view of stowed concentrator panels. This view is for the stowage configuration shown on Page 6-39. The dynamic analysis shows the 0.150-inch panel-to-panel spacing to be adequate during a shuttle launch.

CUT-AWAY VIEW OF STOWED CONCENTRATOR PANELS

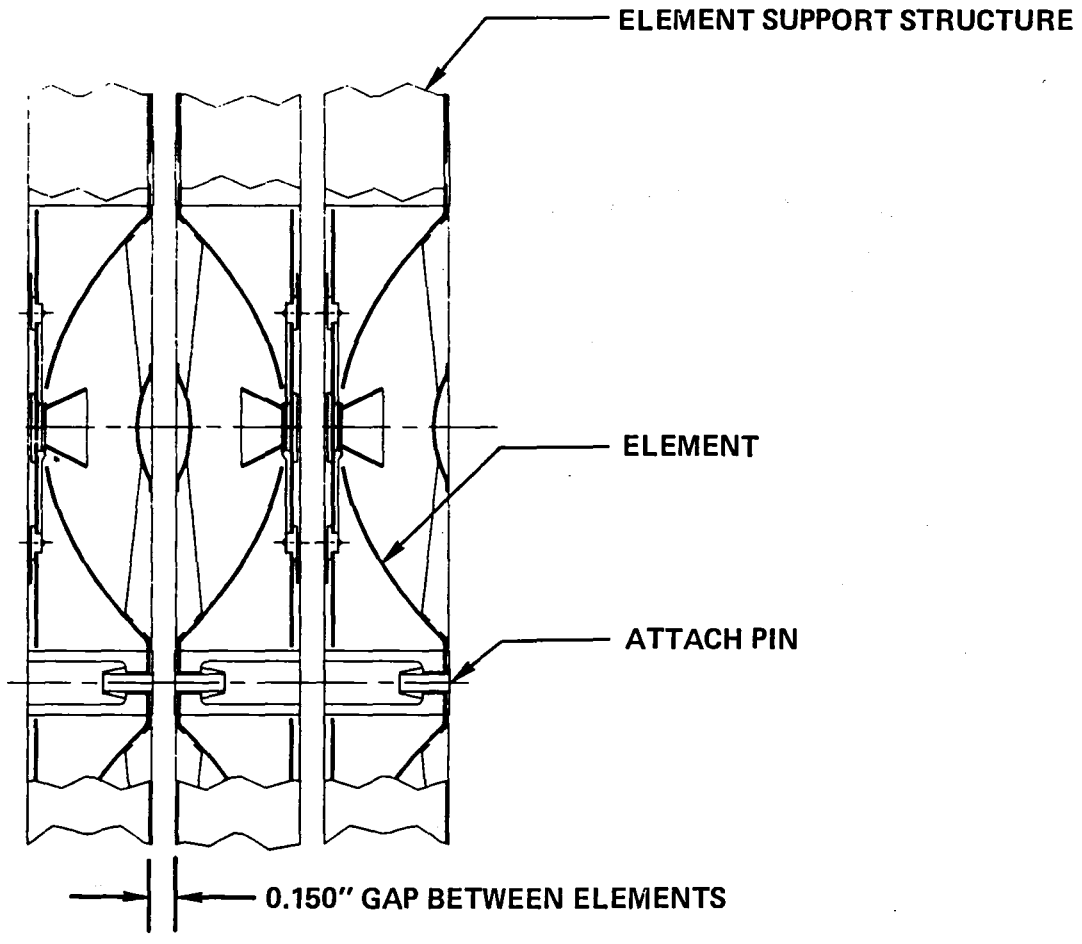

SOLAR ARRAY ATTACHMENT TO THE SPACE STATION STRUCTURE

This shows the eight subwing stacks of panels stowed in the shuttle cargo bay. The space station structure is supported by the Remote Manipulator System (RMS) or a storage/retention arm in position for transferring the subwings to the space station. The RMS connects to a standard grapple fitting, attached to a female half of a subwing mating mechanism, which is then used to pick up all of the other subwing stacks. The subwing mating mechanism is a scaled-down version of the berthing mechanism developed for the Space Platform.

STANDARD MECHANISMS ARE USED FOR SOLAR ARRAY ATTACHMENT TO THE SPACE STATION STRUCTURE

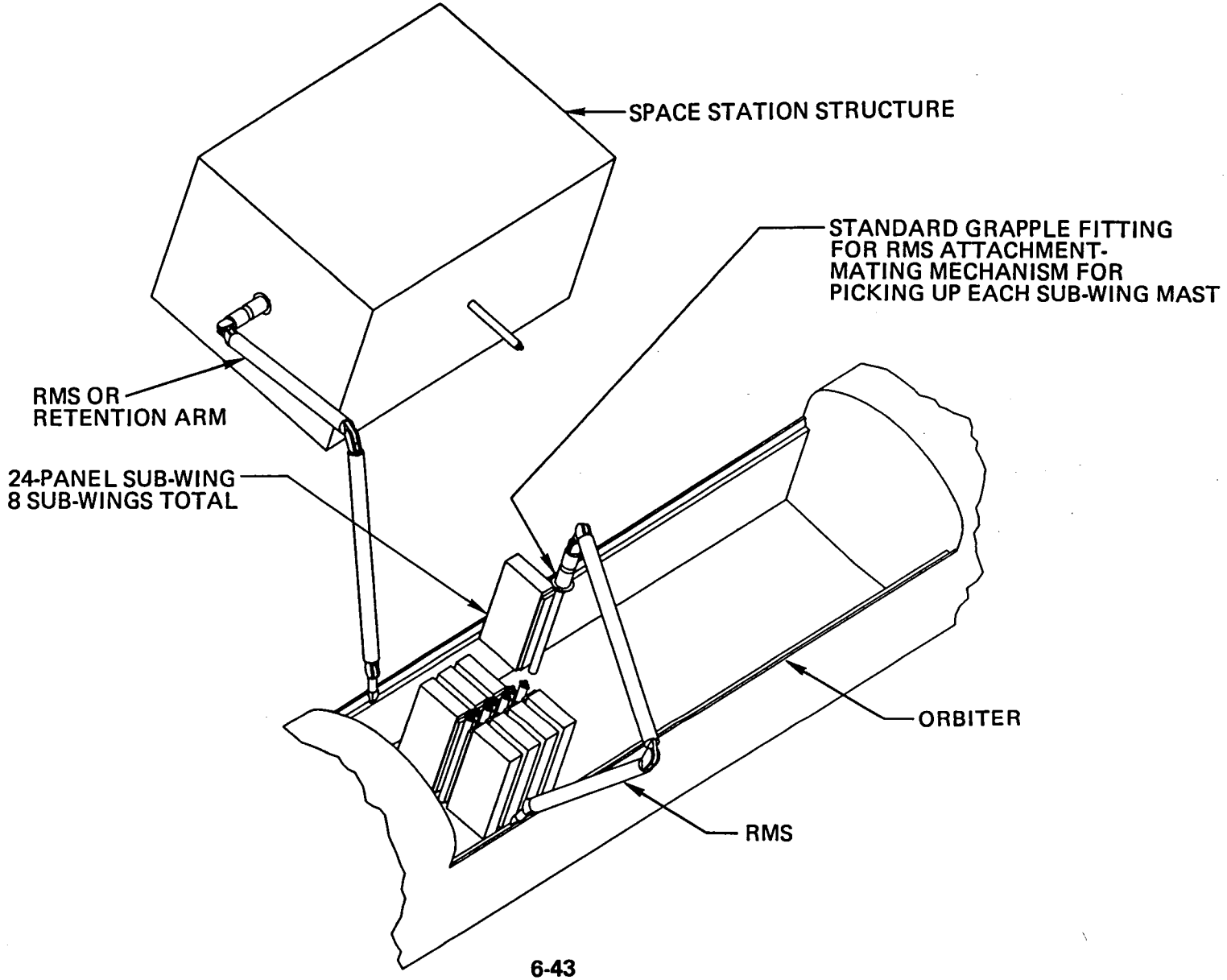

ATTACHMENT OF FOUR STOWED SUBWINGS

This illustrates the sequence of connecting the subwings with the subwing mating mechanisms at the end of each subwing mast. After assembly of one wing the space station is rotated into position for attaching the second wing.

ATTACHMENT OF FOUR STOWED SUB-WINGS TO SPACE STATION STRUCTURE

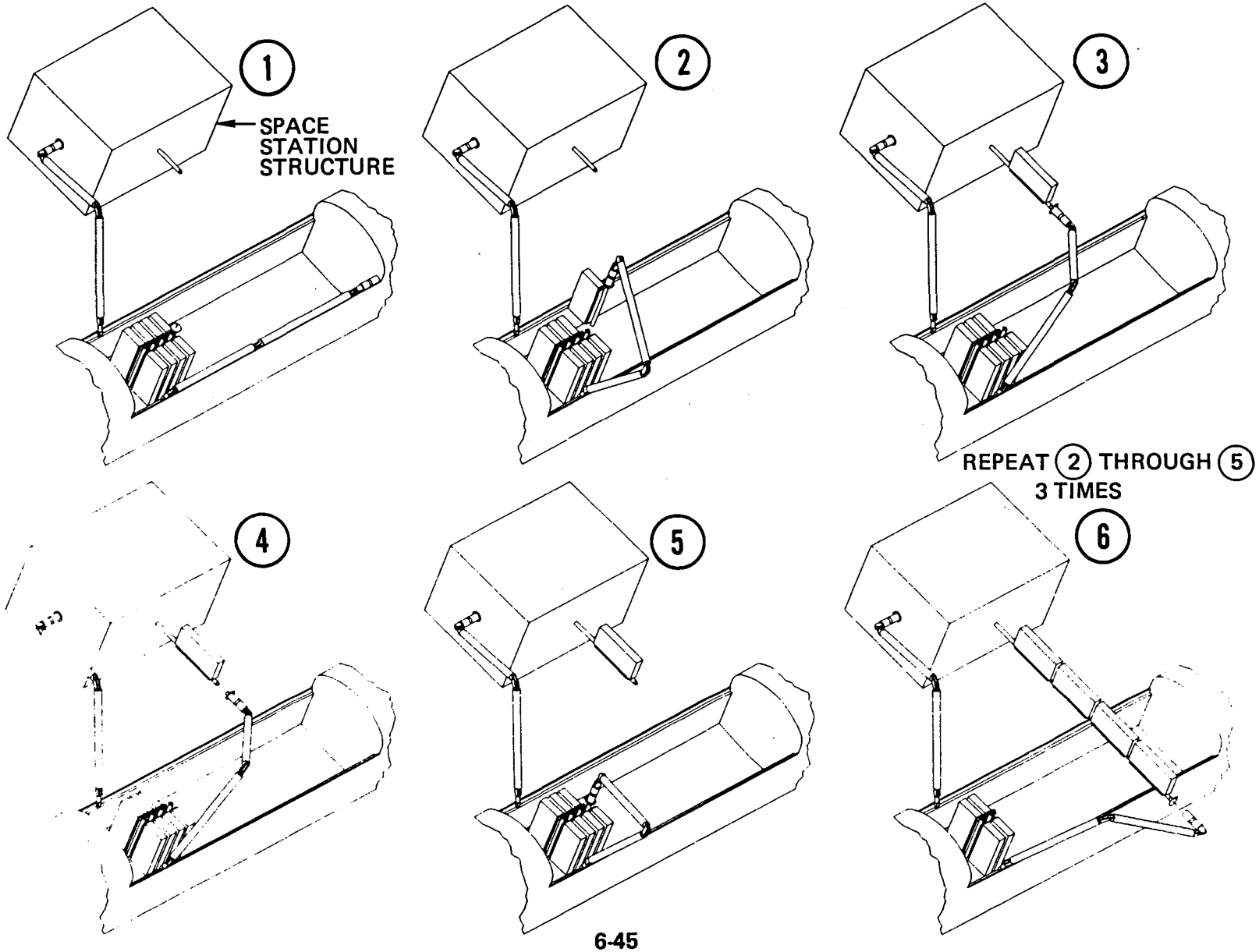

100-KILOWATT ERECTABLE CONCENTRATOR SOLAR ARRAY (CONCEPT A)

This figure illustrates one concept for an array that is erected in space by astronauts. The 56 hexagonal panels provide a high packing factor for storage in the shuttle cargo bay. All connecting joints are preloaded by torquing a single bolt for each to eliminate all free play and minimize pointing errors.

100-KW ERECTABLE CONCENTRATOR SOLAR ARRAY (CONCEPT A)

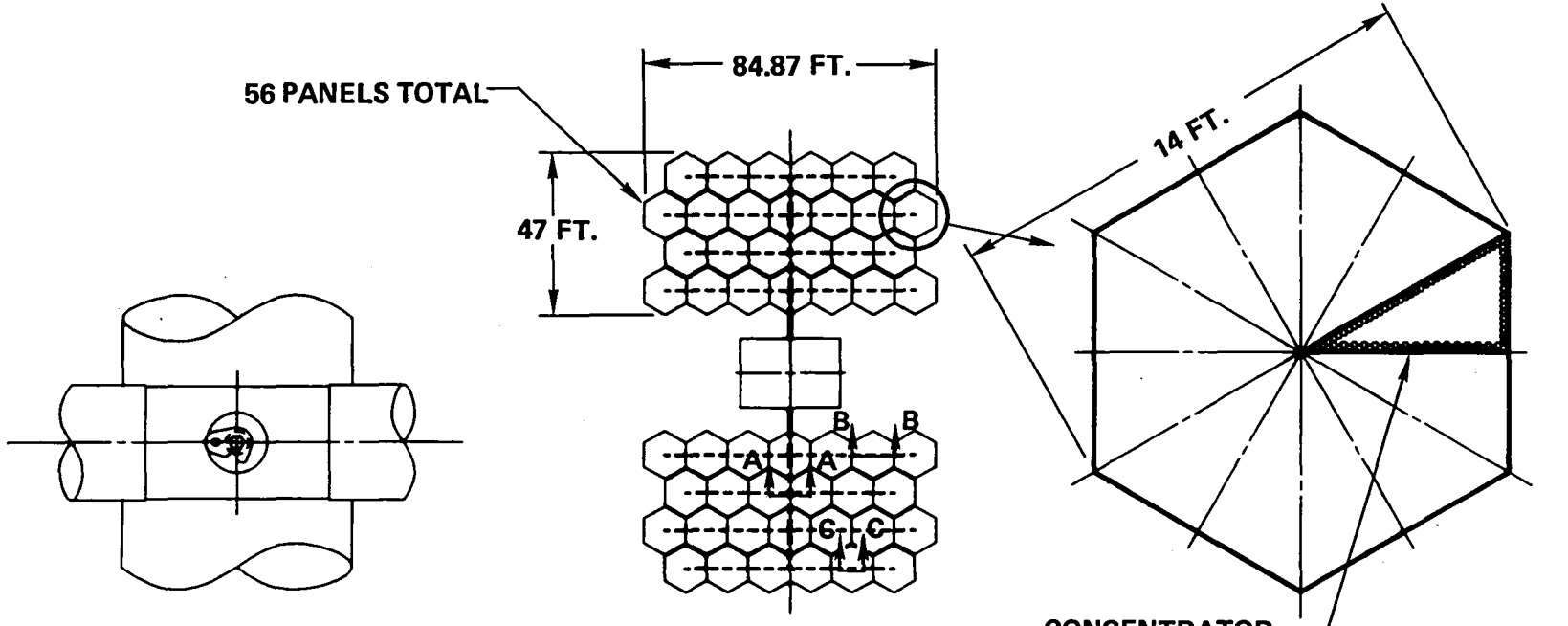

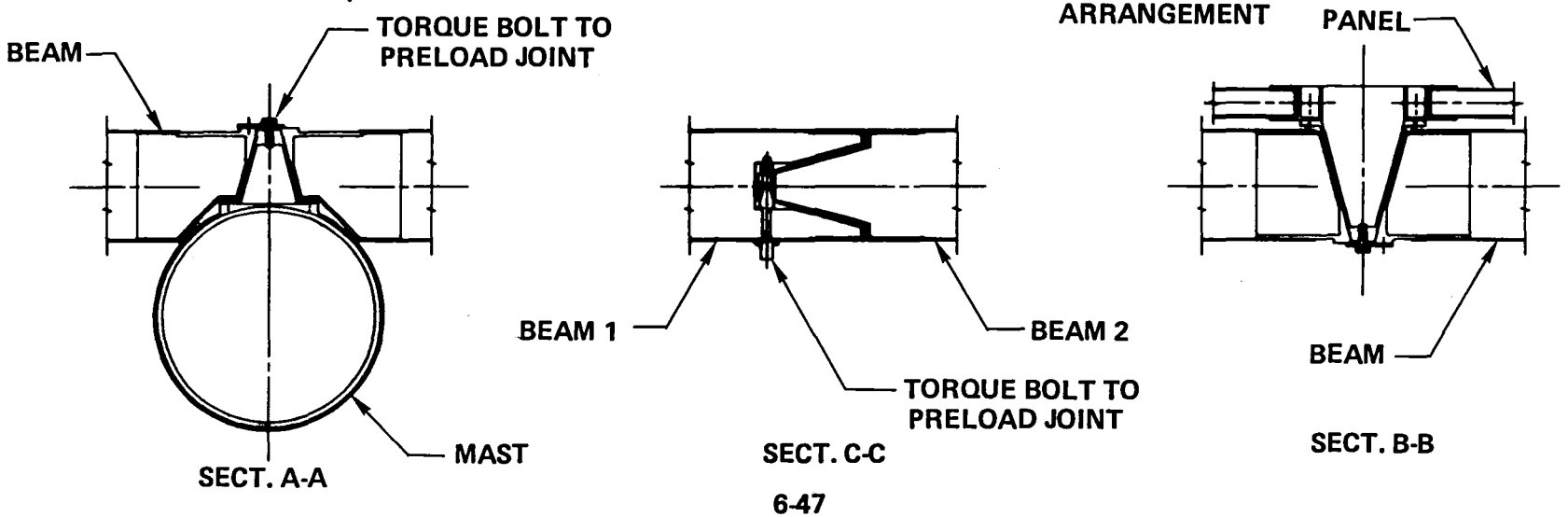

ONE WING OF 100-KILOWATT ERECTABLE CONCENTRATOR SOLAR ARRAY (CONCEPT B)

This concept for an erectable array uses the tetrahedral truss structure developed by NASA, Langley, to provide a very stiff support for the hexagonal array panels.

ONE WING OF 100KW ERECTABLE CONCENTRATOR SOLAR ARRAY (CONCEPT B)

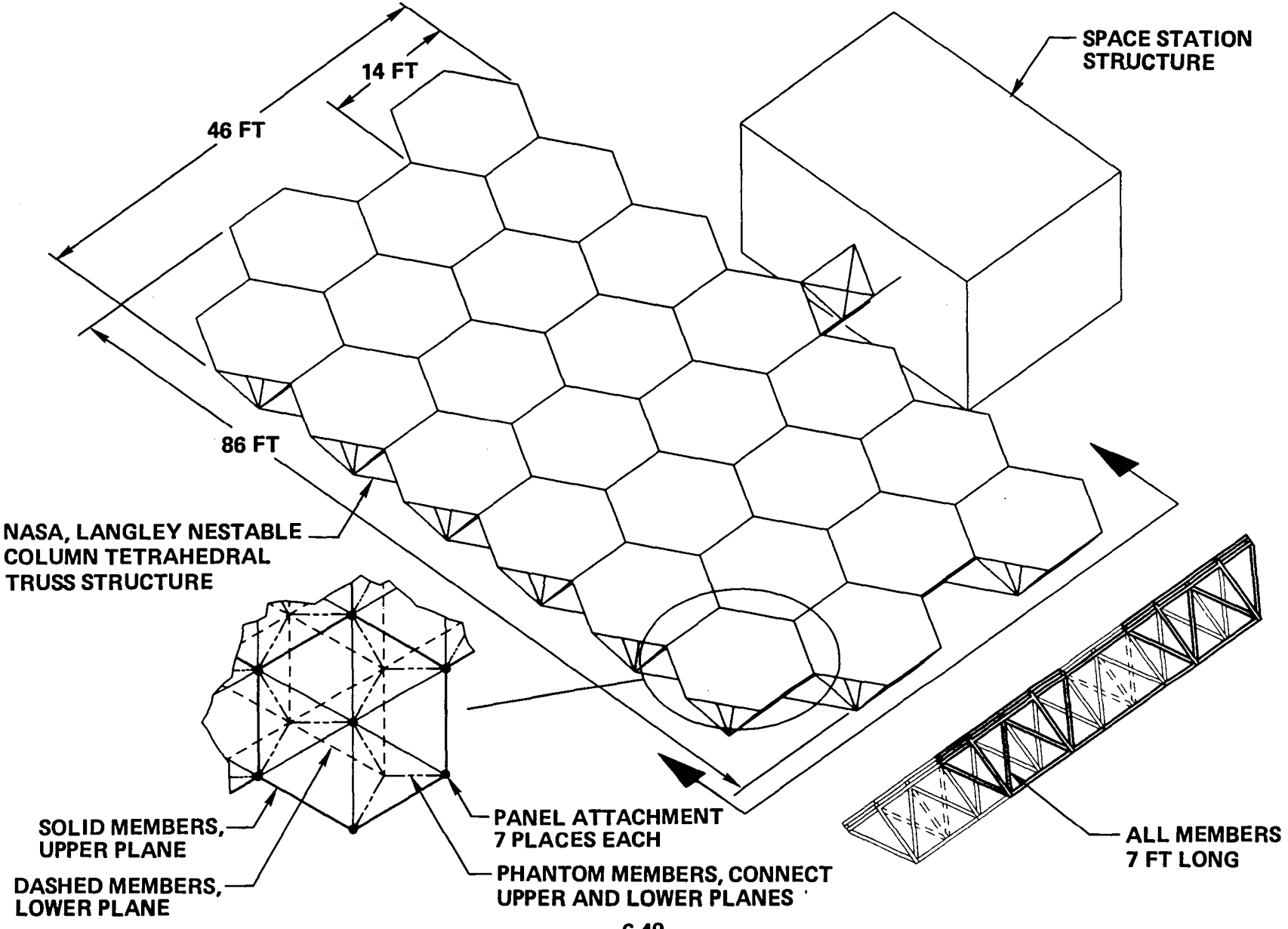

THERMAL DISTORTION ANALYSIS

This figure summarizes the results of the thermal distortion analysis to determine the pointing error for the concentrator elements due to on-orbit operating temperature distribution. The 0.165 degree error applies only to the outermost corner of the array with all contributing errors added end to end. The analysis is for the self-deployable concept and the panel concept shown on Page 6-21.

THERMAL DISTORTION ANALYSIS RESULTS INDICATE MAXIMUM DISTORTION OF < 0.2 DEGREES

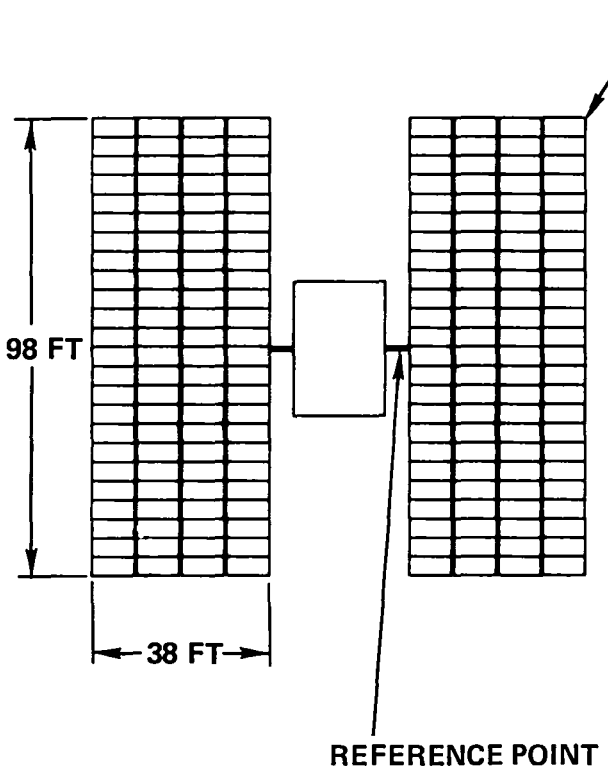

PRELIMINARY ANALYSIS

GRAPHITE EPOXY THERMAL EXPANSION COEFFICIENT: -0.33×10^{-6} IN/IN/^{o}F

PANEL ΔT (FRONT TO BACK) : 5^{o}F

BEAM ΔT (FRONT TO BACK) : 15^{o}F

MAST ΔT (FRONT TO BACK) : 15^{o}F

CALCULATED THERMAL DISTORTION
AT ARRAY WING TIP RELATIVE TO
REFERENCE POINT: 0.165^{o}

POINTING ERROR DUE TO MANUFACTURING

The pointing error for the concentrator elements due to manufacturing tolerances is summarized in this figure. All joints are preloaded throughout deployment or at the end of deployment to eliminate all free play. The analysis is for the self-deployable concept and the panel concept shown on Page 6-21.

MANUFACTURING TOLERANCES CALCULATED TO BE LESS THAN 0.8°

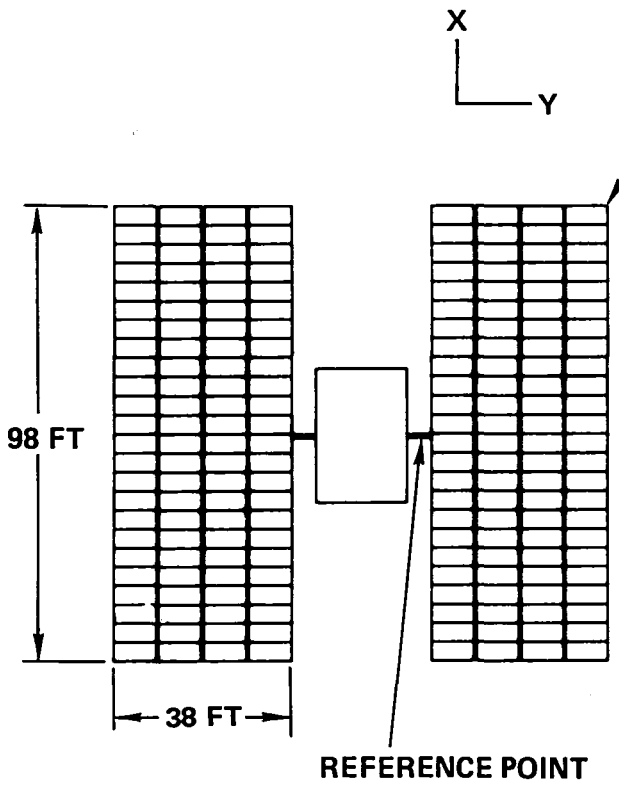

COMPONENT	ASSUMPTION	$\Theta_X \times 10^{-4}$ (RADIANS)	$\Theta_Y \times 10^{-4}$ (RADIANS)
MAST ENDS RELATIVE	BONDED WITH TOOLING 0.003"/8"	3.75	3.75
MAST/BEAM JOINT	BONDED WITH TOOLING 0.0015"/8"	1.88	1.88
BEAM HINGE JOINTS RELATIVE	BONDED WITH TOOLING 0.002"/4.5"	4.44	4.44
BEAM/PANEL PIVOTS	BONDED WITH TOOLING 0.002"/4.5"	4.44	4.44
	PIVOT FITTING REL. TO CELLS 0.001"/2"	5.00	0.00
ELEMENT/PANEL FLATNESS	0.005"/10"	5.00	5.00
PANEL STOPS	0.002"/48"	0	0.42

CALCULATED WORST CASE* ALIGNMENT ERROR DUE TO MANUFACTURING TOLERANCES: 0.74° (ADDITIVE)

* ALL TOLERANCES ADDITIVE

100-KILOWATT BOL CONCENTRATOR ARRAY MASS SUMMARY

The mass of a 100-kilowatt BOL concentrator solar array is 3700 kilograms (8140 pounds). This is based on the use of 0.25-millimeter (10 mil) thick electroformed nickel optics. The element mass comprises 65 percent of the total array mass and, consequently, significant array mass reduction can be achieved by using lighter weight optics. The analysis is for the self-deployable concept and the panel concept shown on Page 6-21.

100-KW BOL CONCENTRATOR ARRAY HAS 3700 Kg MASS

SOLAR ARRAY COMPONENT	UNIT MASS (kg)	QUANTITY	TOTAL COMPONENT MASS (kg) (LB)
PANEL FRAME AND SUBSTRATE	3.6	192	691 (1520)
ELEMENT (CELL STACK AND OPTICS)*	0.0096	250, 368	2404 (5289)
FOLDED BOX BEAM (SUBWING)	18	8	144 (317)
MAST SECTION (SUBWING)	20	8	160 (352)
SUBWING MATING MECHANISM	3	8	24 (53)
SUBWING DEPLOYMENT MECHANISM	4.5	8	36 (79)
BEAM HINGES	0.14	96	14 (31)
PANEL HINGES	0.035	432	15 (33)
PIVOT JOINTS	0.1	96	10 (22)
WIRING, DIODES	202	1	202 (444)
TOTAL	—	—	3700 (8140)

*0.25 mm THICK ELECTROFORMED NICKEL OPTICS

DYNAMIC ANALYSIS OF A SELF-DEPLOYABLE 100-KILOWATT SOLAR ARRAY

Dynamic analysis was performed on the miniaturized Cassegrainian concentrator (MCC) solar array to determine system pointing accuracy on orbit and deflections under launch loads. The MCC solar array requires stringent pointing accuracy to provide power efficiently. Dynamic response due to transient loading conditions is a contribution to pointing error.

Several concentrator mechanical design concepts have been presented. The self-deployable, separate radiator concentrator element, with graphite panel (hexagonal grid) and tubular frame was selected for the dynamic analysis. Other mechanical designs were markedly stiffer and lighter; thus, the design selected for analysis represented the "worst case" relative to dynamic response.

Dynamic models were developed for determining on-orbit and stowed dynamic response. Representative forcing functions were selected for several types of spacecraft disturbances. The forcing functions were coupled to the dynamic models to determine solar array dynamic response.

DYNAMIC ANALYSIS OUTLINE

- ISSUES, APPROACH, AND ASSUMPTIONS
- DEVELOPMENT OF DYNAMIC MODELS
  - SIMPLIFIED PANEL MODEL
  - CANTILEVER WING MODEL
  - ON-ORBIT SPACECRAFT MODEL
- SOLAR ARRAY RESPONSE TO SELECTED FORCING FUNCTIONS
  - SADA SLEW
  - CREW FORCING FUNCTION I
  - CREW FORCING FUNCTION II
  - STEADY STATE GYRO NOISE
  - STATION KEEPING
- DYNAMIC ANALYSIS RESULTS SUMMARY

DYNAMIC ANALYSIS ISSUES APPROACH AND ASSUMPTIONS

Three dynamic models were developed: a stowed model, a cantilever wing model, and an on-orbit model. A stowed model of a quarter solar panel was used to address the issues of stowed panel spacing and stowed natural frequency. The panel deflection under launch is 0.050 inch; thus, the 0.130-inch interpanel spacing is adequate. The panel natural frequency is 200 hertz.

A cantilever wing model was used to address the issue of response due to Solar Array Drive Assembly (SADA) slew. Subwing tip motion is 0.8 inch which is less than the 6.0-inch subwing spacing. Peak solar array off-pointing due to slew is 0.5 degree.

An on-orbit model was used to find peak array off-pointing due to two crew motion forcing functions, a gyro noise forcing function, and a reboost forcing function. The maximum array off-pointing of 0.7 degree was due to a crew forcing function.

DYNAMIC ANALYSIS ISSUES, APPROACH, AND ASSUMPTIONS

ISSUE	APPROACH
• STOWED SPACING DURING LAUNCH.	• DEVELOP DETAILED PANEL MODEL*, AND SUBJECT IT TO 14g LOAD.
• SUBWING SPACING DURING SADA SLEW. • ARRAY OFF-POINTING DURING SADA SLEW.	• DEVELOP CANTILEVER WING MODEL*,**. APPLY SADA SLEW FORCING FUNCTION.
• SUBWING SPACING DURING ANTICIPATED CREW MOTION, GYRO NOISE AND STATION KEEPING DISTURBANCES. • ARRAY OFF-POINTING DURING CREW MOTION, GYRO NOISE, AND STATION KEEPING DISTURBANCES.	• DEVELOP ON-ORBIT SOLAR ARRAY MODEL*,**,*** AND COUPLE WITH SPACE PLATFORM DYNAMIC MODEL. APPLY SELECTED FORCING FUNCTIONS REPRESENTATIVE OF CREW MOTION, GYRO NOISE AND STATION KEEPING DISTURBANCES.

* SINGLE ELEMENT, SEPARATE RADIATOR DESIGN WITH GRAPHIC EPOXY HEX GRID ELEMENT SUPPORT STRUCTURE.

** FOUR 12.5KW SUBWINGS PER WING.

*** TWO 50 KW WINGS.

SOLAR PANEL MODEL FOR STOWED RESPONSE

A detailed model was created using the TRW Structural Analysis Program (TRWSAP) which represented one quarter of a hexagonal grid solar panel and frame assembly (see Page 6-17). The quarter panel was represented by 746 nodes and 1159 members. Eight nodes were constrained in translation to represent interpanel snubbers. Element assemblies and thermal radiators were considered nonstructural and were not modeled, but their weights were distributed along the panel members.

The detailed dynamic model of a quarter integral radiator panel was subjected to a 10g quasi-static load and a 0.025-psi acoustic launch load normal to the panel. Four sets of boundary conditions were used to simulate an entire panel. Primary and secondary reflectors were considered nonload carrying members and the pressure load was applied as an additional one-g load on the panel. The combined launch loads caused a 0.050-inch out-of-plane deflection of the panel, which verifies the adequacy of the 0.130-inch interpanel spacing.

DEPLOYABLE 100-KW CONCENTRATOR SOLAR ARRAY STOWED PANEL SPACING

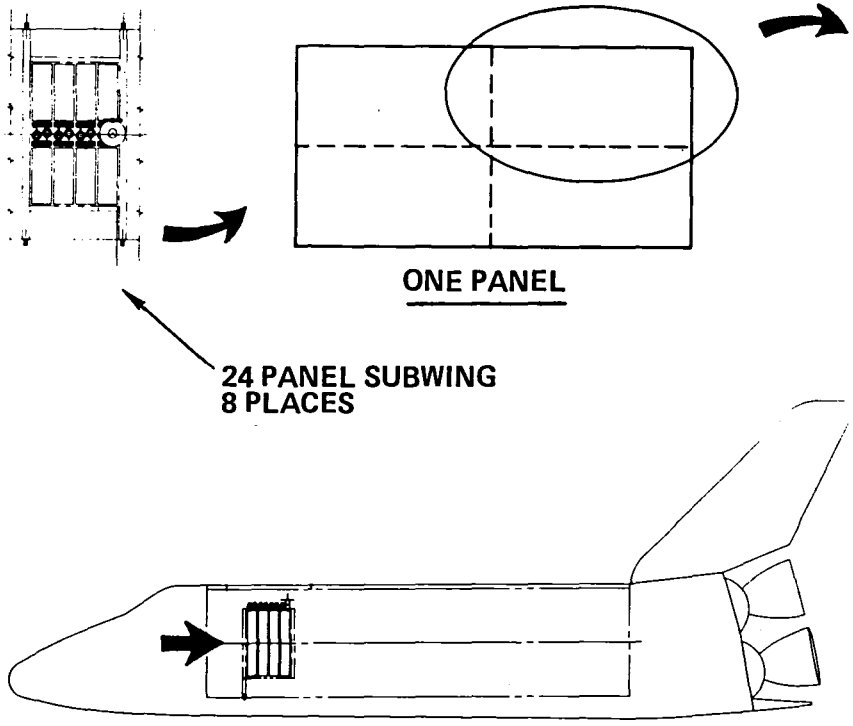

DETAILED QUARTER PANEL
WITH FOUR DIFFERENT BOUNDARY CONDITIONS

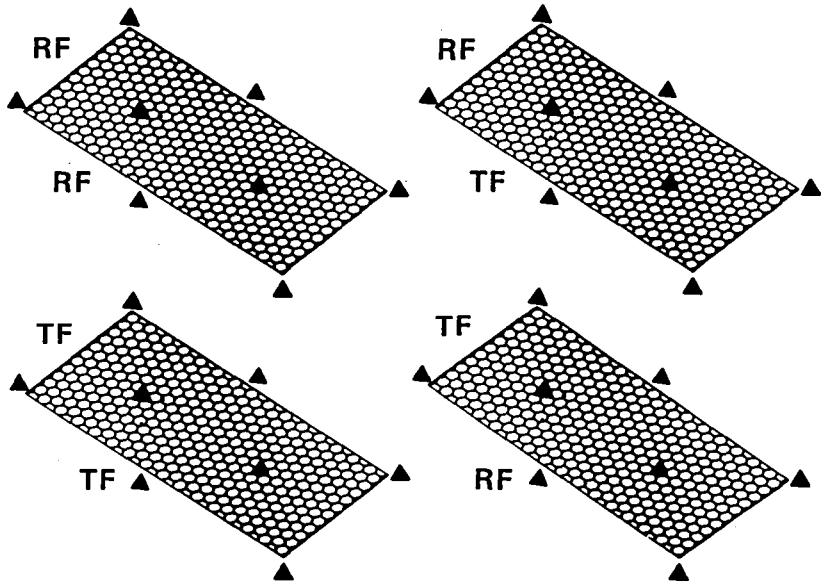

RF = ROTATION FIXED
TF = TRANSLATION FIXED

- MAX PANEL DEFLECTION = 0.050 INCHES IN CENTER
- 0.130 INCH INTER PANEL STOWED SPACING IS ACCEPTABLE

DYNAMIC RESPONSE ANALYSIS PROCESS

Solar array pointing errors were calculated for solar array drive assembly (SADA) slew and crew motion disturbances. Independent open loop and closed loop analysis gave similar results.

SADA slew distortions were less than 0.5 degree and crew motion distortions were less than 0.7 degree. Details of this analysis are presented on Pages 6-64 through 6-81.

CONCENTRATOR SOLAR ARRAY SYSTEM DYNAMIC RESPONSE ANALYSIS PROCESS

- INDEPENDENT ANALYSES (OPEN–LOOP AND CLOSED LOOP) GIVE SIMILIAR RESULTS

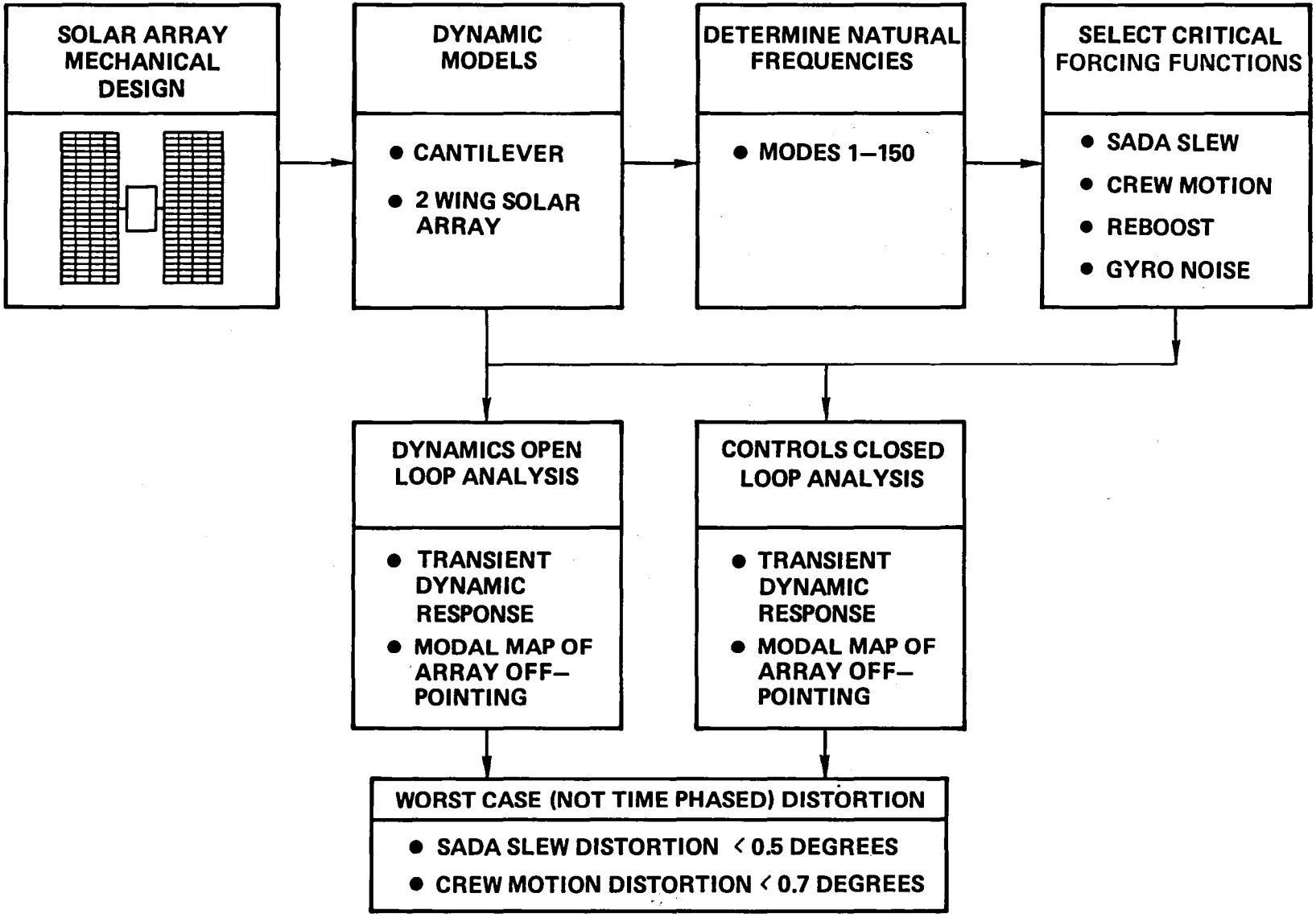

DEVELOPMENT OF THE CANTILEVER DYNAMIC MODEL

A cantilever model of one solar array wing was developed using the TRW Structural Analysis Program. The previously developed detailed quarter panel model was used to calculate the unconstrained or free modes. The material properties of a simplified quarter panel were varied until the simplified model frequencies matched with the detailed model. The simplified panel thickness was 0.1935 inch with a Young's modulus of 1.0×10^7 psi and 1.5×10^7 psi in the X and Y directions, respectively. The shear modulus was 1.86×10^6 psi.

The simplified panel was used to develop a cantilever solar array wing. The wing was left free in torsion about the SADA drive axis so that torques could be applied to the solar array for sun tracking, and SADA slew disturbances.

CASSEGRAINIAN CONCENTRATOR SOLAR ARRAY
DEVELOPMENT OF THE CANTILEVER DYNAMIC MODEL

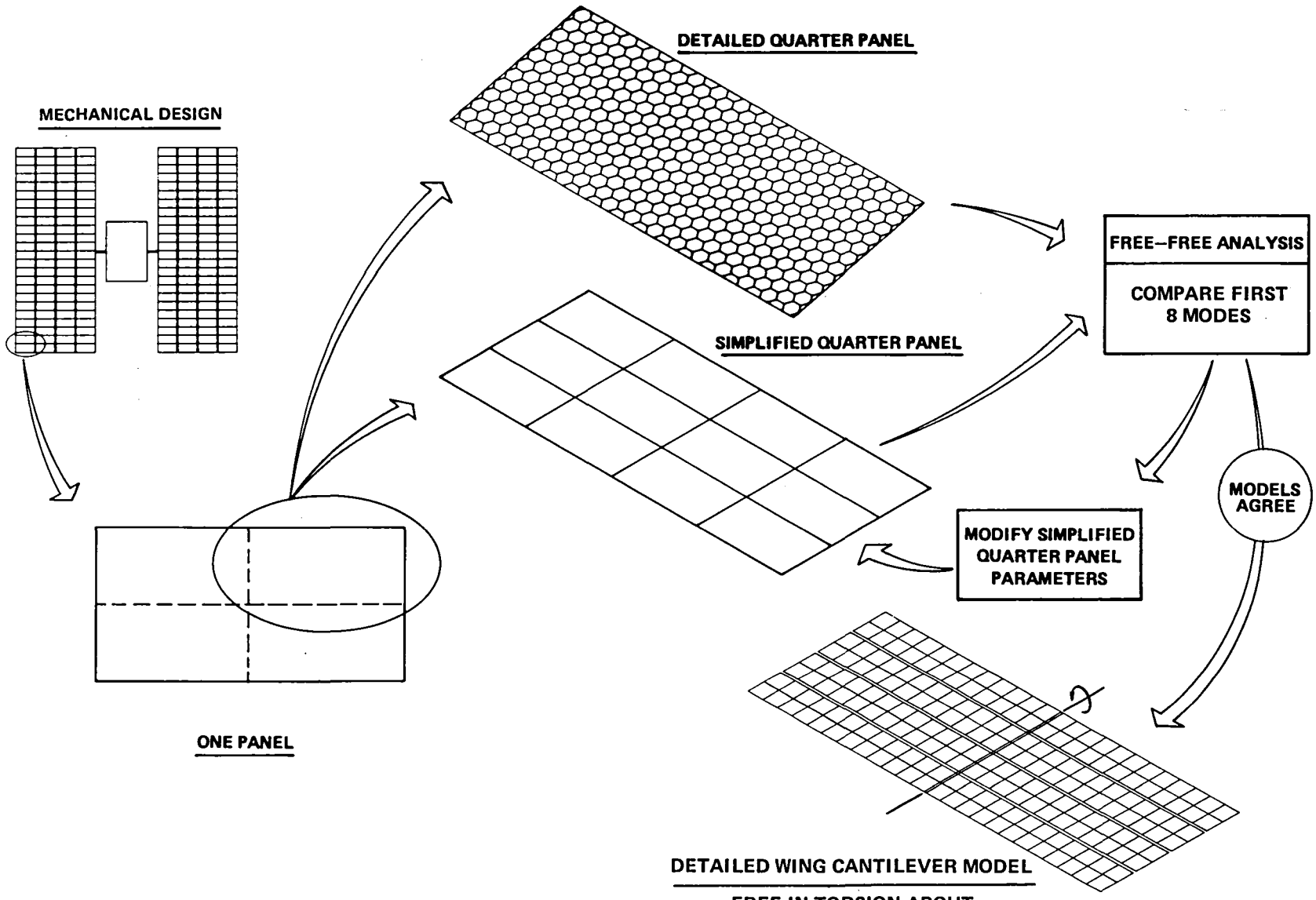

DYNAMIC RESPONSE DUE TO SADA UNWIND

If a cable is used to transfer power from the solar array to the spacecraft main body the solar array must be rotated to unwind the cable; the cable unwinding is referred to as SADA slew. Peak angular response at a point is calculated as the square root of the sum of the maximum θ_x squared and the maximum θ_y squared; since the maximum θ_x and θ_y do not occur at the same time the peak response is not time phased. The peak angular response of 0.422 degree occurs at Point H. Even though a SADA slew function was analyzed, the use of slip rings to transfer power across the SADA has not been ruled out.

DYNAMIC DISTORTION OF THE CONCENTRATOR SOLAR ARRAY DUE TO SADA UNWIND IS LESS THAN 0.5 DEGREES

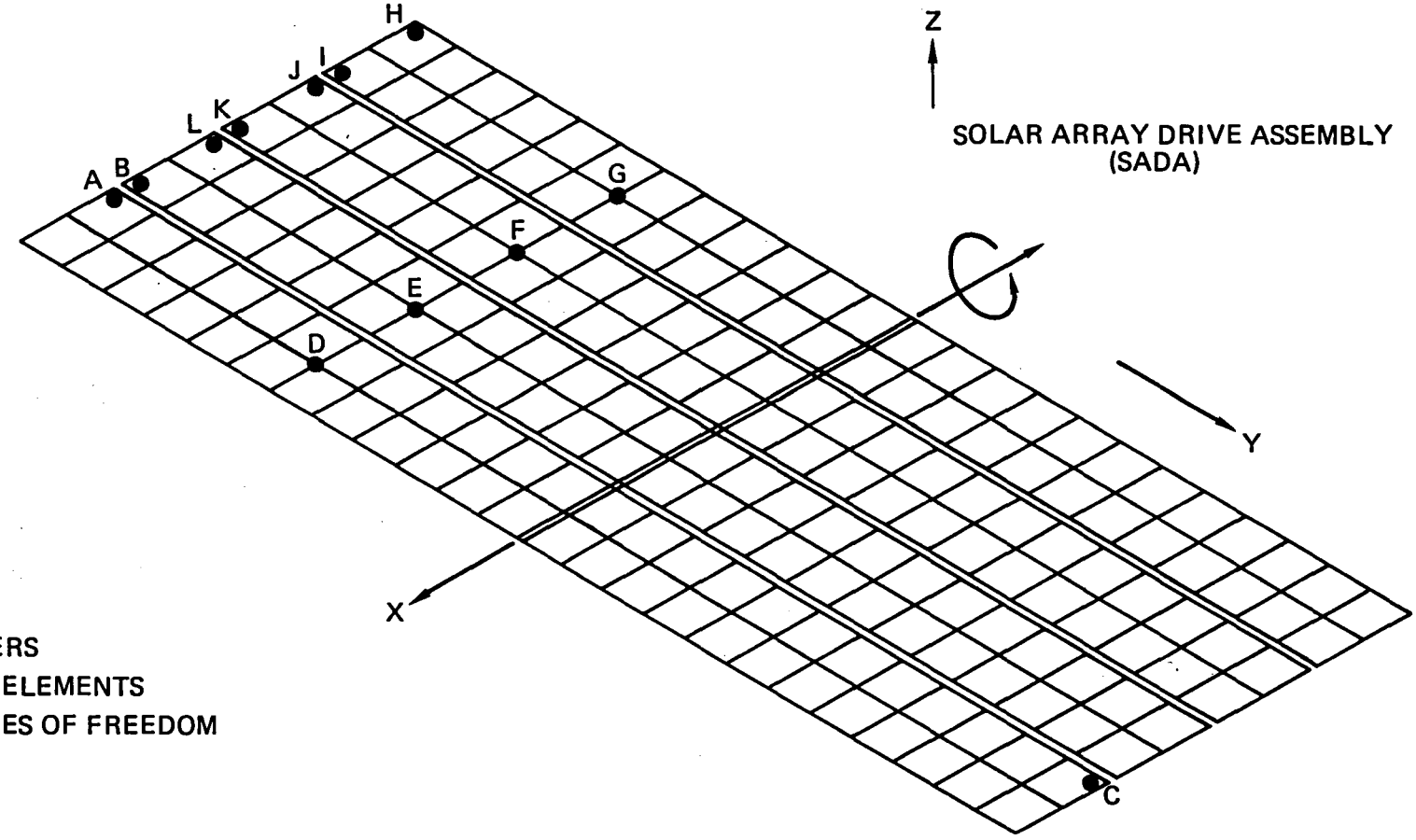

- 741 NODES
- 188 MEMBERS
- 192 SHELL ELEMENTS
- 385 DEGREES OF FREEDOM

DISTUBANCE	FORCING FUNCTION	ANGULAR OFF POINTING ERROR (DEGREES)*							
		A	B	C	D	E	F	G	H
TORQUE ABOUT SADA DRIVE AXIS FOR CABLE UNWIND AT 0.7 DEG/SEC.	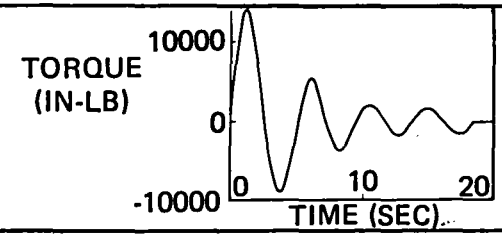	0.283	0.308	0.283	0.214	0.194	0.242	0.376	0.422

* WORST CASE (NOT TIME PHASED)

DYNAMIC CHARACTERISTICS OF THE CANTILEVER DYNAMIC MODEL

A total of 150 modal shapes were calculated for use in the response calculations. The array fundamental mode occurs at 0.175 hertz. All 150 modes are excited to a varying degree. The model force distribution factor is a relative measure of mode excitation. The high frequency content of the SADA slew forcing function excites the first, second, and third mast torsion modes; because the mast torsion modes are excited, the peak response occurs at Point H on the inboard edge of the array instead of the outboard edge of the array as shown on Page 6-67.

CASSEGRAINIAN CONCENTRATOR SOLAR ARRAY DYNAMIC CHARACTERISTICS OF THE CANTILEVER DYNAMIC MODEL

- FUNDAMENTAL CANTILEVER FREQUENCY IS 0.175 HZ
- SLEW TORSION FORCING FUNCTION EXCITES MAST TORSION MODE

MODE NUMBER	FREQUENCY (HZ)	MODAL FORCE DISTRIBUTION FACTOR Q ($X10^{-3}$)	DESCRIPTION OF MODES
1	0.00	0.893	RIGID BODY ROTATION ABOUT SOLAR ARRAY DRIVE AXIS
2 THRU 8	0.175–0186	0.030	OUT OF PLANE BENDING OF SUB ARRAY ELEMENTS
9	0.302	-0.040	IN-PLANE BENDING OF MAST
10–18	0.626–0.669	0.005	TORSION OF SUB ARRAY ELEMENTS
19	0.766	2.459	SECOND OUT OF PLANE BENDING OF SUB ARRAY ELEMENTS COUPLED WITH MAST TORSION
20–27	0.967–1.366	0.538	SECOND OUT OF PLANE BENDING OF SUB ARRAY ELEMENTS
28	1.557	1.198	THIRD OUT OF PLANE BENDING OF SUB ARRAY ELEMENTS COUPLED WITH MAST TORSION

DEVELOPMENT OF THE ON-ORBIT DYNAMIC MODEL

An on-orbit dynamic model (two full wings) was developed to calculate response due to crew forcing functions, gyro noise forcing functions, and reboost forcing functions. To reduce the complexity of the on-orbit model the subarray element model was reduced to a beam model with 10 degrees of freedom. Two wings of eight subarray elements were mounted on the Space Platform center body dynamic model to form the on-orbit dynamic model for this analysis.

CASSEGRAINIAN CONCENTRATOR SOLAR ARRAY DEVELOPMENT OF THE ON-ORBIT DYNAMIC MODEL

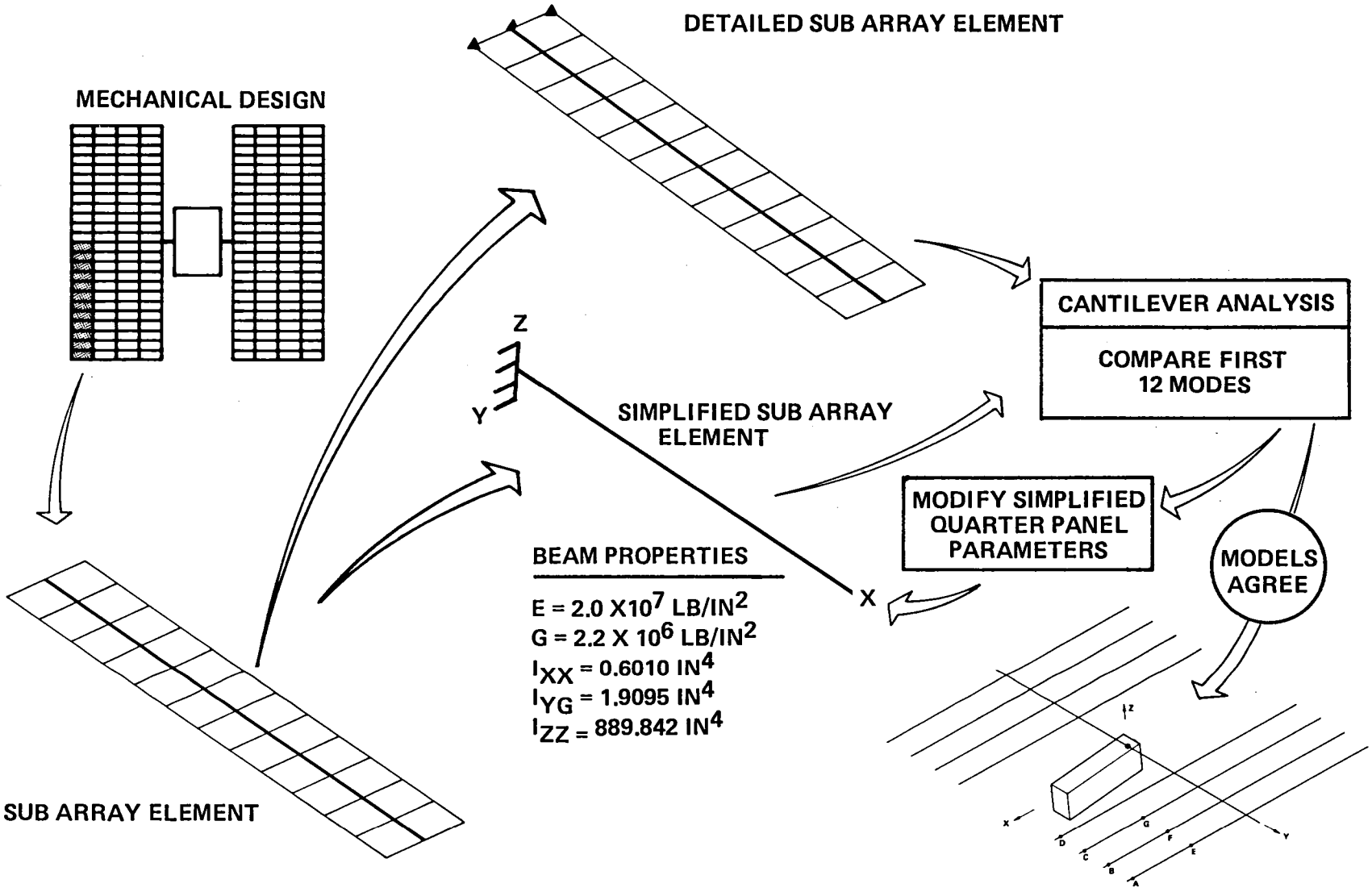

ON-ORBIT DYNAMIC MODEL

For use in response calculations, 150 modes were calculated. The fundamental mode is solar array torsion about the SADA at 0.110 hertz. The SADA stiffness about the drive axis was assumed to be 5×10^6 in-lb/rad. Reducing the SADA stiffness to 1×10^6 in-lb/rad reduced the fundamental frequency to only 1.04 hertz; hence, the solar array torsion is not strongly dependent on SADA stiffness.

CASSEGRAINIAN CONCENTRATOR SOLAR ARRAY DYNAMIC CHARACTERISTICS OF THE ON-ORBIT DYNAMIC MODEL

MODE NUMBER	FREQUENCY (HZ)	MODE DESCRIPTION
1 THRU 6	0.00	RIGID BODY MODES
7	0.110*	SOLAR ARRAY TORSION, SYMMETRIC
8	0.120*	SOLAR ARRAY TORSION, ANTI-SYMMETRIC
9	0.129	OUT OF PLANE MAST / SUB ARRAY ELEMENT BENDING
10 THRU 24	0.158–0.210	OUT OF PLANE SUB ARRAY ELEMENT BENDING

* TORSIONAL STIFFNESS OF SADA: 5×10^6 INCH-LB/RADIAN

DYNAMIC DISTORTION DUE TO CREW MOTION (FORCING FUNCTION I)

The on-orbit spacecraft dynamic model was subjected to two crew motion forcing functions. The forcing functions used were similar to those forcing functions used on the Space Platform study. The first crew motion forcing function (Function I) gives the largest off-pointing error (0.7 degree). This error occurs at one of the outboard corners of solar array wing (Point A). Crew motion is random and distortion due to crew motion is transient.

DYNAMIC DISTORTION OF THE CONCENTRATOR SOLAR ARRAY DUE TO CREW MOTION IS LESS THAN 0.7 DEGREES

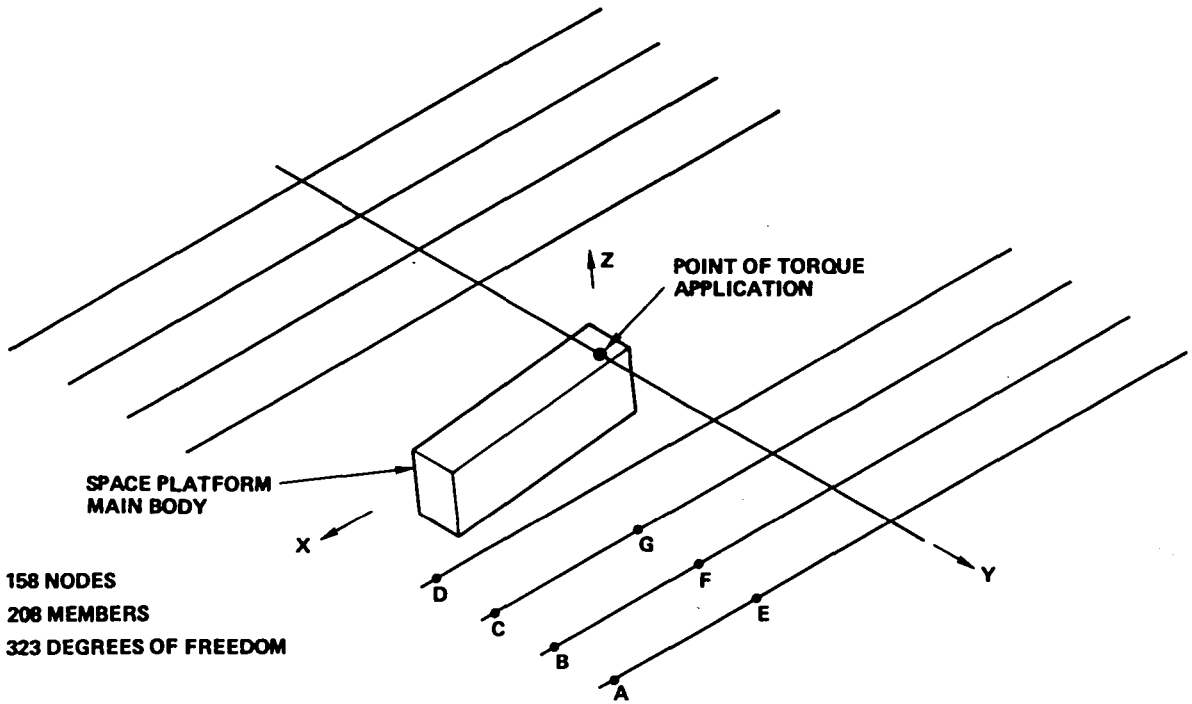

DISTURBANCE	FORCING FUNCTION	ANGULAR OFF POINTING ERROR* (DEGREES)						
		A	B	C	D	E	F	G
CREW FORCING FUNCTION I	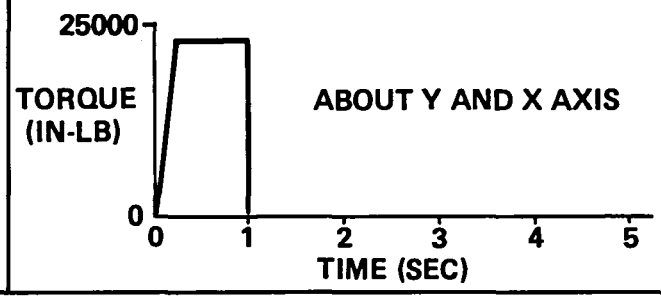	0.651	0.593	0.507	0.362	0.557	0.504	0.430

*WORST CASE (NOT TIME PHASED)

DYNAMIC DISTORTION DUE TO CREW MOTION (FORCING FUNCTION II)

This crew motion forcing function is less severe than Forcing Function I (discussed on Page 6-74) and, consequently, the array dynamic distortion is less (0.2 degree for Forcing Function II versus 0.65 degree for Forcing Function I).

DYNAMIC DISTORTION OF THE CONCENTRATOR SOLAR ARRAY DUE TO CREW MOTION IS LESS THAN 0.7 DEGREES

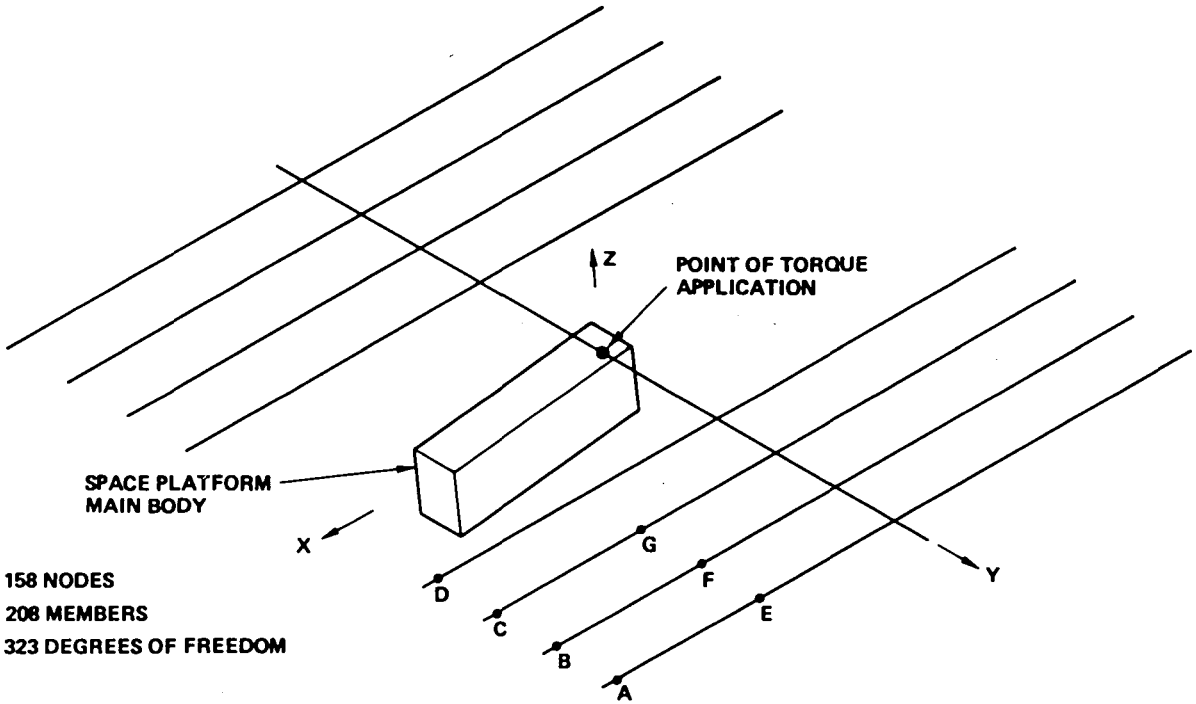

DISTURBANCE	FORCING FUNCTION	ANGULAR OFF POINTING ERROR* (DEGREES)						
		A	B	C	D	E	F	G
CREW FORCING FUNCTION II	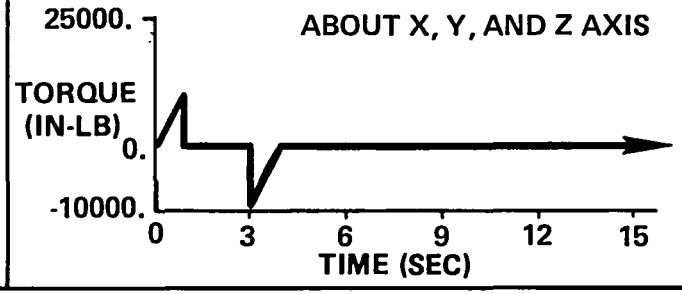	0.196	0.169	0.135	0.097	0.162	0.144	0.118

*WORST CASE (NOT TIME PHASED)

DYNAMIC DISTORTION DUE TO GYRO AND COOLING TORQUE

The on-orbit spacecraft dynamic model was subjected to a gyro and cooling torque. This is a steady-state forcing function which is considered to be continuous throughout mission lifetime. Dynamic distortion due to gyro and cooling torque is less than 0.003 degree and is two orders of magnitude less than for the transient crew motion forcing functions.

DYNAMIC DISTORTION OF THE CONCENTRATOR SOLAR ARRAY DUE TO CONTINUOUS GYRO AND COOLING TORQUE IS LESS THAN 0.003 DEGREES

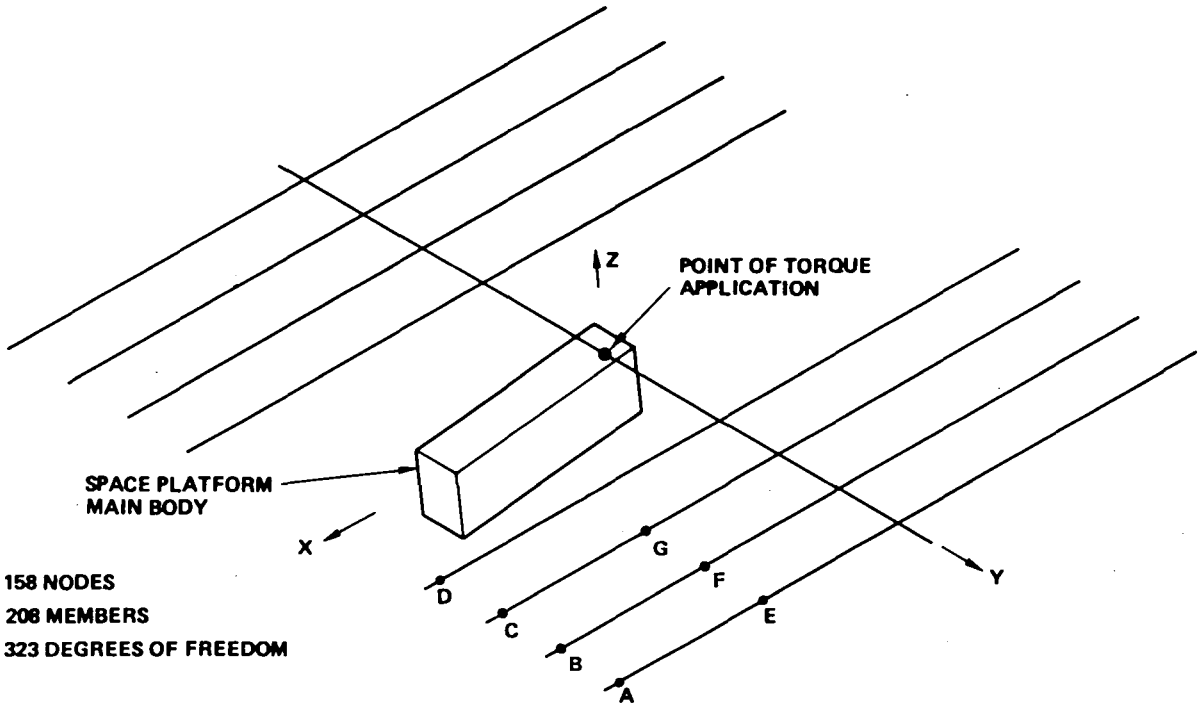

DISTURBANCE	FORCING FUNCTION	ANGULAR OFF POINTING ERROR* (DEGREES)						
		A	B	C	D	E	F	G
GYRO & COOLING TORQUE	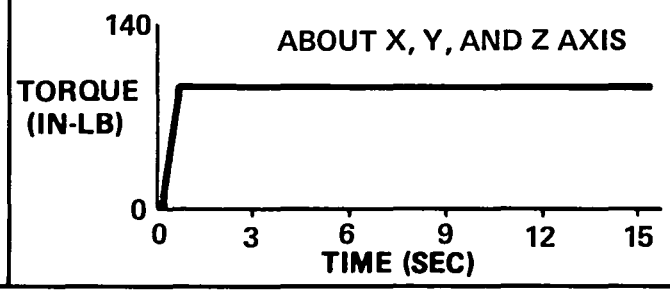	0.0024	0.0020	0.0017	0.0013	0.0022	0.0018	0.0015

*WORST CASE (NOT TIME PHASED)

DYNAMIC DISTORTION DUE TO STATIONKEEPING REBOOST TORQUES

The on-orbit spacecraft dynamic model was subjected to reboost torques for stationkeeping. These torques occur infrequently and at predictable intervals. Dynamic distortion due to reboost torque is 0.017 degree and is an order of magnitude less than for the transient crew motion forcing functions.

DYNAMIC DISTORTION OF THE CONCENTRATOR SOLAR ARRAY DUE TO STATION KEEPING REBOOST TORQUES IS LESS THAN 0.017 DEGREES

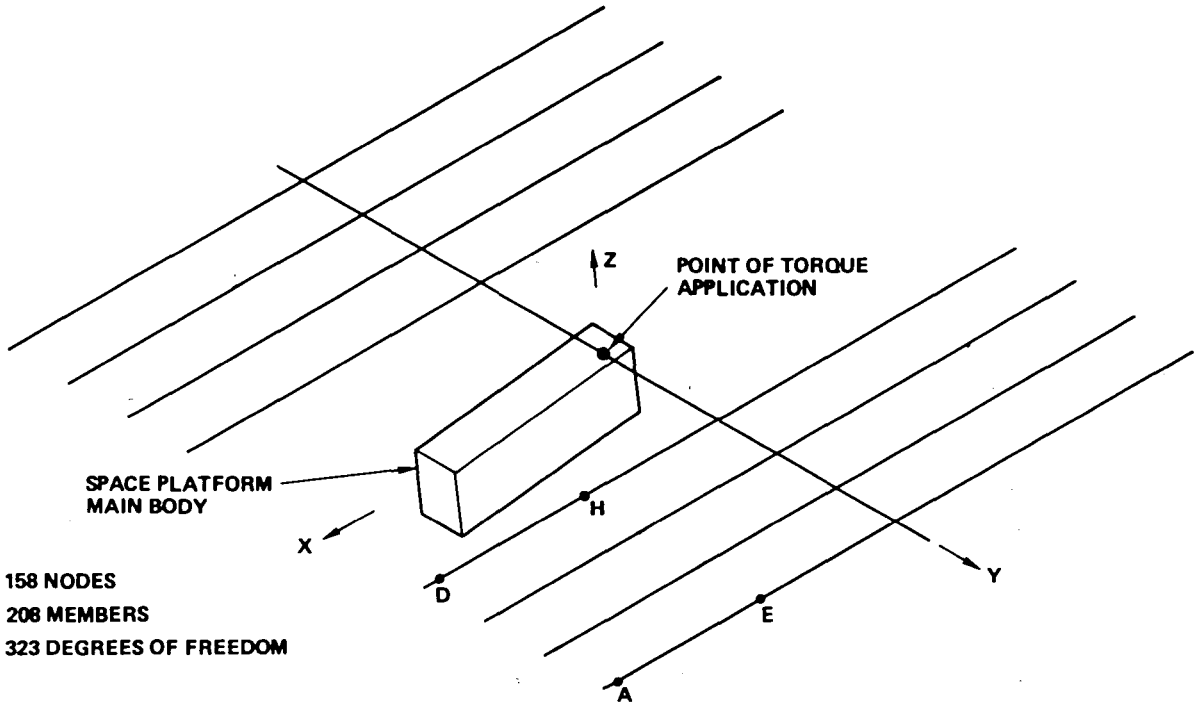

DISTURBANCE	FORCING FUNCTION	ANGULAR OFF POINTING ERROR* (DEGREES)						
		A	D	E	H			
REBOOST TORQUES	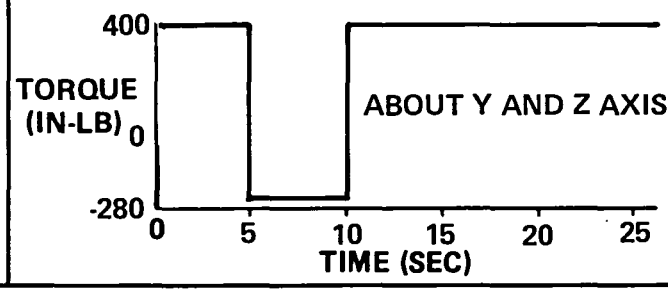	0.0164	0.0128	0.0147	0.0115			

*WORST CASE (NOT TIME PHASED)

DYNAMIC ANALYSIS RESULTS SUMMARY

Dynamic modes were developed and coupled to representative forcing functions to determine solar array dynamic response in the stowed configuration and in the on-orbit configuration. Panel deflection during launch is compatible with panel spacing defined during mechanical design activity. Maximum off-pointing error during orbit occurred for an extremely severe crew forcing function.

DYNAMIC ANALYSIS RESULTS SUMMARY

ASSUMPTIONS

- SELF DEPLOYABLE TWO WING 100KW CONCENTRATOR SOLAR ARRAY (H PATTERN)
- GRAPHITE EPOXY STRUCTURE, HEX GRID
- 0.25 mm NICKEL ELEMENTS WITH SEPARATE RADIATOR
- CONCENTRATOR ELEMENTS ARE NON-STRUCTURAL MEMBERS

RESULTS

(STOWED)
- MAXIMUM OUT-OF-PLANE PANEL DEFLECTION DURING LAUNCH (14g's) IS +0.05 IN

(ON-ORBIT)
- MAXIMUM IN-PLANE ARRAY DEFLECTION ON-ORBIT IS 1.0 IN (CREW FORCING FUNCTION I)
- MAXIMUM OUT-OF-PLANE DEFLECTION ON-ORBIT IS 4.1 IN (CREW FORCING FUNCTION I)
- MAXIMUM OFF-POINTING ERROR IS ±0.7 DEGREES (CREW FORCING FUNCTION I)

This Page Intentionally Left Blank

ELECTRICAL DESIGN OUTLINE

- ELECTRICAL DESIGN SUMMARY
- TYPICAL POWER FLOW FOR A CONCENTRATOR SOLAR ARRAY WING
- TYPICAL PANEL FLOW FOR TWO ADJACENT PANELS
- MAGNETIC MOMENT CANCELLATION
- FLAT RIBBON SUBWING HARNESS

ELECTRICAL DESIGN SUMMARY

The basic unit of the concentrator array is the concentator element which contains a 5 by 5 millimeter, 20 percent efficient (at 85°C) GaAs cell and has an undegraded beginning of life (BOL) output of 0.43 watts. The elements are interconnected in a circuit comprised of 6 cells in parallel by 220 cells in series producing approximately 2.7 amperes at the array bus voltage of approximately 190 volts at beginning of life. The electrical design of a concentrator array is in many respects similar to that of a planar array.

ELECTRICAL DESIGN SUMMARY

- GaAs CELLS, 20% η AT 85°C, 5X5 mm, 4 mm DIAMETER ACTIVE AREA
- 220 ELEMENTS IN SERIES (190 V BUS)
- 6 ELEMENTS IN PARALLEL PER CIRCUIT (2.75 A)
- 192 CIRCUITS PER 100KW SOLAR ARRAY (190 V, 2.75 A)
- 2 FLAT CONDUCTOR HARNESSES PER SUBWING (ONE ON EACH SIDE)
- POWER MODULARITY (12.5 KW PER SUBWING)
- HARNESS LOSSES ARE 3%
- CIRCUIT LAYOUT PROVIDE COUNTERFLOW OF CURRENTS FOR MAGNETIC FIELD CANCELLATION
- REDUNDANT BLOCKING DIODES FOR EACH OF 24 CIRCUITS PER SUBWING

TYPICAL POWER FLOW FOR A CONCENTRATOR SOLAR ARRAY WING

Four identical subwings (12.5-kilowatt BOL power) make up one concentrator wing (50-kilowatt BOL power). Each subwing is divided into 24 circuits. Twelve circuits each are connected to the inboard and outboard subwing flat conductor harnesses which are mirror images of each other. The transition from the flat conductor harness to standard round wire cables is made in boxes that also contain diodes. Each box is permanently attached to its respective subwing mast segment. Adjacent subwing to subwing electrical interconnection is thorugh the subwing mating mechanism shown on Page 6-37.

TYPICAL POWER FLOW FOR A CONCENTRATOR SOLAR ARRAY WING

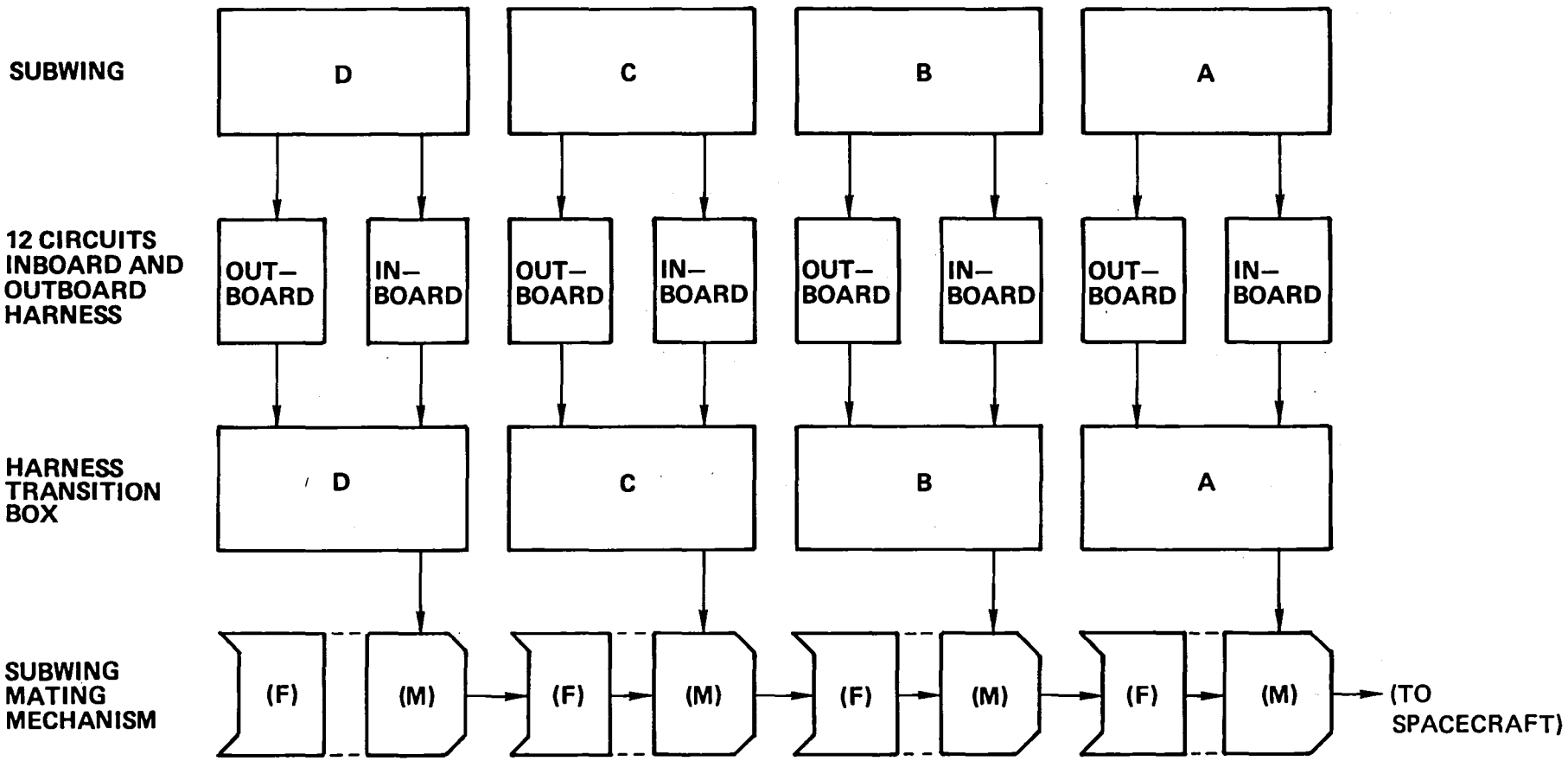

TYPICAL PANEL FLOW FOR TWO ADJACENT PANELS

Concentrator elements on each panel are interconnected into six subcircuits, each consisting of single element series strings of 220 elements. Three substrings on the inboard side of one panel are parallel connected to three substsrings on the inboard side of an adjacent panel to form one complete circuit which is connected to the inboard subwing harness. The outboard subcircuits on two adjacent panels are interconnected in a similar fashion to the outbaord subwing harness. This approach gives a mirror-mirror image current flow pattern for magnetic moment cancellation as shown on Page 6-93.

TYPICAL POWER FLOW FOR TWO ADJACENT PANELS

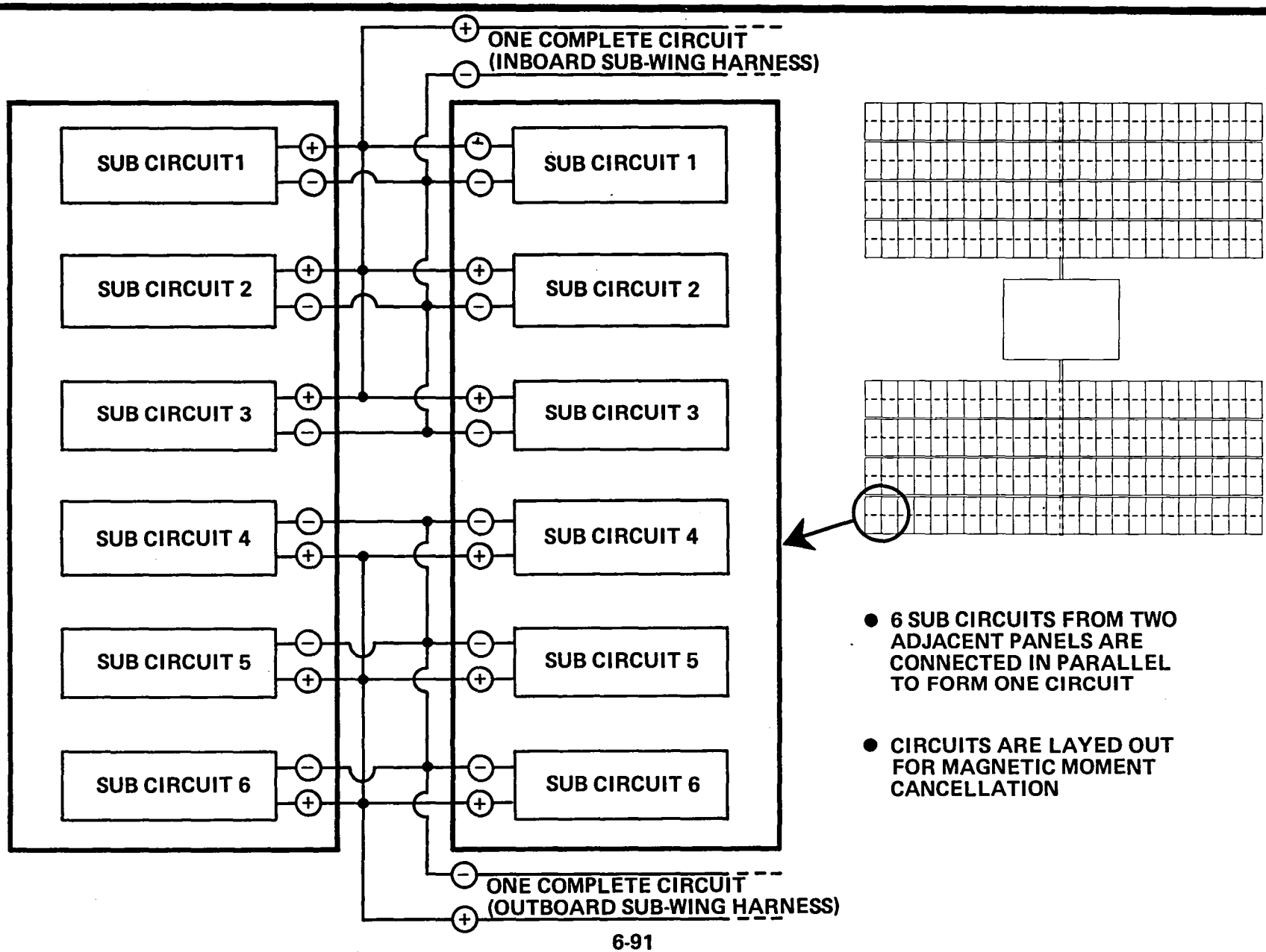

- 6 SUB CIRCUITS FROM TWO ADJACENT PANELS ARE CONNECTED IN PARALLEL TO FORM ONE CIRCUIT
- CIRCUITS ARE LAYED OUT FOR MAGNETIC MOMENT CANCELLATION

PANEL CIRCUITRY LAYED OUT TO MINIMIZE MAGNETIC MOMENTS

The individual current paths of each of the six subcircuits on two adjacent panels are shown. The mirror-mirror current path image which results was designed to provide magnetic moment cancellation.

PANEL CIRCUITS LAYED OUT TO MINIMIZE MAGNETIC MOMENTS

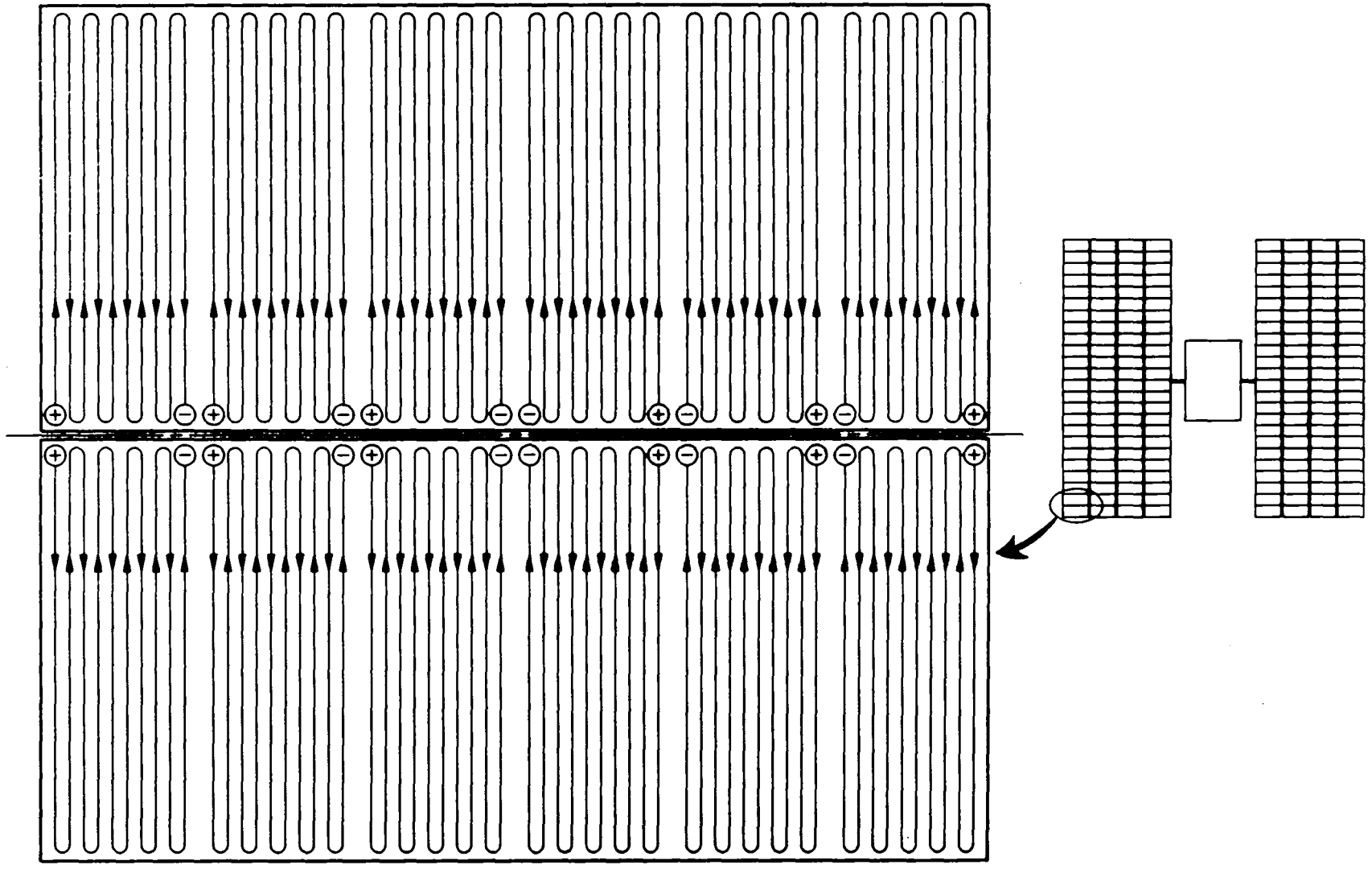

FLAT RIBBON CONDUCTOR SUBWING HARNESS

The flat ribbon conductor subwing harness is designed to provide a low profile for array stowage and to provide flexibility for array deployment. Each subwing harness can consist of either two conductor layers, each 2 inches wide or four conductor layers, each 1 inch wide. The conductor cross sections vary to achieve a uniform 3 percent current-voltage loss for each circuit.

100-KW CONCENTRATOR SOLAR ARRAY
FLAT RIBBON CONDUCTOR SUBWING HARNESS

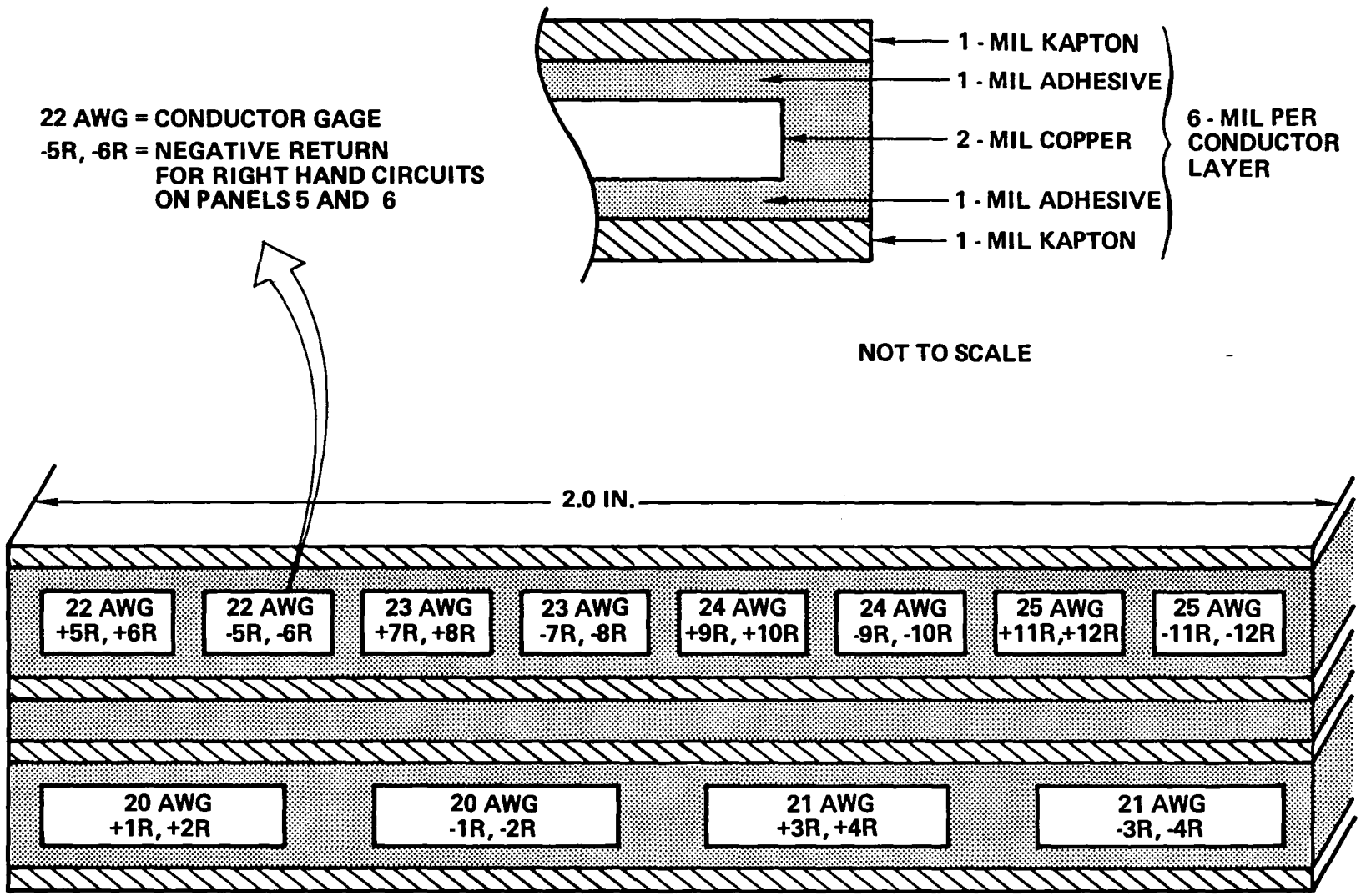

This Page Intentionally Left Blank

ARRAY PERFORMANCE PREDICTION

- OPTICAL EFFICIENCY ASSUMPTIONS
- BASIS OF OFF-AXIS PERFORMANCE FACTOR
- BEGINNING OF LIFE PERFORMANCE (CURRENT TECHNOLOGY)
- PERFORMANCE PROJECTIONS WITH TECHNOLOGY EVOLUTION

BASELINE DESIGN OPTICAL EFFICIENCY

The demonstration hardware had an optical efficiency of 0.55. The 100-kilowatt concentrator array predicted performance on Page 6-103 assumes an element optical efficiency of 0.81. The improvement is based on changing the reflector coating from aluminum to silver and reducing the secondary support blockage.

BASELINE DESIGN OPTICAL EFFICIENCY IS 0.81

PARAMETER	DEMONSTRATION MODULE (TEST RESULTS)	BASELINE DESIGN (ESTIMATED)	COMMENT
PRIMARY REFLECTOR REFLECTANCE	0.84	0.95	● BASELINE HAS Ag COATING ● MODULE HAS Al COATING
SECONDARY REFLECTOR REFLECTANCE	0.84	0.95	● BASELINE HAS Ag COATING ● MODULE HAS Al COATING
SECONDARY REFLECTOR BLOCKAGE	6%*	6%**	● SAME OPTICAL SYSTEMS DESIGN
SECONDARY REFLECTOR SUPPORT BLOCKAGE	14%*	4%**	● BASELINE HAS OUT–OF–PLANE SUPPORTS ● MODULE HAS IN PLANE SUPPORTS
OVERALL EFFICIENCY (η_o)	0.55***	0.81	

*BLOCKAGES COMBINE TO GIVE 0.8 TRANSMISSION FACTOR

**BLOCKAGES COMBINE TO GIVE 0.9 TRANSMISSION FACTOR

***MEASURED TOTAL EFFICIENCY IS 0.01 LESS THAN PRODUCT OF INDIVIDUALLY MEASURED FACTORS

CONCENTRATOR SOLAR ARRAY POINTING ERROR DEGRADATION FACTOR

The predicted curve for the relative performance of concentrator element as a function of pointing error is presented. All identified and analyzed sources of pointing error are shown in the table. Thermal distortion, manufacturing, and dynamic distortion errors are worst case errors at the array tips furthest from the Space Station body. The "average" off-pointing error for the entire array is an integral over the entire array area where the integrand is a function of the off-pointing versus element performance and the thermal distortion, manufacturing tolerance, and dynamic distortion versus array position relationships. These relationships have not been sufficiently defined to perform the integration. As a conservative estimate of "average" off-pointing, the worst case component errors (which occur at the tips of the array furthest from the Space Station body) have been combined using an RSS (square root of the sum of the squares of the individual components) process.

CONCENTRATOR SOLAR ARRAY PERFORMANCE FACTOR DUE TO POINTING ERROR IS 0.98

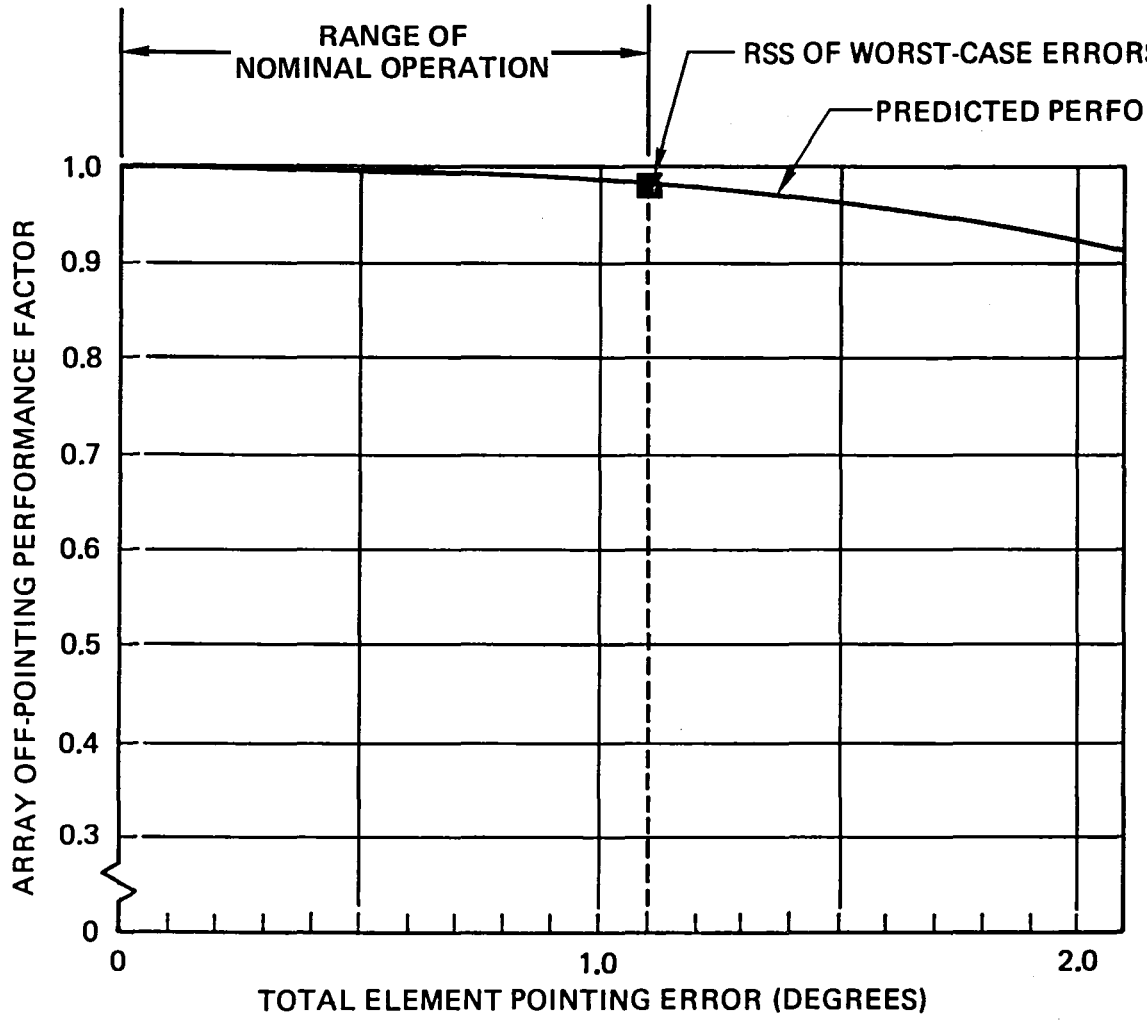

POINTING ERROR COMPONENT	POINTING ERROR (DEGREES)
THERMAL DISTORTION	± 0.2
MANUFACTURING*	± 0.8
CONTROL SENSING	± 0.1
DYNAMIC** DISTORTION	± 0.7
SUM	1.8
RSS	1.1

* WORST-CASE SUM

** WORST-CASE CREW MOTION (NOT TIME PHASED)

PERFORMANCE PREDICTION

The performance prediction for the 100-kilowatt solar array system concept is summarized and shows a beginning of life (BOL) performance of 160 W/m^2 and 28 W/kg. The basis for the optical transmission factor of 0.81 is shown on Page 6-99. The basis for the off-pointing factor of 0.98 is presented on Page 6-101. Assumptions for the calculated thermal distortion are presented on Page 6-51. The manufacturing tolerance analysis is summarized on Page 6-53. The array mass calculation is summarized on Page 6-55. Thermal analysis assumptions are presented on Page 4-33. Array area is total gross panel area and, consequently, areal power is based on total gross panel area.

Array power is based on 250,368 elements (1304 elements per panel, 192 panels) at 0.417 W/element (including all degradation factors). Overall packing factor is 0.79. This corresponds to a basic packing factor of 0.86 for untruncated hexagonal close packing and an edge effect and frame loss factor of 0.92.

BOL PERFORMANCE PREDICTION FOR A 235 NAUTICAL MILE ORBIT

NOMINAL DESIGN FACTORS	
PARAMETER	VALUE
CELL EFFICIENCY	20% AT 85°C
OPTICAL EFFICIENCY	0.81
WIRING & DIODE DROP	0.97
CELL MISMATCH	0.98
OFF-POINTING	0.98

NOMINAL PERFORMANCE	
PARAMETER	VALUE
ARRAY POWER	104 kW
ARRAY AREA	651 m^2
ARRAY MASS	3700 kg
AREAL POWER	160 W/m^2
SPECIFIC POWER	28 W/kg

CASSEGRAINIAN CONCENTRATOR ARRAY ENABLES TECHNOLOGY EVALUATION

Performance of the miniaturized Cassegrainian concentrator (MCC) can be significantly improved upon with technology development. The use of lighter weight optics results in specific power (W/kg) improvement. Lighter weight optics can be achieved by either reducing baseline optical element thickness (0.25-millimeter thick electroformed nickel) or changing to a low density optical element base material (such as as aluminum, copper, or plastic). The use of higher efficiency cells results in specific power and areal power improvements.

The MCC approach offers early opportunity for the application of advanced high efficiency cell types that may be more readily available as small area devices in large quantities from production facilities otherwise limited by market size and capital investment factors. Parallel-processing with surface plasmons ("Plasmon Cell") is a new strategy for efficient solar energy conversion which is being developed by NASA/LeRC and could be applied with the MCC (Reference 6). The "Plasmon Cell" offers the potential of 50-percent conversion efficiency.

CASSEGRAINIAN CONCENTRATOR ARRAY ENABLES TECHNOLOGY EVOLUTION

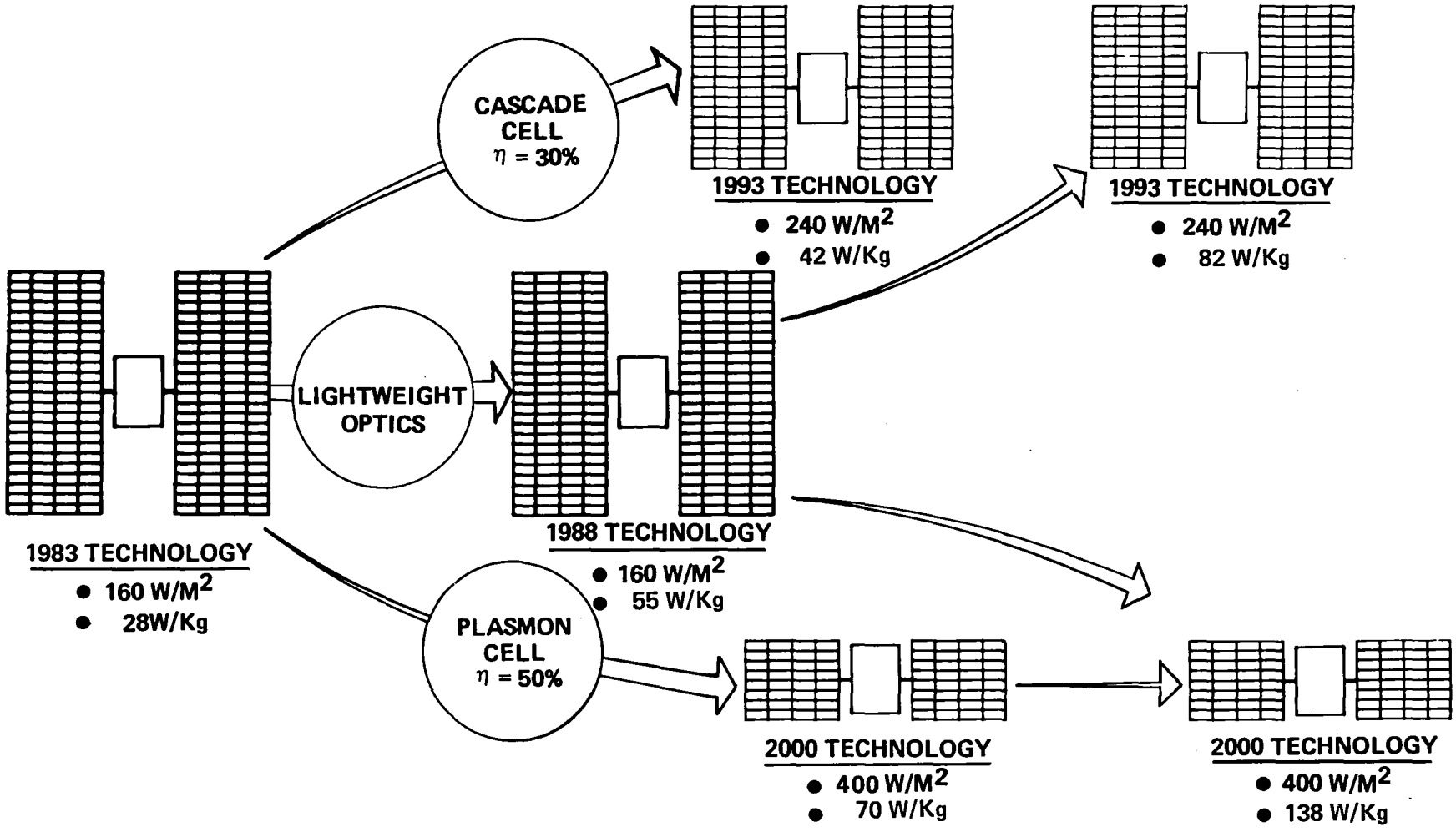

Conclusions

CONCLUSIONS

A miniaturized Cassegrainian concentrator (MCC) module has been designed, assembled, and tested. Results support technical feasibility. Thermal vacuum testing and analysis confirm earlier predictions that miniaturization of the concentrator element enables acceptable cell temperature in a concentrator with effective concentration ratio of 130 with passive control. Electrical performance of the demonstration hardware was as predicted at normal incidence. The light catcher cone improves off-pointing performance but its full predicated effectiveness has not been achieved.

A MCC solar array system study was performed to assess the practicality of assembling the basic MCC element into a total array system capable of producing multihundred kilowatts of power for Space Platform/Space Station or other low earth orbit long lifetime missions. Results of the study support the feasibility of a 100-kilowatt MCC array system with beginning-of-life performance of 160 W/m^2 and 28 W/kg and which would occupy approximately 8 linear feet of Shuttle Cargo Bay in the fully stowed configuration.

The performance numbers are based on 20-percent efficient (at operating temperature) solar cells and 0.25-millimeter thick electroformed nickel optics. These performance numbers can be improved upon significantly with the development of higher efficient solar cells and/or lighter weight optics.

CONCLUSIONS

- THERMAL, OPTICAL AND ELECTRICAL TEST RESULTS DEMONSTRATE ELEMENT TECHNICAL FEASIBILITY
- DESIGN AND ANALYSIS SUPPORT FEASIBILITY OF 100-KW ARRAY SYSTEM WITH BOL PERFORMANCE OF 160 W/m^2 AND 28 W/kg
- NO "TECHNICAL BREAKTHROUGHS" ARE REQUIRED
  - 20% GaAs CONCENTRATOR CELLS HAVE BEEN PRODUCED
  - LOW COST ELECTROFORMED Ni OPTICS ARE USED IN FLASHLIGHTS
  - GRAPHITE-EPOXY TECHNOLOGY IS USED IN SPACE AS WELL AS IN NUMEROUS COMMERCIAL TERRESTRIAL APPLICATIONS
- POTENTIAL OF 60 W/kg WITH TECHNOLOGY DEVELOPMENT

TRW

Related Technology Issues

RELATED TECHNOLOGY ISSUES

Technical feasibility of the miniaturized Cassegranian concentrator (MCC) has been demonstrated at the element level. However, a number of related technology issues have been identified and must be addressed with successful results in order to eventually achieve technology readiness status for the MCC solar array.

CASSEGRAINIAN CONCENTRATOR SOLAR ARRAY RELATED TECHNOLOGY ISSUES

- ENVIRONMENTAL STABILITY OF OPTICS
  - NATURAL PARTICLE RADIATION
  - THERMAL CYCLING
  - PLASMA INTERACTION
  - ATOMIC OXYGEN
  - ULTRA-VIOLET EXPOSURE
  - CONTAMINATION
- LIGHTWEIGHT SUBSTRATE/STRUCTURE DEVELOPMENT
  - LOW COST COMPOSITE FABRICATION
  - DIMENSIONAL STABILITY OF EXPOSED STRUCTURES
- LIGHTWEIGHT OPTICAL ELEMENT DEVELOPMENT
  - LOW COST FABRICATION
  - MAGNETIC EFFECTS ASSESSMENT
- CONCENTRATOR CELL DEVELOPMENT
  - EFFICIENCY IMPROVEMENT
  - CONTACT INTEGRITY
- SADA STIFFNESS
- SUB-WING MATING MECHANISM
- CONCENTRATOR ARRAY PERFORMANCE TESTING
  - PANEL ILLUMINATION TEST EQUIPMENT
  - MECHANICAL ALIGNMENT AND DEPLOYMENT SIMULATION FIXTURES

Recommendations

RECOMMENDED FUTURE WORK

The recommendations presented on the facing page are miniaturized Cassegranian concentrator (MCC) specific and are directed toward near term activity (1 to 2 years). It is also recommended that the more general related technology issues (presented on Page 8-3) be addressed, although not necessarily as specific tasks to the MCC development effort.

RECOMMENDED FUTURE WORK

- CONTINUE ARRAY SYSTEM DESIGN STUDY
- DEVELOP PRE-PROTOTYPE PANEL DESIGN
- INITIATE TECHNOLOGY DEVELOPMENT TASKS
  - ELECTROFORMED NICKEL PRODUCIBILITY
  - ALTERNATE OPTICAL COMPONENT MATERIAL/PROCESSING
  - SUBSTRATE MATERIAL/PROCESSING

References

This Page Intentionally Left Blank

REFERENCES

1 TRW Systems, "Study of Multikilowatt Solar Arrays for Earth Orbit Applications," Mid-term Report on Contract NAS8-32986 to NASA MSFC, July 1980.

2 TRW Systems, "Study of Multikilowatt Solar Arrays For Earth Orbit Applications," Final Report on Contract NAS8-32986 to NASA MSFC, TRW Report No. 33295-6001-UT-00, September 1980.

3 H. Rauschenbach and R. Patterson, "Design Requirements for High Efficiency High Concentration Ratio Space Solar Cells," TRW Space and Technology Group, *Space Photovoltaic Research and Technology, 1980*, NASA Conference Publication 2169, October 1980.

4 R.E. Patterson, H.S. Rauschenback, M.D. Cannady, and U.S. Whang, TRW Space and Technology Group, Redondo Beach, California 90278, and W.L. Crabtree, NASA Marshall Space Flight Center, Huntsville, Alabama 35812, "Low Cost, High Concentration Ratio Solar Cell Array for Space Applications," *16th Intersociety Energy Conversion Conference*, August 9-14,1981.

5 R.E. Patterson, H.S. Rauschenbach, and M.D. Cannady, TRW Space and Technology Group, Redondo Beach, California 90278, "Design and Perfromance Trades for a Miniaturized Photovoltaic Concentration Array," *Sixteenth IEEE Photovoltaic Specialists Conference*, September 27-30, 1982.

6 L.M. Anderson, NASA LeRC, "Parallel-Processing with Surface Plasmons: A New Strategy for Converting the Broad Solar Spectrum," *Sixteenth IEEE Photovoltaic Specialists Conference*, September 27-30, 1982.

End of Document